

EXPERIMENTAL INVESTIGATION OF CENOSPHERE REINFORCED HDPE SYNTACTIC FOAM COMPOSITE

Thesis

Submitted in partial fulfillment of the requirements for the degree of

DOCTOR OF PHILOSOPHY

by

BHARATH KUMAR B. R.



DEPARTMENT OF MECHANICAL ENGINEERING
NATIONAL INSTITUTE OF TECHNOLOGY KARNATAKA,
SURATHKAL, MANGALORE – 575025
SEPTEMBER, 2016

DECLARATION

I hereby *declare* that the Research Thesis entitled “**EXPERIMENTAL INVESTIGATION OF CENOSPHERE REINFORCED HDPE SYNTACTIC FOAM COMPOSITE**” which is being submitted to the **National Institute of Technology Karnataka, Surathkal** in partial fulfillment of the requirements for the award of the Degree of **Doctor of Philosophy** in **Department of Mechanical Engineering** is a *bonafide report of the research work carried out by me*. The material contained in this Research Thesis has not been submitted to any University or Institution for the award of any degree.

Register Number : **138029ME13F13**

Name of the Research Scholar : **BHARATH KUMAR B. R.**

Signature of the Research Scholar :

Department of Mechanical Engineering

Place : **NITK, Surathkal**

Date :

C E R T I F I C A T E

This is to *certify* that the Research Thesis entitled “**EXPERIMENTAL INVESTIGATION OF CENOSPHERE REINFORCED HDPE SYNTACTIC FOAM COMPOSITE**” submitted by **Mr. BHARATH KUMAR B. R. (Register Number: 138029ME13F13)** as the record of the research work carried out by him, is *accepted as the Research Thesis submission* in partial fulfillment of the requirements for the award of degree of **Doctor of Philosophy**.

Research Guide

Dr. Mrityunjay Doddamani.

Assistant Professor

Department of Mechanical Engineering

NITK, Surathkal

Chairman – DRPC

Date:

ACKNOWLEDGEMENT

I would like to extend my gratitude to Dr. Mrityunjay Doddamani, Assistant Professor, Mechanical Engineering, National Institute of Technology Karnataka (NITK), Surathkal for the invaluable constructive guidance and encouragement extended throughout my study. Sincere gratitude is expressed to Dr. Nikhil Gupta for the encouragement and help provided.

I would like to thank my Research Progress Assessment Committee members Dr. S. M. Murugendrappa and Dr. Srinivasa Rao Kola for their valuable inputs. Useful discussions and suggestions of Dr. R. R. N. Sailaja and Dr. Keshav Prabhu are deeply appreciated.

I would like to thank Dr. Prasad Krishna and Dr. K. V. Gangadharan (former and current Head's) and all the members of faculty, Mechanical Engineering, NITK for their support throughout this research work.

Constant encouragement of my family to pursue higher studies has made it possible for me to reach at this stage. I wish to thank all my family members for love, help and encouragement provided. Special note of thanks to all my friends and well wishers for their constant help, encouragement and understanding.

ABSTRACT

Polymer matrix composites can reduce the structural weight and result in improved fuel efficiency and performance in transportation applications. Thermoplastic matrix composites have been used for semi-structural and engineering applications. In addition to the ease of fabrication using a wide range of forming processes, thermoplastic polymers are recyclable, which are the strong driving forces for their current and future applications.

Rapid production of high quality components is the key to cost reduction in industrial applications. The present work is the first attempt of manufacturing syntactic foams, hollow particle filled lightweight composites, using an industrial scale Polymer Injection Molding (PIM) process. High Density Polyethylene (HDPE) is used as the matrix material and fly ash cenospheres as the filler. Development of syntactic foams with cenospheres serves dual purpose of beneficial utilization of industrial waste fly ash and reduction in the component cost. Pressure and temperature used in PIM are optimized to minimize cenosphere fracture and obtain complete mixing of cenospheres with HDPE. The optimized parameters are used for manufacturing syntactic foams with 20, 40 and 60 wt.% cenosphere without any surface treatment initially. With increasing cenosphere content, density and tensile strength reduce and modulus increases. A theoretical model based on a differential scheme is used to estimate the properties of cenospheres by conducting parametric studies because of inherent difficulties in direct measurement of cenosphere properties.

Further, the influence of cenosphere surface treatment, functionalization of HDPE and blending method on tensile properties are investigated. Cenospheres are treated with silane and HDPE is functionalized with 10% dibutyl maleate. Tensile test specimens are cast with 20, 40 and 60 wt.% of cenospheres using injection molding. Modulus and strength are found to increase with increasing cenosphere content for composites with treated constituents. Highest modulus and strength were observed for 40 and 60 wt.% untreated mechanically mixed and treated brabender mixed cenospheres/HDPE blends, respectively. These values are 37 and 17% higher than those for virgin and

functionalized HDPE. Theoretical models are used to assess the effect of particle properties and interfacial bonding on modulus and strength of syntactic foams. Brabender mixing method provided highest ultimate tensile and fracture strengths, which is attributed to the effectiveness of brabender in breaking particle clusters and generating the higher particle-matrix surface area compared to that by mechanical mixing method. Theoretical trends show clear benefits of improved particle-matrix interfacial bonding in the strength results.

Effect of surface treatment and blending method on flexural properties is dealt next. Flexural test specimens are cast with 20, 40 and 60 wt.% of cenospheres using PIM. The flexural modulus and strength are found to increase with increasing cenosphere content. Particle breakage increases with the cenosphere content and the measured properties show increased dependence on processing method. Untreated constituents blended by mechanical mixing provide the highest benefit in flexural modulus. Modulus of syntactic foams is predicted by two theoretical models. Bardella-Genna model provides close estimates for syntactic foams having 20 and 40 wt.% cenospheres, while predictions are higher for higher cenosphere content, likely due to particle breakage during processing. The uncertainty in the properties of cenospheres due to defects contribute to the variation in the predicted values.

Untreated constituents blended by mechanical mixing route as observed in tensile and flexural characterization registered higher tensile modulus and better flexural performance. Thereby, characterization of cenosphere/HDPE syntactic foams synthesized by mechanical mixing route for untreated constituents is dealt in the subsequent investigations.

Quasi-static and high strain rate compressive response is investigated later. Thermoplastic matrix syntactic foams have not been studied extensively for high strain rate deformation response despite interest in them for lightweight underwater vehicle structures and consumer products. Quasi-static compression tests are conducted at 10^{-4} , 10^{-3} and 10^{-2} s^{-1} strain rates. Further, a split-Hopkinson pressure bar (SHPB) is utilized for characterizing syntactic foams for high strain rate compression.

The compressive strength of syntactic foams is higher than that of HDPE resin at the same strain rate. Yield strength shows an increasing trend with strain rate. The average yield strength values at high strain rates are almost twice the values obtained at 10^{-4} s^{-1} for HDPE resin and syntactic foams.

Further, HDPE matrix syntactic foams are characterized for their viscoelastic properties by dynamic mechanical analysis. Tests are conducted over 35-130°C temperatures and 1-100 Hz frequency range and combined using the time-temperature superposition principle to generate a set of isothermal master curves. Storage and loss modulus increase with increasing weight fraction of cenospheres, but with little difference between 40 and 60 wt.%, at all temperatures. The sensitivity of storage modulus to weight fraction of cenospheres increases with increasing frequency. Storage and loss modulus decrease with increasing temperature in the range of 35-130°C, while $\tan \delta$ increases. The Williams-Landel-Ferry (WLF) constants are a linearly increasing function of cenosphere weight fraction.

Structure-property correlations of all the investigated properties are presented with the help of exhaustive SEM images to understand underlying mechanisms. Finally, the potential for using the optimized parameters of injection molding process is demonstrated by casting several industrial components as a deliverable of this work.

Keywords: *Syntactic foam; Injection molding; High density polyethylene; Fly ash cenosphere; Theoretical modeling; Surface treatment; Mechanical properties.*

CONTENT

Declaration	
Certificate	
Acknowledgement	
Abstract	
CONTENT.....	i
LIST OF TABLES.....	vii
ABBREVIATIONS.....	ix
1 INTRODUCTION.....	1
1.1 Composite Materials.....	1
1.2 Syntactic foam composites.....	4
1.2.1 Filler/Reinforcement.....	5
1.2.2 Matrix.....	8
1.2.3 Role of interface and its modification.....	10
1.3 Processing of Syntactic foams.....	14
1.3.1 Compression molding.....	16
1.3.2 Polymer injection molding.....	17
1.4 Literature survey.....	18
1.5 Objectives and Scope of the present work.....	34
1.6 Outline of the thesis.....	35
2 MATERIALS AND METHODS.....	37
2.1 Constituents.....	37
2.1.1 Cenospheres.....	37
2.1.2 HDPE.....	37
2.2 Surface treatment of constituents.....	38
2.2.1 Silane treated cenospheres.....	38
2.2.2 HDPE functionalization.....	39
2.3 Sample preparation.....	40
2.4 Testing.....	44

2.4.1	FTIR spectroscopy and X-ray diffractograms	44
2.4.2	Particle size analysis	44
2.4.3	Density measurement.....	45
2.4.4	Tensile testing	45
2.4.5	Flexural testing.....	45
2.4.6	Quasi-static and high strain rate compression	46
2.4.7	Dynamic mechanical analysis.....	47
2.4.8	Imaging	48
3	RESULTS AND DISCUSSION.....	49
3.1	FTIR and XRD analysis	49
3.2	Particle size analysis.....	51
3.3	PIM process optimization and specimen manufacturing	53
3.4	Density	57
3.5	Tensile behavior	59
3.5.1	Untreated constituents.....	59
3.5.2	Treated constituents	68
3.6	Flexural behavior.....	76
3.7	Quasi-static and high strain rate compression.....	83
3.7.1	Quasi-static	83
3.7.2	High strain rate compression	87
3.8	Dynamic Mechanical Analysis.....	92
3.8.1	Temperature sweep	92
3.8.2	Time-temperature superposition	95
4	CASTING OF PROTOTYPE COMPONENTS.....	99
	CONCLUSIONS.....	103
	SCOPE OF FUTURE WORK	106
	REFERENCES	107
	LIST OF PUBLICATIONS	118
	BIO-DATA	120

LIST OF FIGURES

Figure 1.1 Classification of composites based on the nature of reinforcement.	2
Figure 1.2 Schematic representation of two, three and multi-phased syntactic foams.	5
Figure 1.3 Structure of fly ash particles.	7
Figure 1.4 Polymer consumption in India.	10
Figure 1.5 Reaction between Silane-69 coupling agent and fly ash.	13
Figure 1.6 Illustration of reinforced syntactic foam fabrication method (Gupta, N. et al. 2013).	15
Figure 1.7 Constituents of PMCs and manufacturing options.	16
Figure 2.1 (a) Cenospheres and (b) HDPE matrix used in the present work.	38
Figure 2.2 (a) Brabender (b) blending mechanism and (c) cenosphere/HDPE blend from brabender.	40
Figure 2.3 (a) Image of PIM machine (b) Schematic of the PIM machine used for manufacturing syntactic foam specimens. (c) Schematic of signal/material flow in PIM machine. Mold for manufacturing (d) Tensile (e) Flexural test specimens.	42
Figure 2.4 Fabrication route and the types of cenosphere/HDPE syntactic foams synthesized in the present work.	44
Figure 3.1 FTIR Spectra of (a) neat HDPE and (b) HDPE functionalized with 5, 10 and 15% DBM. Note that the y-scale is different in both figures.	49
Figure 3.2 Freeze fractured micrographs of (a) non functionalized and (b) functionalized HDPE specimens at the same acquisition magnification.	50
Figure 3.3 A section of the FTIR spectra of untreated and silane treated cenospheres.	50
Figure 3.4 X-ray diffractogram of the constituents.	51
Figure 3.5 Micrographs of (a) untreated and (b) silane treated cenospheres.	51
Figure 3.6 Micrographs of broken (a) untreated and (b) silane treated cenospheres. The wall thickness variations within one particle and porosity that exists in the walls of these cenospheres can be observed in these micrographs.	52
Figure 3.7 Particle size analysis of untreated and silane treated cenospheres.	53

Figure 3.8 Syntactic foam samples molded at pressures (a) below 30 bar and (b) above 40 bar. (c) The specimens molded at 30, 35 and 40 bar pressures showed good quality. The figure includes a neat HDPE specimen with three H60-U-MM specimens molded at different pressures.	54
Figure 3.9 Micrographs of syntactic foam specimens containing (a) 30 (H30-U-MM) and (b) 60 wt.% (H60-U-MM) cenospheres manufactured at 160°C, 30 bar.....	55
Figure 3.10 Micrograph of freeze fractured HDPE matrix syntactic foams containing 60 wt.% cenospheres (H60-U-MM) showing (a) uniform dispersion of cenospheres, indicating feasibility of using PIM in developing syntactic foams and (b) lack of bonding between cenospheres and HDPE matrix.....	56
Figure 3.11 (a) Freeze fractured micrographs of H20-T-BM syntactic foam showing dispersion of cenospheres in HDPE resin and (b) the interface between functionalized HDPE matrix and silane treated cenospheres. (c) The region marked by a circle in (b) is shown at higher magnification, where continuity across the interface can be observed. These micrographs are taken prior to the test.	57
Figure 3.12 Tensile stress-strain curves for (a) neat HDPE and (b) syntactic foams having 20, 40 and 60% cenospheres by weight. Note x-scale is different in both the figures.	60
Figure 3.13 A representative failed specimen of (a) HDPE and (b) syntactic foams. Fracture surface of (c) H20-U-MM (d) H40-U-MM and (e) H60-U-MM specimens. The fracture appears different from the fibrous fracture observed for the neat HDPE resin...	61
Figure 3.14 (a) Material flow lines with few separated fibers of HDPE before failure and (b) image close to the fracture zone showing formation of fibers that range from submicron to a few μm in diameter.	63
Figure 3.15 Failure surface of H40-U-MM showing HDPE matrix deformation.	63
Figure 3.16 Fracture surface of H60-U-MM specimen showing (a) plastic deformation of matrix and several intact cenospheres that have not fractured and (b) the higher magnification shows local plastic deformation of HDPE resulting in sub-micron scale diameter fibers of HDPE.....	64
Figure 3.17 (a) Debris of cenospheres in a failed H60-U-MM specimen and (b) A cenosphere in a H60-U-MM syntactic foam specimen.....	65
Figure 3.18 Results from Porfiri-Gupta model. In (a) the particle wall modulus obtained from the rule of mixtures method is kept constant and the radius ratio is varied. In (b) the radius ratio determined by density measurements is maintained constant and the ceramic modulus is varied.	68

Figure 3.19 Comparison of representative stress-strain curves of virgin and functionalized HDPE.	69
Figure 3.20 A representative failed specimen of functionalized HDPE.	69
Figure 3.21 Micrographs of representative tensile tested specimen of (a) virgin and (b) functionalized HDPE.	70
Figure 3.22 Stress-strain behavior of H20, H40 and H60 syntactic foams synthesized by (a) U-MM (b) T _M -MM (c) T-MM and (d) T-BM routes.	71
Figure 3.23 Micrographs of H40 syntactic foams synthesized by (a) U-MM (b) T _M -MM (c) T-MM and (d) T-BM routes. All images are acquired at the same magnification.	73
Figure 3.24 Least squares best fits of (a) Bardella-Genna model for modulus and (b) Pukánszky model for tensile strength represented with respect to the properties of neat resin. Solid lines with symbols represent experimental data and dashed lines are model fits. Note y-scale is different in both the figures.	75
Figure 3.25 Stress-strain behavior of non functionalized and functionalized neat HDPE.	77
Figure 3.26 Freeze fractured SEM images of (a) non functionalized and (b) functionalized HDPE samples after the test, acquired at same magnification. Tiny islands are observed for functionalized HDPE.	77
Figure 3.27 Stress-strain behavior of H20, H40 and H60 prepared by (a) U-MM (b) T _M -MM (c) T-MM and (d) T-BM routes.	78
Figure 3.28 Comparison of stress-strain response for (a) H20 (b) H40 and (c) H60 syntactic foams as a function of blending methodology.	79
Figure 3.29 (a) Flexural modulus and (b) flexural strength of syntactic foams at different cenosphere contents.	80
Figure 3.30 Comparison of model predictions with experimental data on modulus of syntactic foams.	82
Figure 3.31 Comparison of stress-strain curves at different quasi-static compressive strain rates for (a) H (b) H20 (c) H40 and (d) H60.	83
Figure 3.32 A representative compressive stress-strain curve at 10 ⁻³ strain rate for H60 syntactic foam showing three regions of different deformation behaviors (I: elastic deformation, II: post yield plastic deformation, III: plastic deformation beyond densification).	84

Figure 3.33 Yield strength of HDPE and its syntactic foams normalized by their density at different compressive strain rates.	86
Figure 3.34 SEM image of compressed (a) H20 specimen at 0.01s^{-1} (b) H20 specimen at 0.001s^{-1} (c) H40 compressed at 0.01s^{-1} (d) H40 specimen at 0.001s^{-1} (e) H60 specimen at 0.01s^{-1} and (f) H60 specimen at 0.001s^{-1} . Intact cenospheres are found in the material even after densification strain is reached. No significant change in the failure mode is observed in the material even after two orders of magnitude change in strain rate.....	88
Figure 3.35 A representative set of strain signals for HDPE tested at 3430 s^{-1} showing (a) incident and transmitted signals and (b) stress and strain rate with respect to strain.	89
Figure 3.36 Compressive stress-strain curves at three different high strain rates for (a) HDPE (b) H20 (c) H40 and (d) H60. The strain rates are recovered from the test results so they are not exactly the same for all materials.	89
Figure 3.37 Yield strength of HDPE and its syntactic foams at low and high strain rates.	90
Figure 3.38 SEM images of (a) H20 specimen compressed at 1770 s^{-1} (b) H40 specimen compressed at 1850 s^{-1} and (c) H60 specimen compressed at 1740 s^{-1}	91
Figure 3.39 (a) Storage modulus (b) loss modulus and (c) $\tan \delta$ results from DMA temperature sweep at 1 Hz.....	94
Figure 3.40 Representative data set from combined temperature-frequency sweep on a specimen of H60.	96
Figure 3.41 Time-temperature superposition results from DMA frequency sweep calculated for reference temperatures of (a) 60° (b) 80° and (c) 100°C	97
Figure 3.42 Williams-Landel-Ferry constants for syntactic foams.	97
Figure 4.1 Eco-friendly components cast using injection molding technique 1. Bearing cover 2. Automobile component used in liquefied petroleum gas cylinder for gas mixtures 3. Gear 4. Electrical junction box 5. Water filter cap 6. End cap for closure 7. Square base attachment for pipes 8. Jerry can cap and 9. Bottle cap. Several original components made of pure HDPE are also displayed in the center.	99
Figure 4.2 Prototype components cast in the study: (a) an example of an electrical junction box cast of pure HDPE (b) the electrical junction box cast on the same machine with syntactic foam. Other syntactic foam prototypes: (c) a part bearing cover (d) a bottle cap and (e) bottom cap of a chair leg.	100

LIST OF TABLES

Table 1.1 Literature review on Tensile behavior.	19
Table 1.2 Review of Flexural studies.	22
Table 1.3 Review on compression and high strain rate response.	25
Table 1.4 Review on dynamic mechanical analysis.	29
Table 1.5 Literature survey on surface treated constituents of composites.	31
Table 2.1 Chemical, physical and sieve analysis details of cenospheres*.	37
Table 2.2 Characteristics of HDPE grade HD50MA180*.	38
Table 2.3 Chemicals used for surface treatment of constituents.	39
Table 2.4 Injection molding machine specifications.	43
Table 2.5 Processing conditions for injection molded syntactic foam composites*.	43
Table 2.6 Syntactic foam types fabricated in the present study.	43
Table 3.1 Density values of H30-U-MM and H60-U-MM cast in the pilot study for optimization of process parameters.	55
Table 3.2 Theoretical and experimental density values of syntactic foams and cenosphere breakage during fabrication.	58
Table 3.3 Average modulus, strength, elongation and fracture behavior of HDPE and syntactic foams with untreated constituents.	61
Table 3.4 Specific tensile properties of HDPE and syntactic foams.	65
Table 3.5 Tensile properties of virgin and functionalized HDPE. The values are presented in average.	70
Table 3.6 Modulus, elongation at UTS and fracture strain of syntactic foams.	71
Table 3.7 UTS and fracture strength of syntactic foams.	71
Table 3.8 Flexural modulus and strength of materials.	80
Table 3.9 Mechanical properties of HDPE and its composites under varying low strain rate compression conditions.	85

Table 3.10 Slope and y-intercept values of yield strength (MPa) trend lines with respect to varying low strain rates for the different composites.	85
Table 3.11 Storage modulus and loss modulus values of HDPE at different temperatures.	92
Table 3.12 Comparison of storage modulus at three representative temperatures.	94
Table 3.13 Comparison of loss modulus at three representative temperatures.....	94
Table 3.14 Comparison of damping parameter at three representative temperatures.....	95
Table 4.1 Details of cast syntactic foam components.....	101

ABBREVIATIONS

APTS	: 3-Amino propyl tri ethoxy silane
ASTM	: American Society for Testing and Materials
DBM	: Dibutyl Maleate
FTIR	: Fourier Transform Infrared spectroscopy
HDPE	: High Density Polyethylene
HSR	: High Strain Rate
PIM	: Polymer Injection Molding
REB	: Relative Elongation at Break
RIS	: Relative Impact Strength
RTS	: Relative Tensile Strength
RYM	: Relative Young's Modulus
SEM	: Scanning Electron Microscope
SF	: Syntactic Foam
SHPB	: Split-Hopkinson Pressure Bar
T _g	: Glass transition temperature
UTS	: Ultimate Tensile Strength
WLF	: Williams-Landel-Ferry
XRD	: X-ray Diffraction

1 INTRODUCTION

1.1 Composite Materials

The development of mankind is defined in terms of advances in materials: the Stone Age, the Bronze Age, and the Iron Age. Today the development of any country is decided based on the amount of steel and concrete used. The Industrial revolution to a large extent made possible advances in the use of materials in industrial equipments. In the last half century, the growth of materials technology has been explosive and its impact on our daily lives, pervasive. In last few decades the developments in materials technology is fuelled mainly by composite materials. Composite materials are extending horizons of designers in all branches of engineering, and yet the degree to which this is happening can easily pass unperceived. The eye, after all, does not see beyond the glossy exterior or the race performance of a glass fiber reinforced plastics (GRP) yacht, nor does it sense the complexity of the structure of a composite helicopter rotor blade or of a modern carbon fiber reinforced plastics (CFRP) tennis racket. Nevertheless, this family of synthesized materials offers the possibility of exciting new solutions to difficult engineering problems (Harris 1999). In composites, materials are combined in such a way as to enable us make better use of their virtues while minimizing to some extent the effect of their deficiencies. This principle, when extended to physical, chemical and mechanical properties that can accrue, has opened a Pandora's box where the combinations to be thought of and tried for optimizing any of the above properties are only limited by one's imagination. This process of optimization can release a designer from the constraints associated with the selection and manufacture of conventional materials. One can make a use of tougher and lighter materials, with properties that can be tailored to suite particular design requirements.

Composites are classified according to either of the constituents, the matrix or the reinforcement (Chawla 2001). Based on the matrix material, composites are classified as Metal Matrix Composite (MMC), Ceramic Matrix Composite (CMC) and Polymer Matrix Composite (PMC). PMC's are becoming promising materials for variety of structural and automotive applications since these possess favorable combinations of

mechanical properties (Benchechou et al. 1998). Metal and ceramic matrix composites find less extensive applications compared to PMC's, because of the involved processing methods and higher cost. The applications of the former two varieties are typically seen in high performance/high temperature and cost intensive categories. On the other hand, PMC's have particularly attracted a wider usage and lot of interest because of their relative ease of processing, low density, desirable electrical/thermal properties and excellent chemical/corrosion resistance. Hence, they find applications ranging from specialized functions in aerospace and electronics engineering to day-to-day consumer industries like construction and transportation. Classification of composites based on the nature of reinforcement is simplified and presented in Figure 1.1 (Agarwal and Broutman 1980).

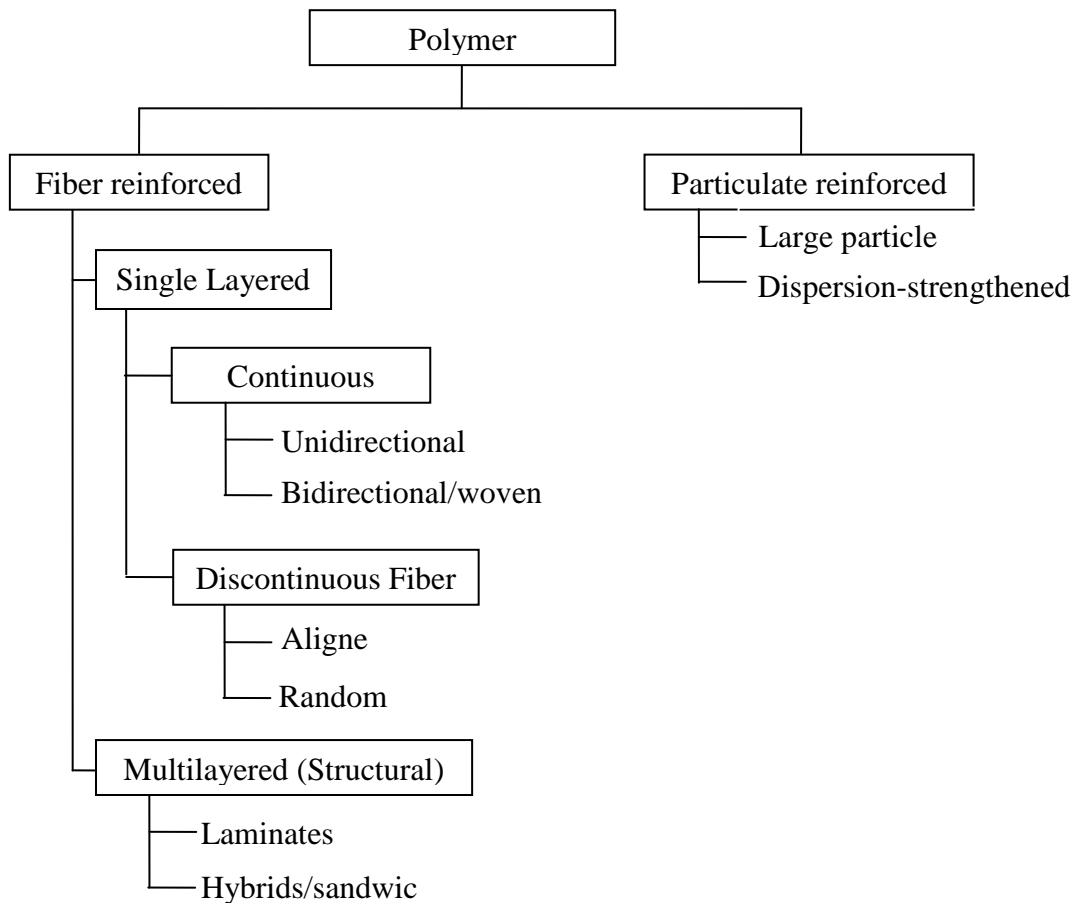


Figure 1.1 Classification of composites based on the nature of reinforcement.

PMCs consists of a polymer (epoxy, polyester, urethane etc.) reinforced by thin- diameter fibers (graphite, aramids, boron etc.). The reasons for this are two-fold. Foremost, in general the mechanical properties of polymers are inadequate for many structural designs. In particular, their strength and stiffness is low compared to metals and ceramics. This implies that there is a considerable benefit to be gained by reinforcing polymers and that the reinforcement, initially at least, did not have to have special properties. Secondly, the processing of PMCs need not involve high pressures and temperatures. It follows that problems associated with the degradation of the reinforcement during manufacture are less significant for PMCs than for composites with other matrices. Also the equipment required for PMCs are simpler. For these reasons polymer matrix composites developed rapidly and soon became accepted for structural applications. Today glass-reinforced polymers are still by far the most used composite material in terms of volume with the exception of concrete.

To see the advantages in using composite materials, a comparison between their properties and those of newer class of composites should be done in terms of specific values (per unit of weight). When it comes to weight saving without sacrificing structural performance, composites and in particular from the lightweight materials regime, syntactic foam (SF) composites are without doubt far superior to other traditional composites. In the present scenario, SF a special class of structural composite have become very popular due to high specific strength and bending stiffness. Low density of these materials makes them especially suitable for use in aeronautical, space, marine and sports applications (Gupta, N. 2002). Syntactic foams are lightweight porous composites that found their early applications in marine structures due to their naturally buoyant behavior and low moisture absorption. This lightweight feature is beneficial in weight sensitive aerospace structures too. Syntactic foams have pushed the performance boundaries for composites and have enabled the development of vehicles for travelling to the deepest parts of the ocean and to other planets. The high volume fraction of porosity in syntactic foams also enabled their applications in thermal insulation of pipelines in oil

and gas industry. The possibility of tailoring the mechanical and thermal properties of syntactic foams through a combination of material selection, hollow particle volume fraction, and hollow particle wall thickness has helped in rapidly growing these applications. The low coefficient of thermal expansion and dimensional stability at high temperatures are now leading their use in electronic packaging, composite tooling and thermoforming plug assists. Methods have been developed to tailor the mechanical and thermal properties of syntactic foams independent of each other over a wide range, which is a significant advantage over other traditional particulate and fibrous composites (Gupta, N. et al. 2005).

1.2 Syntactic foam composites

Syntactic foams are examples of particulate composites. These foams are made by mixing hollow particles called cenospheres/microspheres/microballoons in a matrix material. They possess lower density due to the hollow microballoons incorporated in the matrix compared to solid particulate and fiber reinforced composites. These foams are found to possess high specific strength and low thermal conductivity (Gupta, N. et al. 2005). SF's are used in a wide variety of applications. Most of the applications are related to the marine environment, where structural designs depend on the buoyancy obtained from such lightweight materials with high compressive strength and modulus. These materials were developed in the 1960s as buoyancy aid materials, for deep sea applications. Currently they are used in aircraft, spacecraft and ship structures (Gupta, N. 2002). One of the major advantages of syntactic foams is their ability to be designed and fabricated according to the physical and mechanical property requirements of the application. Depending upon the service conditions, the matrix resin can be chosen from a wide range of thermosetting and thermoplastic resins. Similarly, microballoons of polymer, ceramic or metal can be chosen based on the availability (Gupta, N. et al. 2013).

A schematic representation of two, three and multi phase structures of syntactic foams are presented in Figure 1.2. Syntactic foams are usually a two phase structures, namely

matrix and microballoons. These foams are classified as closed pore/cell foams, due to the existence of enclosed porosity within the microballoons (Gupta, N. 2007). However, during fabrication of syntactic foams, air or voids might get entrapped in the matrix. The presence of air or voids within the matrix is termed as open cell porosity and thus making syntactic foams a three phase structure. Syntactic foams when reinforced with fibers results in multi-phase structure.

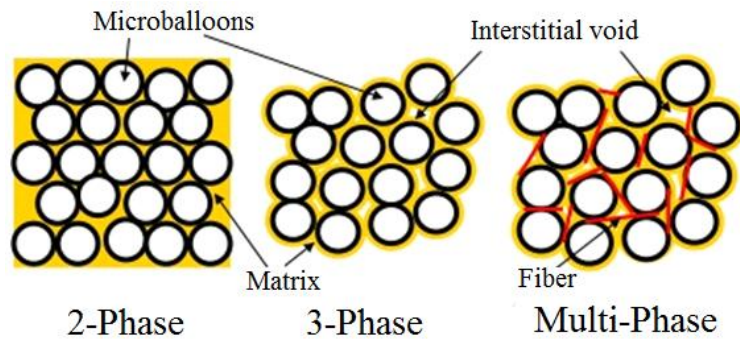


Figure 1.2 Schematic representation of two, three and multi-phased syntactic foams.

Interest in utilizing the advantage of low density of syntactic foams in variety of applications has made it necessary to characterize these materials for mechanical behavior. Though SF's are widely used, thrust on developing these with variety of hollow particulate fillers is overgrowing.

1.2.1 Filler/Reinforcement

Fillers are often incorporated in matrix resin to improve tensile and compressive strengths, tribological characteristics, toughness, dimensional and thermal stability etc. Selection of filler material is primarily dependant on the requirements expected in the end product, the interface compatibility, shape, size and packing factor. Large number of materials can be selected as fillers for the polymers which include particles of minerals, metals, ceramics, polymers and also some industrial wastes (Shaikh and Channiwala 2006). Some common examples of filler materials are particles of alumina, silica, hollow and solid particles of glass, wood chips, fly ash and carbon black. Selection of one of

these materials is mainly based on the desired properties of the composite. The shape of the filler particles plays important role in determining the properties of the composite. Spherical particulate fillers are more popular compared to the other types. The principal advantages of spherical fillers are (Ferrigno 1978):

- Low surface area to volume ratio
- Regularity of shape
- Control of surface properties
- High crush strength
- Closely controlled particle size
- Better rheology

One of the materials available in abundance in particulate form as far as fillers are concerned is 'Fly ash'. It has attracted interest lately because of the abundance in terms of material volume generated and the environmental linked problems in the subsequent disposal (Ferrigno 1978). Fly ash is a predominantly inorganic residue obtained from the flue gases of furnaces at pulverized coal power plants. When coal is burnt in pulverized coal boilers, the minerals entrained in the coal are thermally transformed into chemical species that are reactive or could be chemically activated, for example by the addition of calcium hydroxide (Chawla 2001). The finely divided glass phase, the predominant phase in fly ash, reacts as a pozzolan, defined by Manz (1999) as "...a siliceous and aluminous material that in itself possesses little or no cementitious value but will, in finely divided form and in the presence of moisture, chemically react with calcium hydroxide at ordinary temperatures to form compounds possessing cementitious properties".

Fly ash can be classified as either cementitious or pozzolanic. The cementitious fly ash is labeled as Class C making up at least 50 mass percent. In pozzolanic fly ash, Class F makes up more than 70 mass percent of the total fly ash composition (Kruger 1997, Scheetz and Earle 1998). There are two primary sources of fly ash: fly ash from a pulverised coal power plant and fly ash from a municipal waste incineration plant. The fly

ash produced from the burning of pulverized coal in a coal fired boiler is a fine-grained, powdery particulate material that is carried off in the flue gas and usually collected from it by means of electrostatic precipitators, bag houses or mechanical collection devices such as cyclones. It is the finely divided mineral residue resulting from the combustion of ground or powdered coal in electric generating plant (ASTM C 618). Since the particles solidify while suspended in the exhaust gases, fly ash particles are generally spherical in shape (Kruger 1997) and are usually silt size (0.074 - 0.005 mm). As these have aspect ratios closer to unity, near isotropic characteristics are displayed by them. These are inexpensive and possess good mechanical properties.

Fly ash mainly consists of alumina and silica which are expected to improve the composite properties. It also consists to some extent, hollow spherical particles termed as cenospheres (Pedlow 1978, Mohapatra and Rao 2001) which aid lowering the composite density. A schematic with SEM image showing the structure of the fly ash particles is presented in Figure 1.3.

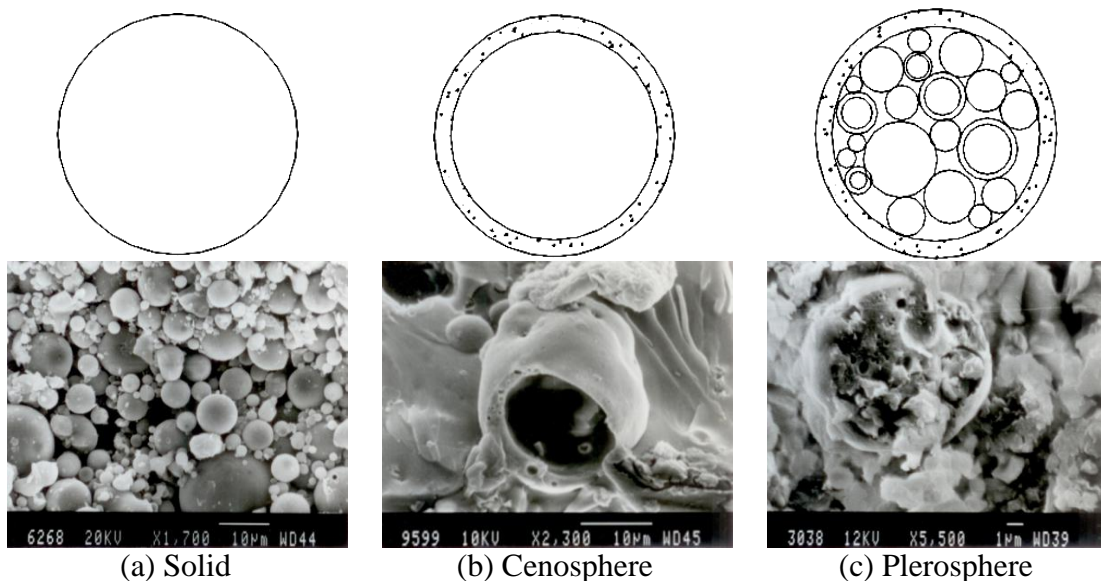


Figure 1.3 Structure of fly ash particles.

Hollow fly ash particles are generally termed as Cenospheres. Composite particles, which consist of smaller solid and hollow spherical particles, are referred as Plerospheres and the SEM picture above displays one such Plerosphere. Cenospheres are unique free flowing powders composed of hard shelled, hollow, minute spheres. A small proportion of the pulverized fuel ash produced from the combustion of coal in power stations is formed as Cenospheres. Cenospheres are made up of silica, iron and alumina. They are also referred to as microspheres, hollow spheres, hollow ceramic microspheres or microballoons. These spheres have been used to improve the properties of a variety of finished consumer products. Thermosetting synthetic foams made with cenospheres have demonstrated superior mechanical properties when compared to those manufactured with fabricated microspheres (Gupta, N. et al. 2013).

When used with well established matrix materials, these help in reducing the cost and either retain or improve desirable and specific mechanical properties (Scheetz and Earle 1998). The feature of inbuilt porosity in cenospheres is of considerable significance in weight specific applications. As the fillers are of near spherical shape, the resin spread is also better. Developing newer and utilitarian thermoplastic systems using fly ash displaying near isotropic properties should be an interesting and challenging task.

1.2.2 Matrix

Polymers are long chain organic molecules or macromolecules with many desirable properties such as high ductility, ease of forming and non-corrosiveness (Srinivasan and Ramakrishnan 1983). A wide variety of such materials are available to a designer. Two such classes are thermosetting and thermoplastic polymers. Their initial target applications were in aerospace and later became viable alternative material in the sporting, automotive and in construction industries. In thermosetting polymers, there are covalent cross bonds (cross link) between molecules, in addition to Van der Waals forces. Owing to these cross bonds, a thermosetting polymer remains rigid on heating (Arzamasov 1989). Thermoplastic polymers can be re-shaped by repeated heating and

cooling without losing their properties (Arzamasov 1989). They soften on heating and become rigid on cooling. On the other hand, thermosets remain rigid during reheating till they are converted into char. This difference in behavior on heating is due to the relatively weak Van der Waals forces acting between the molecules of thermoplastic polymers. On heating, the bonds between the molecules weaken substantially and the material becomes soft and yieldable.

Many thermoplastics are now accepted as engineering plastics. The term engineering plastics probably originated as a classification distinguishing those plastics that can satisfactorily substitute the metals such as Aluminum in small devices and structures requiring lower mechanical properties. Engineering plastics are the main source for developing high performance composites which possess advantages like high stiffness, high strength to weight ratio and increased chemical and atmospheric inertness compared to conventional materials.

Though PMCs have higher initial material costs, low cost ones could be developed from reinforcing plastics with low cost environmental pollutants like cenospheres. In the year 1997, the estimated per capita demand of plastics in India was 0.800 Kgs. which was one of the lowest in Asia (Esha Shah and Rajaram 1997, Rigoberto et al. 2004, Burgiel et al 1994, Scott 2000). The projected demand in 2000 A. D. was 2.16 kg/capita (KSSPMA 1992). A boom in the consumption of plastic in India is experienced with the economic liberalization since 1991. Plastic consumption in India has more than doubled from 0.85 million tons during 1990-91 to 1.79 million tons during 1995-96. Demand for commodity plastics is growing at the rate of 15% per year.

As per a survey conducted by the All India Plastic Manufacturers Association, the total capacity to produce PE, PVC, PP and PS was 1.39 million mega tonne (MMT) against the demand of 1.55 million MT in 1995 which has increased to 1.8-1.9 million MT for 1996-97. This is concentrated in three major sectors according to the Plast India figures:

infrastructure (power, roads, bridges, telecommunications and construction) which is 30% of the total, packaging is 25% of the total and 24% for agriculture and water (Nanavaty 1997). The consumption of polymers in the year 2012 in India is 9 MMT which is 10 times higher than that seen in 1990 and is estimated to grow upto 13 MMT by 2015 (Figure 1.4) (Shekhar 2012). Polymers used in packages have about 50% of share in this consumption.

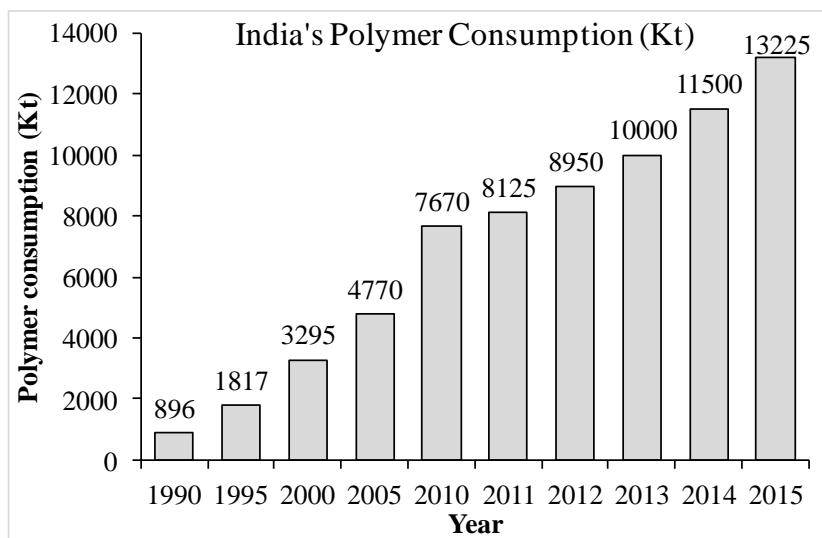


Figure 1.4 Polymer consumption in India.

With such a drastic growth prevailing in the consumption of plastic, thermoplastic syntactic foam composites with filler such as fly ash cenospheres may be an essential requirement to avoid issues regarding plastic management and environmental linked problems. Further, when matrix is reinforced with fillers, role of interface between them and related compatibility issues needs attention.

1.2.3 Role of interface and its modification

For stresses to efficiently get transferred from thermoplastic matrix to cenospheres, interfacial bonding between them plays a very vital role. Surface modification of the constituents might improve the performance of these SF's owing to better compatibility. Compatibilizers are often used as additives to improve the morphology and resulting

properties of the composite blend. Compatibilization reduces interfacial energy between the constituents in order to increase adhesion. Similarly, it is often challenging to disperse hollow fillers effectively in the matrix polymer. Generally, adding compatibilizer also results in finer dispersion, alongside more regular and stable morphologies. If a polymer (or blend) contains reinforcing fillers (such as inorganic fibers), an additive that can compatibilize the polymers in a blend may also act as a “coupling agent”, helping the fillers to disperse and bond to polymers increasing the stiffness, strength and impact toughness of the composite.

A key region that influences mechanical properties of the composite is the matrix/reinforcement interface. A series of phenomena takes place at such interfaces. The structure of interface and the stresses generated during different stages of processing and services have a bearing on the fracture and failure of the composite (Ranney et al. 1974). Hence it is essential to consider the interfaces in detail and examine their influence on the mechanical properties of the composite, so as to alter the properties to suit one’s need in the end product. A good bonding at the interface is essential to have efficient load transfer from the matrix to the reinforcement. The interfacial characteristics can be modified in a number of ways, an effective one being the chemical treatment. Reinforcing materials such as fly ash cenospheres contain oxides like Al_2O_3 , SiO_2 and Fe_2O_3 which form links to hydroxyl groups during their contact with moisture and convert into water molecule. The presence of water, additionally, reduces the wettability of the reinforcement as it lowers the surface energy. Coatings that function as coupling agents hence are expected to raise the effective surface energy of the reinforcement. The coupling agents primarily provide a chemical link between the oxide groups on the filler surface and the polymer molecule of the thermoplastic.

The silane coupling agents have a general formula R-Si-X_3 , wherein this multifunctional molecule reacts at one end with the surface of the filler and at the other with the polymer phase. The ‘X’ group in these is a hydrolysable one and hence the silane is hydrolyzed to

corresponding silanol (R-OH) in the presence of aqueous solution. These silanol molecules compete with water molecules to form hydrogen bonds with the hydroxyl groups bound to the reinforcement surface (Hull and Clyne 1996). When the reinforcement is dried, the free water is driven off and the condensation reaction occurs, both at silanol/surface junction and between neighboring silanol molecules. The result is a polysiloxane (X-R-Si (OH)₃) layer bonded to the filler/reinforcing surface presenting an array of 'R' functional groups to the environment. These open functional groups involve in curing reaction with the matrix polymer and establish a bond (Hull and Clyne 1996). Besides improving the bonding and the mechanical properties, the coupling enhances the electrical, thermal and magnetic properties due to increased effective contact at the interface. Another important feature is the increased resistance to environmental effects. The bonding also serves to reduce the effect of hostile environments at the reinforcement causing degradation and thus retains useful mechanical properties of the composite in spite of its exposure to such environments.

Silane treatments help in better wetting while those wherein dirt or greasy/oily layers envelope the fillers, the effectiveness of the medium to wet reinforcements/fillers reduces (Farinha et al 2000). Their presence also affects the properties including the mechanical behavior. The mechanical property of polymer-cenosphere composite is inferior owing to poor interfacial interactions between the hydrophilic cenospheres surface and hydrophobic polymer (Guhanathan et al. 2001).

However, surface treated cenosphere is found to improve the interfacial interactions (Thongsang and Sombatsompap 2006). A mechanism of interaction between Silane-69 (Bis (3-triethoxy silyl) propyl tetrasulfide) coupling agent and fly ash, as explained by Nabil et al. (2004), is shown in Figure 1.5.

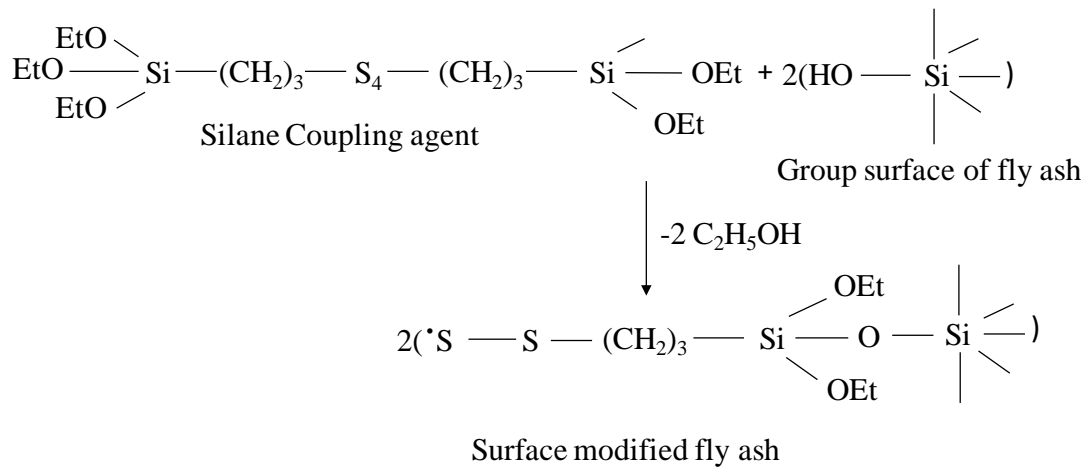


Figure 1.5 Reaction between Silane-69 coupling agent and fly ash.

Mechanical and morphological properties of recycled HDPE filled with Calcium Carbonate and fly ash are investigated by Atikler et al. (2006). Authors investigated the effect of surface treated fly ash on the mechanical properties of HDPE as compared to conventional calcium carbonate filler. Tensile strength slightly increased on addition of fly ash when compared to conventional calcium carbonate. However, higher increase is noticed when modified fly ash is used with 30% filler content. The decrease in elongation at break is higher for ash filled composites when compared to calcium carbonate ones. This decrease in property is higher in case of treated fly ash. Authors concluded that ash is a good replacement for calcium carbonate. Further, no compatibilizers are used and also thermal characterization of the composites is not reported in their study.

Effect of surface coverage of silane treated CaCO_3 on the tensile properties of polypropylene composites are analyzed by Demjen and Pukanszky (2004). Amino functional silanes showed a strong reactive coupling effect leading to a maximum tensile strength (Phueakbuakao et al. 2008). Effect of silane and zirconate coupling agents on mechanical properties of mica/epoxy composites is investigated by Bajaj et al. (1992). Tensile modulus and flexural strength are improved by the surface treatment. Mathew et al. (2004) reported that the properties of silica filled styrene-butadiene rubber composites are improved through plasma surface modification of silica. The filler dispersion as

revealed by scanning electron microscopy was found to be greatly improved by the plasma as well as silane treatment. Kulkarni and Kishore (2002) reported that the fly ash filled epoxy composite showed improved compression strength after exposure to aqueous media but the surface treated fly ash particles in epoxy showed reduction in compression strength. Ramakrishna et al. (2006) concluded that the toughened epoxy/fly ash composites showed improved compressive and impact strength. However, the tensile strength decreases and modulus increases with increase in fly ash content (Srivastva and Shembekar 1990, Seena et al. 2010, Ferreira et al. 2010). Development of suitable process and its optimization influences mechanical behavior alongside aids in lowering the component cost. Processing of syntactic foam composites is described in the section to follow.

1.3 Processing of Syntactic foams

Every material possesses unique physical, mechanical and processing characteristics and hence a suitable manufacturing route must be selected to transform the material to its final shape. In the last half of the twentieth century, the processes used for fabrication of parts made from composite materials evolved from operations relying on manual labour, to manufacture by automated equipment controlled from sophisticated microprocessor systems. Early pioneers combined raw materials and formed the final structure by hand lay-up or spray-up in open molds. The parts are cured at ambient temperature. As the advantages of PMC's are felt, these synthetic materials began to penetrate virtually every other market worldwide, from consumer products, automotive and marine to primary structural elements of aircraft and bridges. Such widespread growth in product applications mandated corresponding growth in materials technology, design approaches, and fabrication processes (Arza Seidel 2012).

In case of syntactic foam composites, if the processing route is not carefully designed, hollow particles reinforcement may provide unintentional effect of increased matrix porosity by stabilizing gas bubbles in polymer matrix. The processing methods are also

required to be efficient in promoting wetting of reinforcement by the matrix resin, breaking clusters without fracturing the reinforcement material and obtaining uniform distribution of reinforcement in the matrix resin. In addition, the hollow particles should not be excessively fractured during the manufacturing process. A commonly used fabrication method for reinforced syntactic foams is illustrated in Figure 1.6. In this method, a three-step mixing process is used. In the first step, the reinforcement is added to the neat resin and mixed. After thorough mixing of reinforcement, hollow particles are added and stirred until slurry of consistent viscosity is obtained. In the final step, the hardener or catalyst is added to the resin and stirred slowly. The mixture is cast in molds and cured as per the requirements of the resin. Additional rigorous mixing of reinforcement before hollow particles helps in reducing the possibility of hollow particle breakage during processing.

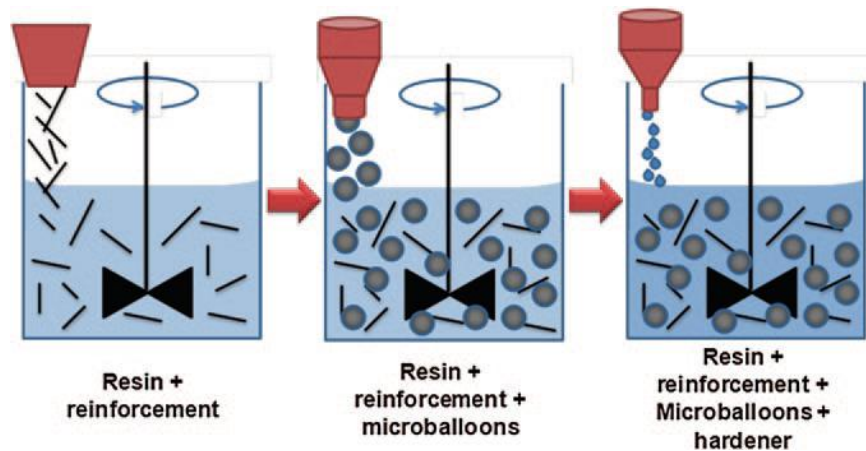


Figure 1.6 Illustration of reinforced syntactic foam fabrication method (Gupta, N. et al. 2013).

Some of the fabrication processes widely practiced on the shop floor include open mold processes like hand layup, autoclave, press cure oven cure process. Closed mold processes include compression molding, injection molding, transfer molding and thermostamping. Some of the processing options for thermoset and thermoplastic materials with variety of reinforcement are presented in Figure 1.7 (Reinhart 1998).

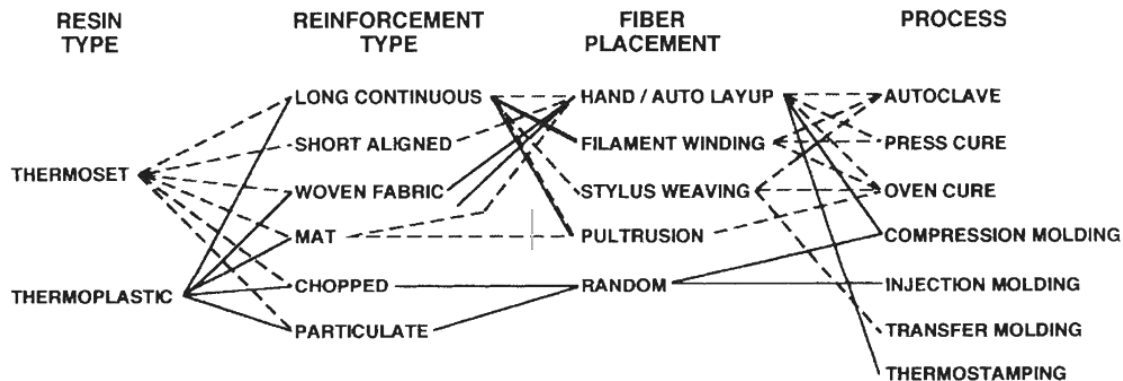


Figure 1.7 Constituents of PMCs and manufacturing options.

Particulate reinforced thermoplastics are processed using Compression and Injection molding routes as seen from Figure 1.7.

1.3.1 Compression molding

Compression molding machine is a kind of press which is oriented vertically with two molding halves (top and bottom). It is high-pressure method suitable for molding complex, high strength fiber glass reinforcements. Compression mold consists of two components namely male and female plate. Male plate is fixed and the female plate is movable. Thermoplastics blended with filler are placed inside the mold which is been preheated to a set temperature depending on the materials requirement. Pressure is applied through hydraulic means to the preheated mold to form the required shape. Advanced composite thermoplastics can also be compression molded with unidirectional tapes, woven fabrics, randomly oriented fiber mat or chopped strand. Materials such as polystyrene, polypropylene and polythene are used with this method. Compression molding is a cost effective process when compared to the injection molding and stamping. It is the oldest and unique process for molding of plastic components that produce parts of near net shape (Manas and Salil 2006). In compression molding of thermosets, the mold remains hot throughout the cycle. As soon as a molded part is ejected, a new charge of molding powder can be introduced. On the other hand, unlike thermosets, thermoplastics must be cooled to harden. Compression molding of HDPE composites was prepared and characterized for impact and wear performance by Navin Chanda et al. (2010). They observed considerable improvement in both the properties.

Divya et al. (2015) developed multi walled carbon nanotubes reinforced cenosphere/HDPE syntactic foam sheets at 15 MPa pressure and 160°C temperature using compression molding and investigated for mechanical properties. Further, Deepthi et al. (2014) developed HDPE reinforced with silicon nitride and nanoclay using compression molding at 15 MPa pressure and 130°C temperature and dealt with mechanical characterization. Compression molding is not as efficient as PIM with regard to cycle time, complexity of components and volume of production.

1.3.2 Polymer injection molding

Polymer injection molding (PIM) is one of the most widely processes to manufacture thermoplastic products. It is considered as the promising alternative technique for mass-fabrication of the polymer micro/nano engineered surfaces due to rapid cycle time, low material cost and variety of material options. It offers a number of advantages such as low material consumption, improved dimensional stability, shorter cycle time, lower injection pressures and clamp forces. Furthermore, injection molded products show better thermal, acoustic insulation and improved mechanical properties compared to compression molded counterparts. PIM is a widely used manufacturing method for low and high density polyethylene (LDPE and HDPE), polymethyl methacrylate and polylactic acid (Bachmatiuk A et al. 2010, Alkan C et al. 1995). Injection molding is capable of economically producing precision plastic parts with various shapes and complex geometries at low cost. Use of these resins in fabricating syntactic foams (Bunn, P and Mottram, J. T. 1993, Gupta N et al. 2004) can provide opportunities of saving weight in existing applications and also in developing new material systems. One of the advantages of using thermoplastic resins is the possibility of using rapid manufacturing industrial techniques for making syntactic foam parts. However, the existing studies have not utilized such mainstream industrial production methods for producing syntactic foams. If such rapid manufacturing technique can be developed for syntactic foam parts, the cost of such lightweight eco-friendly components can be lowered (Gupta N et al. 2013). The available studies on thermoplastic syntactic foams process materials under controlled conditions at laboratory scale, which usually provides syntactic foams with

high quality. However, processing of materials with industrial scale manufacturing equipment may not yield similar quality thereby the effect of such manufacturing environment needs to be studied.

Rapid manufacturing is a key to satisfying the ever growing demands of useful and durable products. The present work deals with utilization of one such technique, injection molding, with optimized temperature and pressure to synthesize cenosphere/HDPE syntactic foam composites.

1.4 Literature survey

Syntactic foams are lightweight composites used prominently in weight saving applications. However, the extent to which these can be tailored to produce a target mechanical performance - i.e., the design of SF, strongly depends on the resultant effective properties and more importantly, on how these properties relate to its microstructure. Therefore investigating mechanical, thermal and or other relevant properties for a given microstructure and its spatial distribution plays a significant role in the design and development of SF. A number of reviews dealing with various aspects of syntactic foams under different loading conditions have been published in recent years and are presented in tabular form herewith.

Notations used while presenting the summary of literature is as below:

ρ	Density	g/cm^3
$d_{\mu\text{m}}$	Particle diameter	μm
d_{nm}	Particle diameter	nm
Φ_w	Filler content	wt. %
Φ_v	Filler content	vol. %
η	Radius ratio	---

Table 1.1 Literature review on Tensile behavior.

Author	Reinforcement	Matrix	Remarks
Jena, H., Pandit, M. K. and Pradhan, A. K. (2013)	<i>Cenosphere</i> (CS300) $\rho : 0.45-0.80$ $d_{\mu m} : 60-94$ $\Phi_w : 0, 1.5, 3, 4.5, 6$ <i>Bamboo fiber</i> $\rho : 0.95$	Epoxy L12 with K6 Hardener	<ul style="list-style-type: none"> • Increase in strength by 20 and 9% for 1.5 and 3 cenosphere wt.% and decreases in strength by 17.5 and 42.8% for 4.5 and 6 cenosphere wt.% respectively for 3, 5, 7 and 9-layered bamboo–epoxy composites compared to neat samples. • Increase in strength by 25.4, 6.5 and 4.1% for 3, 5, and 7-layered bamboo-epoxy composite while 23.5% decrease in strength is observed for 6 wt. % cenosphere when number of layers is increased more than seven.
Kulkarni, M. B., Mahanwar, P. A. (2014)	<i>Fly ash</i> $\rho : 0.65$ $d_{\mu m} : 100$ $\Phi_w : 0, 10, 20, 30, 40$	PP with 3% PP- g-MAH compatibilizer	<ul style="list-style-type: none"> • Strength decreases by 35% and modulus increases to 33.48% with increasing filler content. • The values of yield stress (52.7%) and breaking strength (25.4%) of compatibilized PP-g-MAH/FA-based PP composites showed higher values compared to that of untreated FA-filled PP composites at corresponding filler content.
Singh, A. K., Siddhartha. (2014)	<i>Cenospheres</i> $\rho : 0.67, 0.65, 0.64$ $d_{nm} : 900, 600, 300$ $\Phi_w : 10$	Polyester resin with Methyl ethyl ketone peroxide catalyst	<ul style="list-style-type: none"> • Strength increases to the tune of 11% with decreasing particle size. • Strength for 300 nm particle reinforced composite is observed to be 16% higher compared to neat polyester.

Thakur, S., Chauhan, S. (2014)	<i>Cenosphere</i> ρ : 0.97, 0.67, 0.66 $d_{\mu m}$: 2 d_{nm} : 900, 400 Φ_w : 10	Vinylester with HY951 Hardener	<ul style="list-style-type: none"> • Marginal improvement in strength (2.56%) is observed for 400 nm cenosphere reinforced composites. • It is observed that the volume fraction of void for 2μm, 900 nm and 400 nm is 9.4529, 8.0904 and 10.434 respectively.
Hu, G., Yu, D. (2011)	P(DVB-GMA) ρ : 0.97, 0.67, 0.66 $d_{\mu m}$: 2.2, 1.1 d_{nm} : 900, 400 Φ_v : 5, 10, 15, 20, 25	Epoxy E44	<ul style="list-style-type: none"> • Decrease in tensile strength upto 30-50% and modulus upto 40% with increasing volume fraction from 0-25%. • Density of the composites decreases by 14.85% with increase in the volume fraction from 0-25%.
Yu, M., Zhu, P. Ma, Y. (2012)	<i>Ceramic microsphere</i> ρ : 0.6-0.8 $d_{\mu m}$: 130 Φ_v : 0, 10, 20, 30, 40, 50	Epoxy E51 with PA651 Hardener	<ul style="list-style-type: none"> • With the increase of filler content strength and failure strain decrease to 61.65 and 58% respectively, compared to neat resin.
Gupta, N., Nagorny, R. (2006)	<i>Glass microballoon</i> ρ : 0.22, 0.32, 0.38, 0.46 Φ_w : 30, 40, 50, 60 η : 0.9702, 0.9565, 0.9474, 0.9356	Epoxy DER332 with DEH24 Hardener	<ul style="list-style-type: none"> • All types of syntactic foams showed 60-80% decrease in the tensile strength compared to neat resin. • The modulus is found to increase in the range 30-90% with the increasing microballoon density. Lower radius ratio microballoons performed better in both strength and modulus.

Wouterson, E. M., Boey, F., Xiao Hu. Wong (2005)	<i>Glass microballoon (K15, K46)</i> $\rho : 0.25, 0.15, 0.46$ $\Phi_v: 0, 10, 20, 30, 40, 50$	Epoxy epicote 1006	<ul style="list-style-type: none"> Strength gradually decreases as the filler content increases from 10-50% for all particle densities. The modulus is found to decrease upto 55% with the filler addition (10-50%) for all particle densities.
Dimchev, M., Ryan Caeti, Nikhil Gupta (2010)	<i>Glass microballoon</i> $\rho : 0.254, 0.328, 0.377, 0.465$; $\Phi_v: 30, 40, 50$ <i>Carbon nano fibers</i> $\rho : 1.950$	Epoxy DER332 with DEH24 Hardener	<ul style="list-style-type: none"> Strength and modulus of syntactic foams, shows 20-50% and 10-20% rise respectively owing to the presence of nanofibers. The trends in tensile properties with respect to the hollow particle wall thickness and volume fraction are similar with and without nanofiber addition.
Gupta, N., Ye, R. and Porfiri, M. (2010)	<i>Glass microballoon</i> $\rho : 0.22, 0.32, 0.37, 0.46$ $\Phi_v : 30, 40, 50, 60$ $\eta : 0.970, 0.956, 0.947, 0.936$	Vinylester with Methyl ethyl ketone peroxide catalyst	<ul style="list-style-type: none"> Tensile modulus found 50-75% higher than the neat vinyl ester resin for 40 vol. %. A comparison shows that the compressive modulus values are 15-30% lower than the tensile modulus values for the same type of syntactic foam. Relation between the relative Young's modulus and the wall thickness of microballoons is non-linear.
Rizzi, E., Papa, E. and Corigliano, A. (2000)	<i>Glass microballoon (K1)</i> $\rho : 0.125$ $\omega : 0.58$	Amperg Epoxy ultra slow Hardener	<ul style="list-style-type: none"> The average tensile strength for syntactic foams is found to be about 55% lower as compared to the compression strength. Tensile modulus is observed to be 35% higher than that of compressive modulus.

Table 1.2 Review of Flexural studies.

Author	Reinforcement	Matrix	Remarks
Jena, H., Pandit, M. K. and Pradhan, A. K. (2013)	<i>Cenosphere (CS300)</i> $\rho : 0.45-0.80$ $d_{\mu m} : 60-94$ $\Phi_w : 0, 1.5, 3, 4.5, 6$ <i>Bamboo fiber</i> $\rho : 0.95$	Epoxy L12 with K6 Hardener	<ul style="list-style-type: none"> Strength increases by 32, 9 and 11.2% in 3, 5, 7-layered bamboo-epoxy composite. Strength decreases by 8.97% as cenosphere content increases to 3 wt. % in 9-layered bamboo-epoxy composite. Strength increases by 30.6, 9.09 and 14.75% for 1.5, 3 and 4.5 cenosphere wt.% while decreases to 24.4% for 6 wt.% in 3, 5, 7 and 9-layered bamboo-epoxy composites respectively.
Kulkarni, M. B., Mahanwar, P. A. (2014)	<i>Fly ash</i> $\rho : 0.65$ $d_{\mu m} : 100$ $\Phi_w : 0, 10, 20, 30, 40$	PP with 3% PP-g- MAH compatibilizer	<ul style="list-style-type: none"> The flexural strength values of the compatibilized PP/PP-g-MAH/FA composites showed comparable performance with that of PP up to 40% and followed by gradual reduction to 16.8% at higher filler contents.
Labella, M., Zeltmann, S. E., Shunmugasamy, V. C., Gupta, N. & Rohatgi, P. K. (2014)	<i>Fly ash (fillite 300)</i> $\rho : 0.7$ $\Phi_v : 30, 40, 50, 60$	Vinylester resin with methyl ethyl ketone peroxide Hardener	<ul style="list-style-type: none"> The flexural strength and modulus showed a maximum decrease and increase of 73 and 47% in comparison to the matrix for 60 vol.% syntactic foams. It is observed that the increase in specific flexural modulus of 111% can be achieved for 60 vol.% cenospheres syntactic foam in comparison to neat matrix.

Wouterson, E. M., Boey, F. Y.C., Xiao Hu. and Wong, S. C. (2005)	<i>Glass microballoon</i> (K15, K46, BJO) ρ : 0.25, 0.15, 0.46 Φ_v : 0, 10, 20, 30, 40, 50	Epoxy Epicote 1006	<ul style="list-style-type: none"> Flexural strength of syntactic foams at 50% volume fraction decreases by 64.8, 60.08 and 50.5% for K15, K46 and BJO with respect to neat resin. Strength gradually decreases as the filler content increases from 0-50%.
Kishore, Shankar, R. & Sankaran, S. (2005)	<i>Glass microballoon</i> ρ : 0.25 Φ_v : 38.5, 50.2, 54.5, 57.7	Epoxy Araldite LY556 with HT972 Hardener	<ul style="list-style-type: none"> Strength increases (3.87 to 5.79 MPa) as glass microballoons content decreases (57.7 to 38.5 vol. %).
Maharsia, R., Gupta, N. and Jerro, H. D. (2006)	<i>Glass microballoon</i> (S22, S32, K38, K46) ρ : 0.22, 0.32, 0.38, 0.46 η : 0.9703, 0.9561, 0.9474, 0.9356; Φ_v : 65 <i>Rubber particle</i> $d_{\mu m}$: 40, 75; Φ_v : 2 <i>Nanoclay</i> Φ_v : 2, 5	Epoxy DER332 with DEH24 Hardener	<ul style="list-style-type: none"> Addition of 2% nanoclay particles resulted overall reduction in flexural strength of the syntactic foams to the tune of 11%. Addition of 5% nanoclay particles has resulted in an increase in strength of low density syntactic foams by around 22%. However a reduction in strength is observed in syntactic foams. Flexural stiffness and modulus of foams are observed to increase by 7% with decrease in η. With decrease in rubber particle diameter, strength increases by 16%.

<p>Gupta, N., Gupta, S. K., and Benjamin, J. M. (2008)</p>	<p><i>Glass microballoon</i> (S22, S32, K37, K46) ρ : 0.22, 0.32, 0.37, 0.46 Φ_v : 30, 40, 50, 60 η : 0.9703, 0.9561, 0.9457, 0.9356</p>	<p>Epoxy DER332 with DEH24 Hardener</p>	<ul style="list-style-type: none"> • In volume fraction based functionally graded syntactic foams (FGSFs), flexural modulus and strength decreases by 39.5 and 34.18% as η and filler content (30-60%) increase. • Flexural modulus and strength of radius ratio type FGSFs shows that with increase in microballoon volume fraction, the strength and modulus decreases by 52 and 13% respectively.
<p>Singh, A. K., Siddhartha. (2014)</p>	<p><i>Cenospheres</i> ρ : 0.67, 0.65, 0.64 d_{nm}: 300, 600, 900 Φ_w : 10</p>	<p>Unsaturated polyester resin with methylethyl- ketone peroxide hardener and cobalt naphthalene accelerator</p>	<ul style="list-style-type: none"> • Flexural strength of polyester composites gradually increases (10-25%) with decrease in the practical size. • Composite with particle size of 300 nm shows the highest flexural strength (25%) among all the studied samples.
<p>Thakur, S., Chauhan, S. (2014)</p>	<p><i>Cenosphere</i> ρ : 0.97, 0.67, 0.66 $d_{\mu m}$: 2 d_{nm}: 900, 400 Φ_w : 10</p>	<p>Vinylester with HY951 Hardener</p>	<ul style="list-style-type: none"> • Gradual improvement in strength with reduction in particle size. • Strength of 400 nm cenosphere filled vinylester composite is higher (27.11%) as compared with 900 nm (15.25%) and 2 μm (10.16%) cenosphere filled vinylester composite.

Table 1.3 Review on compression and high strain rate response.

Author	Reinforcement	Matrix	Remarks
Thakur, S., Chauhan, S. (2014)	<i>Cenosphere</i> $\rho : 0.97, 0.67, 0.66$ $d_{\mu m}: 2; d_{nm}: 900, 400$ $\Phi_w : 10$	Vinylester with HY951 Hardener	<ul style="list-style-type: none"> The compressive strength of the vinylester composites reinforced with 2 μm, 900 nm and 400 nm is higher by 225, 275 and 300% respectively, compared to unfilled vinylester composites.
Gupta, N., Woldesenbet, E., Mensah, P. (2004)	<i>Cenospheres</i> $\rho : 0.205, 0.32, 0.37,$ $0.38, 0.46; \Phi_w : 65$ $\eta : 0.922, 0.907, 0.891,$ $0.888, 0.863$	Epoxy DER332 with DEH24 Hardener	<ul style="list-style-type: none"> Increase in compressive modulus from 1550 to 2640 MPa is observed with decrease in radius ratio. Peak compressive strength shows increasing trend with decrease in radius ratio and changes from 30 to 72 MPa within the chosen range of η.
Gupta, N. (2007)	<i>Cenospheres (S22, S32,</i> <i>S37, K38, K46)</i> $\rho : 0.22, 0.32, 0.38, 0.46$ $\Phi_w : 50, 60, 65$ $\eta : 0.9703, 0.9561,$ $0.9474, 0.9356$	Epoxy DER332 with DEH24 Hardener	<ul style="list-style-type: none"> The compressive strength and modulus of FGSF's are found to be dependent on the weakest layer. FGSF is found to be capable of withstanding 60-75% compression. Modulus values are 1134, 1344 and 1440 MPa and compressive yield strength values are 23.7, 32.7 and 41 Mpa for FGSFs having volume fraction of 65, 60 and 50% respectively. The area under the stress-strain curves is found to be 300-500% higher compared to plain syntactic foams, indicating significantly higher energy absorption in FGSFs.

Gupta, N., Karthikeyan C. S., Sankaran, S. and Kishore (1999)	<i>Glass microballoon</i> $\rho : 0.25, \Phi_w : 35$ $d_{\mu m} : 10-100$ <i>Epoxy compatible</i> <i>E-glass fibers</i> : 6 mm length, $\Phi_w : 9.7$	Epoxy Araldite LY5052 with HY5052 Hardener	<ul style="list-style-type: none"> Compressive strength for unreinforced (fiber free) system exceeds that of reinforced (with fiber) system by 27.79 MPa. The void content in reinforced foam is 11.1% as compared to unreinforced foam (8.4%).
Gupta, N., Ye, R. and Porfiri, M. (2010)	<i>Glass microballoon</i> $\rho : 0.22, 0.32, 0.37, 0.46$ $\Phi_v : 30, 40, 50, 60$ $\eta : 0.970, 0.956, 0.947,$ 0.936	Vinylester with methyl ethyl ketone peroxide Hardener	<ul style="list-style-type: none"> Compressive modulus of syntactic foams increases with decreasing η. The specific moduli for composites are found 10-47% higher than the neat resin tested for 30, 40, 50 and 60 vol. %. The compressive strength increases by 7-11% with increase in filler content as compared to neat resin.
Gupta, N., Maharsia, R. and Jerro, H. D. (2005)	<i>Glass microballoon</i> (S22, S32, S38, K46) $\rho : 0.22, 0.32, 0.38,$ 0.46; $\Phi_v : 63$ $\eta : 0.922, 0.907, 0.888,$ 0.863 <i>Rubber particles</i> $\rho : 1.12-1.15; \Phi_v : 2$	Epoxy DER332 with DEH24 Hardener	<ul style="list-style-type: none"> Compressive modulus is found to decrease by approximately 50%, whereas a reduction of approximately 10% is observed in the compressive strength due to the incorporation of rubber particles by 0.02 vol. %. Compressive toughness and damage tolerance of these high-strength foams is increased by 11%. The effect of microballoon η is found to be similar in hybrid foams and syntactic foams. Decrease in η, corresponds to increase in strength.

Wouterson, E. M., Boey, F. Y.C., Xiao Hu. and Wong, S. C. (2005)	<i>Glass microballoon (K15, K46)</i> $\rho : 0.25, 0.15, 0.46$ $\Phi_v : 0, 10, 20, 30, 40, 50$	Epoxy Epicote 1006	<ul style="list-style-type: none"> • The compression tests revealed the excellent compressive properties of syntactic foam and in particular the superior performance of K46 microspheres (10, 20 and 30%) giving rise to higher compressive yield strengths (84.61, 80.64 and 76.63 MPa), and moduli (0.95, 1.14 and 1.14 GPa) compared to K15 and phenolic microspheres. • Strength and modulus decreases by 10-70% and 8-50% with increasing filler content (0-50 vol.%).
Singh, A. K., Siddhartha. (2014)	<i>Cenospheres</i> $\rho : 0.67, 0.65, 0.64$ $\Phi_w : 10$ $d_{nm} : 900, 600, 300$	Polyester resin with methylethylketone peroxide Hardener	<ul style="list-style-type: none"> • The value of compressive strength increases from the unfilled polyester composite to the smallest cenosphere particle size reinforced composite. • Composite B300 shows the highest flexural strength (244%) compared to B900 (133%) and B600 (177%) composites.
Shunmugasamy, V. C., Gupta, N., Nguyen, N. Q., Coelho, P. G. (2010)	<i>Glass microballoon (S22, K46)</i> $\rho : 0.22, 0.46$ $\Phi_v : 30, 60$	Vinylester with methyl ethyl ketone peroxide	<ul style="list-style-type: none"> • Strength is found to be 200-300% higher than the quasi-static compressive strength of same types of syntactic foams. • The quasi-static modulus (20.73%) and strength (66.6%) of SF220-60 are lower than those of SF220-30. • The modulus of VE460-60 is higher (16.5%) than VE460-30. Strength of VE460-60 composites is significantly lower (53.79%) relative to VE460-30 at quasi-static compression strain rates.

<p>Labella, M., Zeltmann, Shunmugasamy, V. C., Gupta, N. and Rohatgi (2014)</p>	<p><i>Fly ash (fillite 300)</i> $\rho : 0.7$ $\Phi_v: 30, 40, 50, 60$</p>	<p>Vinylester resin with methyl ethyl ketone peroxide Hardener</p>	<ul style="list-style-type: none"> • 40 vol. % composites showed a maximum of 42% increase in the compressive modulus compared to neat resin. • The densities of 30, 40, 50 and 60 vol. % composites are 11.5, 14.4, 17.8 and 26.4% respectively lower than neat resin. • The specific strength of the neat resin is 12-19% higher while the specific modulus is 50–70% lower than the syntactic foams.
<p>Poveda, R., Dorogokupets, G., Gupta, N. (2013)</p>	<p><i>Glass Microballoons</i> $\rho : 0.22, 0.46$ $\Phi_v: 30, 50$ <i>Carbon Nanofiber</i> $\Phi_w: 1$</p>	<p>Epoxy DER332 with DEH24 Hardener</p>	<ul style="list-style-type: none"> • High strain rate strength is found to be 1.3 to 2.2 times higher for both wet and dry syntactic foams depending on thin and thick walled glass microballoons and volume fraction (30-50%). • Compressive strength of wet CNF/epoxy composites is 28% lower than that of dry specimens. The strength of all syntactic foams is decreased by 25-35% due to the moisture exposure in CNF/epoxy composites.

Table 1.4 Review on dynamic mechanical analysis.

Author	Reinforcement	Matrix	Remarks
Hu, G., Yu, D. (2011)	<i>P(DVB-GMA)</i> ρ : 0.97, 0.67, 0.66 $d_{\mu m}$: 2.2, 1.1 d_{nm} : 900, 400 Φ_v : 5, 10, 15, 20, 25	Epoxy E44	<ul style="list-style-type: none"> The loss factor ($\tan \delta$) increases with increase in temperature in the range of -20 to 90°C.
John, B., Nair, C. P. R., Ninan, K. N. (2010)	<i>Glass microballoons (K37)</i> ρ : 0.37 Φ_v : 70 <i>Nano clay</i> Φ_v : 2, 4	BACY with Zincocotate Nonylphenol catalyst	<ul style="list-style-type: none"> The addition of nanoclay by 4 vol. % decreases glass transition temperature (T_g) as a result of increase in plasticization of the matrix. Storage modulus is improved by 10% with addition 4 vol. % nanoclay and decreases by 90% with temperature increase in the range of 100-350°C.
Sankaran, S., Ravi Sekhar, K., Govinda Raju., Jagdish, M. N. (2006)	<i>Glass microballoons</i> ρ : 0.45 Φ_v : 0.62, 0.68, 0.72	DGEBA Epoxy with cycloaliphatic amine and aromatic amine Hardeners	<ul style="list-style-type: none"> Reduction in use temperature for syntactic foams is up to 25%. 1.7-24.9% higher T_g for syntactic foams over the neat resin. Tan δ is the highest for cycloaliphatic amine based syntactic foam at room temperature.

Poveda, R., Achar, S., Gupta, N. (2014)	<i>Glass microballoons</i> Φ_v : 0.15, 0.3 ρ : 0.22, 0.46 <i>Carbon nanofibers</i> Φ_w : 1, 2, 5, 10	Epoxy resin DER 332 and Hardener DEH 24	<ul style="list-style-type: none"> • With respect to neat epoxy, the storage modulus and loss modulus for CNF/epoxy composites increase with CNF content by 14.6 and 22.6% at room temperature. The loss modulus of CNF/syntactic foams is shown to increase by 25.3% at room temperature compared to neat epoxy. • The glass transition temperatures of CNF/syntactic foams are observed to increase by 27.1 and 25% as compared to neat resin.
Shunmugasamy, V. C., Pinisetty, D., Gupta, N. (2013)	<i>Glass microballoons</i> Φ_v : 0.3, 0.4, 0.5, 0.6 ρ : 0.22, 0.32, 0.46 η : 0.970, 0.956, 0.9363	Vinylester resin with methyl ethyl ketone peroxide Hardener	<ul style="list-style-type: none"> • Storage modulus of the neat resin is 76-96% lower than syntactic foam in the temperature range of 30-140°C. • T_g decreases by 14-66% with increase in filler content. • Loss modulus decreases by 28-74% with increase in density.
Das, A., Satapathy, B. (2011)	<i>Cenospheres (CS-300)</i> ρ : 0.45-0.80 Φ_w : 0, 5, 10, 15, 20.	Polypropylene Homopolymer (REPOL H110MA)	<ul style="list-style-type: none"> • Enhancement in the energy dissipation ability of the composite with 10 wt.% of cenosphere and an increase in the storage modulus up to 30% in the composites relative to the soft PP-phase. • Storage modulus is relatively higher with increasing cenosphere content upto 10 wt.% at lower temperatures (-25 to 0°C).

Table 1.5 Literature survey on surface treated constituents of composites.

Author	Reinforcement	Matrix	Remarks
Sailaja, R. R. N. and Deepthi, M. V. (2010)	<i>Lignin phthalate (ligph)</i>	LDPE 24FS040 LDPE-g-maleic Benzoyl peroxide initiator (0-15 g) Maleic anhydride	<ul style="list-style-type: none"> • Onset of weight loss is at 408°C, maximum being at 481°C with 97% weight loss. The compatibilized counterpart showed a similar trend with lower char content. • RIS reduces drastically as filler content increases from 20-40%. An optimal compatibilizer loading is observed at 9% of filler. Compatibilized blends for 40% ligph loading registered 54% rise. • Addition of compatibilizer shows RTS exceeding 0.95. For 40% ligph loading, RTS drops by 20% for the uncompatibilized blends. • RYM increases as ligph loading increases from 20-40%. For compatibilized blends, it reduces to 2.3 and 2.25 for 20 and 30% ligph loadings respectively. • Compatibilization of the blends slightly improves REB. For higher ligph loading (40%), it increases from 0.19 (without compatibilizer) to 0.3 (3% compatibilizer addition).

<p>Deepthi, M. V., Sailaja, R. R. N., Sampathkumar, P., Seetharamu, S. and Vynatheya, S. (2014)</p>	<p><i>Silicon nitride</i> Φ_v: 10, 20, 30 <i>Surface modified Nanoclay (NC)</i></p>	<p>HDPE 24FS040 Dibutyl Maleate (DBM) Dicumyl peroxide initiator HDPE-g-DBM</p>	<ul style="list-style-type: none"> • RTS reduces as Silicon Nitrate (SN) loading increases from 10-30%. RYM increases from 1.0 (neat HDPE) to 2.74 (with 30% SN) without compatibilizer with addition of SN. Nanoclay addition of 2, 5 and 10% with compatibilization further improves RYM. • REB reduces to 0.71 and 0.68 for 20 and 30% SN loading (without compatibilizer) respectively. For 30% SN loading, REB increases from 0.33 (without compatibilizer) to 0.43 on compatibilization. Addition of compatibilizer improves the flexural strength by 24.63, 9.55, 10% and modulus value by 37.34, 12.28, 14.2% for 10, 20, 30% SN loadings respectively. Addition of compatibilizer improves the compressive strength by 38.63, 16.54, 21.42% and modulus value by 14.93, 12.41, 9.55% for 10, 20, 30% SN loadings respectively.
<p>Sailaja, R. R. N. (2006)</p>	<p>Bleached kraft eucalyptus pulp PEGMA with 8 wt.% of GMA compatibilizer</p>	<p>LDPE MMA monomer Manganicpyrophosphate as initiator</p>	<ul style="list-style-type: none"> • Compatibilized composites show substantial improvement in RIS values. For higher filler loadings, the impact strength increases by 60% on compatibilization.
<p>Sailaja, R. R. N. and Seetharamu, S. (2008)</p>	<p>Tapioca starch (TS)</p>	<p>LDPE LDPE-g-itaconic Dicumyl peroxide initiator</p>	<ul style="list-style-type: none"> • RTS decreases as TS loading increases. For 40% TS loading, RTS is 83% of neat LDPE. RIS is around 70% of neat LDPE for 50% TS loading. • As the TS loading increases, REB decreases.

Deepthi, Sharma, M., Sailaja, Anantha, P., Sampathku maran and Seetharamu, S. (2010)	<i>Cenospheres</i>	HDPE 24FS040 HDPE-g-DBM Φ_v : 5, 10, 15	<ul style="list-style-type: none"> • Addition of compatibilizer increases the tensile strength by 70% as compared to neat resin. • RYM increases by 14.38% as the silane coated cenosphere loading increased from 10-30% . • REB reduces to 27.21% with increase in cenosphere content.
---	--------------------	--	--

From the existing literature, it is very clear that environmental pollutant like fly ash has not exploited well to synthesize and develop thermoplastic based syntactic foams using industrial scale injection molding technique. Hence, present work deals with development and characterization of eco-friendly and lightweight cenosphere/HDPE syntactic foam composites.

1.5 Objectives and Scope of the present work

From the foregoing literature survey, clear is the fact that the research reports on development of cenosphere/HDPE syntactic foam composites using industrial scale injection molding technique is not available. Development and performance analysis of a low cost cenosphere filled HDPE is proposed in the present investigation. The perusal of literature review on syntactic foam prompted a thorough and systematic study on these composites by performing experimental characterization for physical and mechanical behavior. Thereby the work undertaken pursues the following objectives:

1. Synthesize cenosphere (environmental pollutant) filled High Density Polyethylene (HDPE) using two blending methods (mechanical and brabender mixing) with untreated and treated constituents and develop them through industrial scale injection molding technique.
2. Optimize the injection molding parameters based on experimental density estimations and investigate the influence of blending method and surface modification on tensile and flexural behavior and compare experimental values with available theoretical models.
3. Investigate quasi-static, high strain rate compressive response and dynamic mechanical analysis on cenosphere/HDPE composite fabricated by most influential blending method and constituent configuration and perform micrography of as cast and fractured samples for structure-property correlations followed by development of several industrial components to show the feasibility of injection molding technique to synthesize cenosphere/HDPE syntactic foam composite products.

The available studies on thermoplastic syntactic foams, process materials under controlled conditions at laboratory scale, which usually provides foams with high quality. However, processing of materials with industrial scale manufacturing equipment may not yield similar quality, thereby the effect of such manufacturing environment needs to be studied and is the focus of present work. Rapid manufacturing is a key to satisfying the ever growing demands of useful and durable products. The present work deals with utilization of one such technique, injection

molding, with optimized temperature and pressure parameters to synthesize thermoplastic syntactic foams.

Scope of the present work includes, injection molding of cenosphere reinforced HDPE syntactic foam composites with cenosphere varying as 20, 40 and 60% by weight. Injection molding machine parameters are optimized to get quality samples, being this work is the first attempt of its kind to use industrial scale injection molding machine to fabricate eco-friendly and lightweight syntactic foam composites. Optimization is carried out based on the density estimation of the prepared samples. Based on the optimized temperature and pressure values, cenosphere/HDPE samples are fabricated using untreated and treated configurations with two different blending methods namely, mechanical and brabender mixing, prior to loading the blend in injection molding machine hopper. Such cast samples are tested under tensile and flexural conditions to investigate the effect of blending method and the surface condition of the constituents. Theoretical models are used to estimate the effectiveness of cenospheres in reinforcing syntactic foams.

Based on the experimental results, environmental and economic feasibility most influential blending method and constituent surface condition are chosen and further cenosphere/HDPE samples are prepared and tested for quasi-static, high strain rate compressive response and dynamic mechanical analysis.

Finally, potential for using the optimized injection molding process is demonstrated by casting several industrial scale components.

1.6 Outline of the thesis

The systematic study conducted with respect to above objectives is presented in the thesis. A brief skeletal structure of the thesis is detailed as below.

- Chapter 1 aims at providing necessary details of the research in syntactic foam composites along with an exhaustive literature survey followed by objective and scope of the work.

- Chapter 2 focuses on the constituents used for thermoplastic syntactic foam composites, surface treatment details, processing route adopted and testing methodology.
- Chapter 3 presents the performance evaluation of cenosphere/HDPE syntactic foam composites prepared and tested as mentioned in Chapter 2. The results of the tests conducted on these samples are presented here. Further, the results of the experimental investigation of tensile and flexural behavior are compared with theoretical models.
- Chapter 4 presents the deliverables of the present investigation.
- Chapter 5 highlights the significant conclusions drawn from the results presented earlier.

2 MATERIALS AND METHODS

2.1 Constituents

In the present work, hollow fly ash cenospheres are used as filler and HDPE matrix is utilized to prepare lightweight thermoplastic syntactic foam composite. Details about these constituents are dealt with in the section to follow.

2.1.1 Cenospheres

Cenosphere of CIL-150 grade, supplied by Cenosphere India Pvt. Ltd., Kolkata, India, are used as hollow fillers (Figure 2.1a). Cenospheres are used in the as supplied condition, without any surface treatment in the initial phase of study. Later they are surface treated with silane for comparison (discussed in section 2.2.1). Chemical, physical and sieve analysis details of cenospheres are presented in Table 2.1. Cenospheres primarily comprise of alumina, silica, calcium oxide and iron oxides as observed in this table.

Table 2.1 Chemical, physical and sieve analysis details of cenospheres*.

Physical properties		Chemical analysis		Sieve analysis	
True particle density	800 kg/m ³	SiO ₂	52-62%	+ 30 # (500µm)	Nil
Bulk density	400 – 450 kg/m ³	Al ₂ O ₃	32-36%	+ 60 # (250µm)	Nil
Hardness (MOH)	5 – 6	CaO	0.1-0.5%	+100 # (150µm)	Nil
Compressive strength	180 – 280 kg/m ²	Fe ₂ O ₃	1-3%	+120 # (125µm)	Nil
Shape	Spherical	TiO ₂	0.8-1.3%	+150 # (106µm)	0-10%
Packing factor	60-65%	MgO	1-2.5%	+ 240 # (63µm)	70-95%
Wall thickness	5-10% of shell dia.	Na ₂ O	0.2-0.6%	- 240 #	0-30%
Color	Light grey – light buff	K ₂ O	1.2-3.2%		
Melting point	1200 – 1300 °C	CO ₂	70%		
pH in water	6 – 7	N ₂	30%		
Moisture	0.5% max.				
Loss on ignition	2% max.				
Sinkers	5% max.				
Oil absorption	16 – 18 g/100g				

*As specified by supplier.

2.1.2 HDPE

HDPE of grade HD50MA180 supplied by Reliance Polymers, Mumbai, India is used as the matrix material. The resin is in granular form (3 mm diameter) having

molecular weight of 97500 g/mol. Table 2.2 presents the details about the matrix used. HDPE (Figure 2.1b) is used in both as received and treated (functionalized) mode (section 2.2.2).

Table 2.2 Characteristics of HDPE grade HD50MA180*.

Property	Test Method	Typical Value	Unit
Melt Flow Index (190 ⁰ C/2.16 kg)	ASTM D1238	20.0	gm/10 min.
Tensile Strength at Yield	ASTM D638	22	MPa
Elongation at Yield	ASTM D638	12	%
Flexural Modulus	ASTM D790	900	MPa
Notched Izod Impact Strength	ASTM D256	30	J/m
Vicat Softening Point	ASTM D1525	123	°C

*As specified by supplier



Figure 2.1 (a) Cenospheres and (b) HDPE matrix used in the present work.

2.2 Surface treatment of constituents

The chemicals used for surface treatment of constituents are listed in Table 2.3. Functionalization of HDPE matrix resin is performed in a Brabender mixer (CMEI, MODEL-16 CME SPL, Western Company Keltron) with Dibutyl Maleate and Dicumyl Peroxide.

2.2.1 Silane treated cenospheres

A potential application of Cenospheres as lightweight filler in polymer matrices can be a suitable material from techno-economic perspective. Apart from cenospheres

volume fraction and size, the cenosphere-HDPE interaction plays a major role in determining the mechanical properties of the developed composite system.

Table 2.3 Chemicals used for surface treatment of constituents.

Material	Role	Supplier
3-Amino propyl triethoxy silane (APTS)	Silane coating on cenospheres	Sigma Aldrich, USA.
Dibutyl maleate (DBM)	Functionalization of HDPE	S.D. Fine Chem Ltd., Mumbai.
Dicumyl peroxide	Initiator for compatibilization between silane coated cenosphere and functionalized HDPE	S.D. Fine Chem Ltd., Mumbai.

The mechanical properties of cenosphere reinforced polymer composites are inferior owing to poor interfacial interactions between the hydrophilic cenosphere surface and the hydrophobic polymer (Guhanathan et al. 2001). Thus, tetrasulfane modified cenospheres are used as reinforcing filler as reported by Thongsan and Sombatsompap (2006). Silane coupling agents are usually used as adhesion promoters between inorganic filler and an organic matrix.

In the present work, cenospheres have been surface treated with silane. 50 g of cenospheres are mixed into 100 ml solution of water/ethanol (20:80 wt. %) and is maintained at 80°C. Further, 2% by volume of APTS is added into the solution and continuously stirred for 30 minutes at 80°C in a microve reactor (Enerzi microwave systems, Bangalore). Finally, the resultant product is filtered and washed at least three times using a mix of water/ethanol and then dried in an oven to extract the coated cenospheres. The cenospheres are analyzed by FTIR to confirm the silane coating.

2.2.2 HDPE functionalization

Dicumyl peroxide (0.15g) is added to 50 g of HDPE, 5 ml of DBM and mixed in the Brabender at 210°C for 10 minutes. Resultant blend thus obtained is analyzed by FTIR to confirm the HDPE functionalization.

Further, cenosphere/HDPE syntactic foam composites with untreated and treated constituents are prepared using two different mixing routes prior to injection molding. Details about sample preparation are discussed in the next section.

2.3 Sample preparation

Two methods, mechanical and brabender mixing (MM and BM), are used in this work to mix HDPE (non functionalized and functionalized) and cenospheres (untreated and treated) prior to feeding in PIM machine. Mechanical mixing is carried out manually resulting in no bonding between the constituents, whereas brabender mixing is carried out at 210°C (Deepthi et al. 2010) using brabender with the parameters as detailed in section 2.2.2. Figure 2.2a shows the image of brabender used for blending while blending mechanism is presented in Figure 2.2b. Material is fed through feeder which melts in the heating zone and later carried to twin screws/lobes (Figure 2.2b) rotating at 30 rpm. Blend of cenosphere/HDPE from brabender in the granular form having average mean diameter of 7 mm is shown in Figure 2.2c.

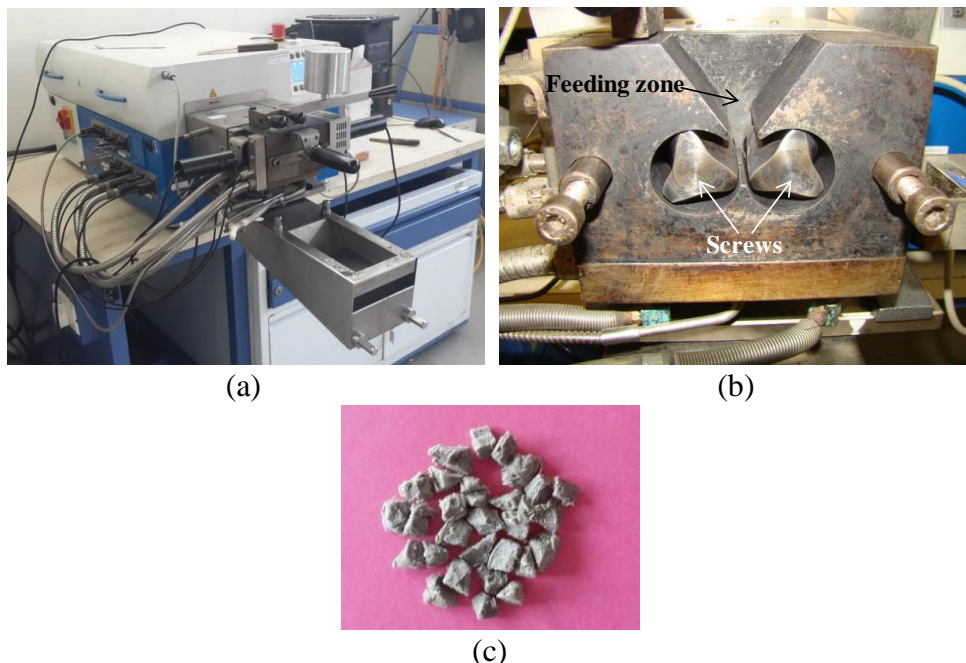


Figure 2.2 (a) Brabender (b) blending mechanism and (c) cenosphere/HDPE blend from brabender.

The mechanically or brabender-mixed blend of cenospheres with HDPE in desired proportions is fed into an industrial scale horizontal type single screw PIM machine (WINDSOR, 80 ton capacity). The photograph of the machine is shown in Figure 2.3a and the schematic representation is presented in Figure 2.3b for clarity. The specifications of the machine are listed in Table 2.4.

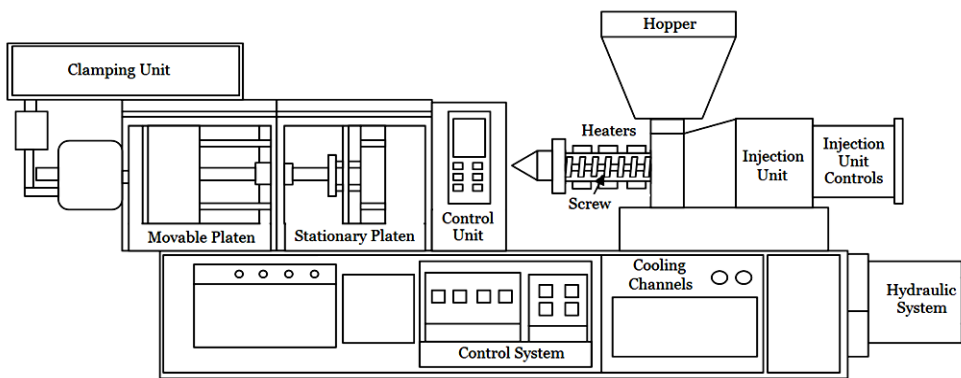
The schematic of signal/material flow in the PIM machine is presented in Figure 2.3c and the tensile and flexural test specimen molds (cartridge type) used are shown in Figure 2.3d-e, which produces specimens in accordance with ASTM D638-10 and D790-10 standards respectively. In the PIM machine, a single screw rotates at 30 rpm in the heating zone to uniformly disperse cenospheres in plasticized HDPE. Subsequently, the mixture is injected through the nozzle into the mold of desired cavity shape (Figure 2.3d-e).

Processing conditions for PIM of syntactic foam composites is presented in Table 2.5. These parameters are fixed in the present study. Injection temperature and pressure are maintained at 160°C and 30 bars which are the outcomes of pilot study as discussed in section 3.3. Table 2.6 lists the four types of syntactic foams fabricated in the present investigation. Specimens of each type are fabricated with 0, 20, 40, and 60 wt.% cenospheres.

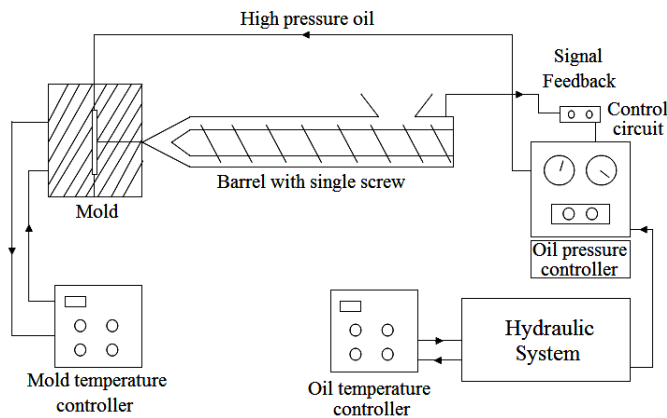
The specimens are named according to the convention HXX-Y-ZZ, where H denotes the HDPE matrix, XX is the weight fraction of cenosphere and Y-ZZ is the processing type name as described in Table 2.6. An overview of the different processing routes is presented in Figure 2.4 for casting cenosphere/HDPE samples and characterized for mechanical properties as detailed in the next section. Brabender is used for reactive blending purposes wherein constituent is surface treated. Thereby, untreated constituents are not blended using brabender.



(a)



(b)



(c)



(d)



(e)

Figure 2.3 (a) Image of PIM machine (b) Schematic of the PIM machine used for manufacturing syntactic foam specimens. (c) Schematic of signal/material flow in PIM machine. Mold for manufacturing (d) Tensile (e) Flexural test specimens.

Table 2.4 Injection molding machine specifications.

Machine	Parameters	Typical Value
General specifications	Make	Windsor, India
	Capacity	80 Ton
Injection Unit	Plasticizing capacity	40 kg/h
	Capacity molded per shot barrel/screw unit with pressure on material	1020 bar, 110 cm ³
	Screw diameter	42 mm
	Injection stroke	80 mm
	Screw speed infinitely variable	0 – 200 rpm
	Capacity of hopper	30 kg
Locking unit	Mold clamping force	80 Ton
	Size of mold plates	500×500 mm
	Distance between tie bars	330×330 mm
	Maximum mold opening	450 mm
	Maximum mold thickness	150 mm

Table 2.5 Processing conditions for injection molded syntactic foam composites*.

Parameters	Typical Value
Mold temperature (°C)	50-60
Nozzle temperature (°C)	160
Heating zone temperature (°C)	160
Screw speed (RPM)	30
Injection speed (mm/s)	18
Injection time (s)	04
Holding time (s)	06
Cooling time (s)	20
Total cycle time (s)	30

*As specified by Konkan Speciality Polyproducts Pvt. Ltd., Mangalore, Karnataka, India.

Table 2.6 Syntactic foam types fabricated in the present study.

Specimen Type	Cenospheres	HDPE	Mixing method
U-MM	Untreated	Virgin	Mechanical Mixing
T _M -MM	Untreated	Functionalized	Mechanical Mixing
T-MM	Silane Treated	Functionalized	Mechanical Mixing
T-BM	Silane Treated	Functionalized	Brabender Mixing

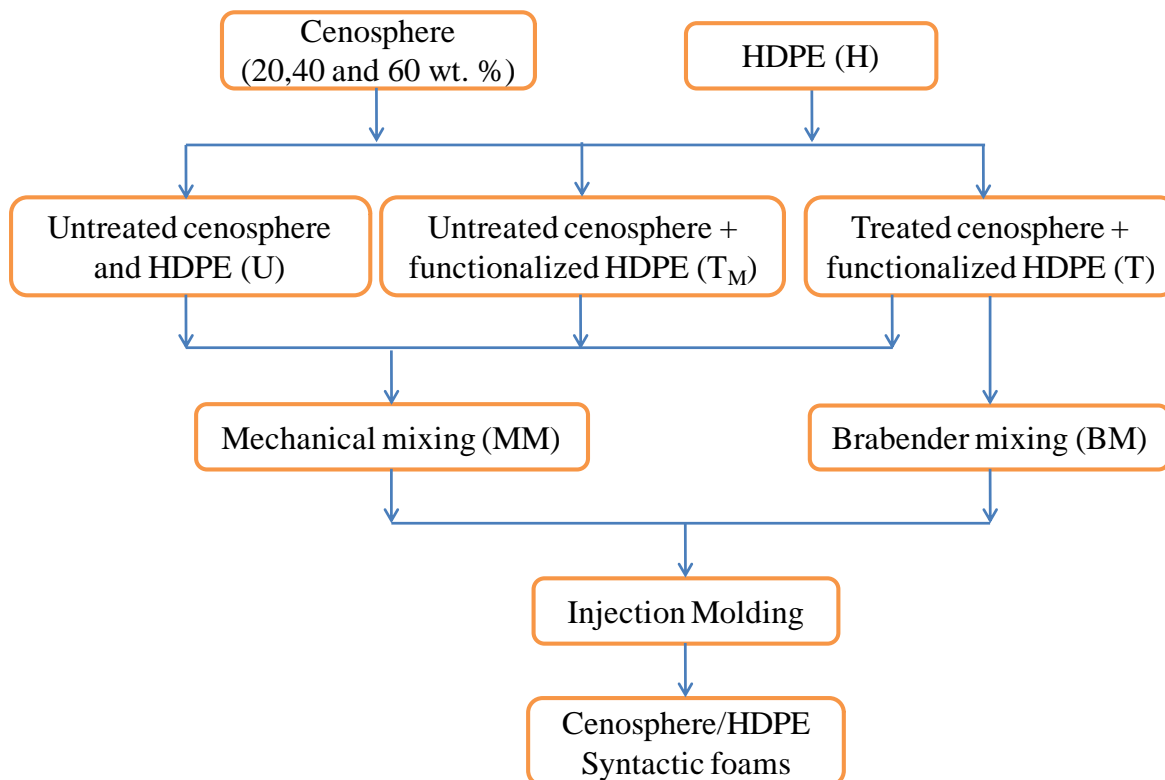


Figure 2.4 Fabrication route and the types of cenosphere/HDPE syntactic foams synthesized in the present work.

2.4 Testing

2.4.1 FTIR spectroscopy and X-ray diffractograms

Cenospheres are analyzed by FTIR spectroscopy (JASCO 4200, Japan, Automated Total Reflection mode, wave number 4000 to 650cm^{-1}) to confirm the silane coating. X-ray diffractograms are also looked into for crystallinity of HDPE and 2θ values using DX GE-2P, JEOL, Japan having Nickel filter material with scanning speed of $2^\circ/\text{min}$ and $\text{Cu K}\alpha$ ($\lambda=1.514\text{\AA}$) radiation.

2.4.2 Particle size analysis

Particle size and shape analysis is conducted using a Sympatec (Pennington, NJ) QICPIC high speed image analysis system. The particles are dispersed using the RODOS and VIBRI systems, which aerosolize a stream of particles in a jet of compressed air. A pulsed laser illuminates the particles as they pass a camera that images the particles at 175 frames/sec. For each particle imaged, the equivalent diameter is calculated as the diameter of a sphere having a projected area equal to the projection captured by the camera. Five runs of each particle type are conducted and

the values presented are averaged from these runs, with weight according to the number of particles in each run. Approximately 375,000 and 550,000 particles are measured for untreated and treated particles, respectively.

2.4.3 Density measurement

ASTM D792-13 standard is adopted to measure the density of all fabricated specimens. The densities of five specimens are measured and the average values and standard deviations are reported.

2.4.4 Tensile testing

A computer controlled universal test system (Z020 Zwick Roell, USA) with 20 kN load cell is used for tensile testing. A constant crosshead displacement rate is maintained at 5 mm/min during the tests (ASTM D638-10). The acquired load and displacement data are used to calculate the stress and strain, respectively. Average modulus and strength values of five specimens for each composite type are reported.

2.4.5 Flexural testing

The flexural testing is performed in three-point bend configuration using a computer controlled Zwick (Zwick Roell Z020, ZHU) machine having a load cell capacity of 20 kN. ASTM D790-10 is adopted for testing. A pre-load of 0.1 MPa is set and crosshead displacement rate is maintained at 1.54 mm/min. All specimens have span length of 52 mm to maintain 16:1 span length/thickness ratio. Five specimens are tested and the average values of the measured properties are presented. Tests are continued until 10% strain to check the possibility of specimen failure and the stress-strain data is acquired. The specimens did not show complete fracture in any syntactic foam at this strain level; therefore, results are reported in figures only up to 5% strain for clarity. The flexural modulus (E) is calculated by,

$$E = \frac{L^3 m}{4bd^3} \quad (2.1)$$

where L is the support span (mm), b is the width of beam (mm), d is the thickness of beam (mm) and m is the slope of the tangent to the initial straight-line portion of the load-deflection curve. The flexural stress (σ_{fM}) is estimated by,

$$\sigma_{fM} = \frac{3PL}{2bd^2} \quad (2.2)$$

where P is the load (N) at a given point on the load-deflection curve. The reported flexural strength values are taken at 5% strain for comparison.

2.4.6 Quasi-static and high strain rate compression

Quasi-static compression testing is performed on an Instron 4467 Universal Testing System with a 30 kN load cell. Bluehill 2.0 software is used for data acquisition. Tests are conducted at 10^{-4} , 10^{-3} and 10^{-2} s⁻¹ initial strain rates, corresponding to cross-head displacement velocities of 0.02, 0.2 and 2 mm/min, respectively. The end of test criteria is set at 70% strain. The data is analyzed using an in-house developed MATLAB code and yield strength and modulus are calculated for every specimen.

High Strain Rate (HSR) compression tests are conducted using a split-Hopkinson pressure bar (SHPB) system. The length and diameter of Inconel alloy incident and transmitter bars are 200 and 1.27 cm, respectively. Young's modulus of 200 GPa and density of 8497 kg/m³ are taken for the Inconel alloy in calculations. Dow Corning 111 lubricant is used between the specimen and the bars. A brass pulse shaper is used at the front end of the incident bar.

The incident, reflected, and transmitted strain pulses are acquired by two strain gages of type CEA-13-240UZ-120 (Vishay Precision Group, Malvern, PA) that are bonded at the midpoint of the bars. The acquired pulses are recorded by a Tektronix TDS 2014B (Beaverton, OR) oscilloscope. The specimen's response over time is calculated by,

$$\dot{\varepsilon}(t) = \frac{2c_b \varepsilon_r(t)}{l_0} \quad (2.3)$$

$$\sigma(t) = \frac{AE \varepsilon_t(t)}{A_0} \quad (2.4)$$

$$\varepsilon(t) = \int_0^t \dot{\varepsilon}(\tau) d\tau \quad (2.5)$$

where ε_r and ε_t are reflected and transmitted pulses respectively, $\dot{\varepsilon}(t)$ is the strain rate obtained within the specimen, τ is the time variable used in integration, $\sigma(t)$ is the stress within the specimen, c_b is the sound wave velocity in the bar, A and E are the cross-sectional area and Young's modulus of the bar material, respectively, while l_0 and A_0 are the length and cross-sectional area of the specimen, respectively (Shim, J. and Mohr, D. 2009).

2.4.7 Dynamic mechanical analysis

Dynamic mechanical analysis (DMA) is conducted using a TA Instruments (New Castle, DE) Q800 DMA. Specimens of nominal dimensions $60 \times 12.7 \times 3.3 \text{ mm}^3$ are tested in the dual cantilever configuration with a span length of 35 mm. Testing is conducted in the strain control mode with a maximum displacement of 25 μm .

Dynamic mechanical analysis is conducted in two phases. In the first phase, the behavior of the syntactic foams at high temperature is studied using the temperature sweep mode at constant frequency. The behavior at higher frequencies is studied using the frequency sweep mode in the second phase. The results of temperature and frequency sweeping are combined using the time-temperature superposition principle to generate master curves describing the behavior over a wider range of frequencies.

In the temperature sweep test, the temperature is ramped from 35°C to 150°C at a rate of 1°C/min with the deformation occurring at a constant frequency of 1 Hz. Testing is halted once the storage modulus reaches a value of 20 MPa to prevent total melting of the specimen. At least five specimens of each type are tested in this phase. In the frequency sweep testing, the temperature is stepped from 35°C to 120°C in increments of 5°C. At each temperature step the specimen is soaked for 5 minutes to

ensure thermal equilibrium. The dynamic properties are measured at 20 discrete frequencies logarithmically spaced between 1 and 100 Hz at each temperature step. At least five specimens of each type are tested in this phase.

2.4.8 Imaging

Scanning electron microscope (JSM 6380LA, JEOL, Japan) is used for micro structural analysis. All the samples are sputter coated using JFC-1600 auto fine coater (JEOL, Japan). Nikon D7000 camera with Nikkor 35 mm F1.8G lens is used for optical imaging. Tokina AT-X pro 100 mm F2.8D macro lens is used for imaging fractured features.

Results of the tests envisaged here are elaborately discussed in the section to follow.

3 RESULTS AND DISCUSSION

3.1 FTIR and XRD analysis

Figure 3.1 presents FTIR spectra of non functionalized and functionalized HDPE. DBM is added in dissolved solution of HDPE in proportions of 5, 10 and 15% by volume to check the variations in transmittance in FTIR (Figure 3.1b). As observed from the figure, the variation in the spectra of specimens containing 5 and 10 vol.% DBM is negligible. HDPE functionalized with 10 vol.% DBM is chosen for use in the present work based on the previous published literature (Deepthi et al. 2010).

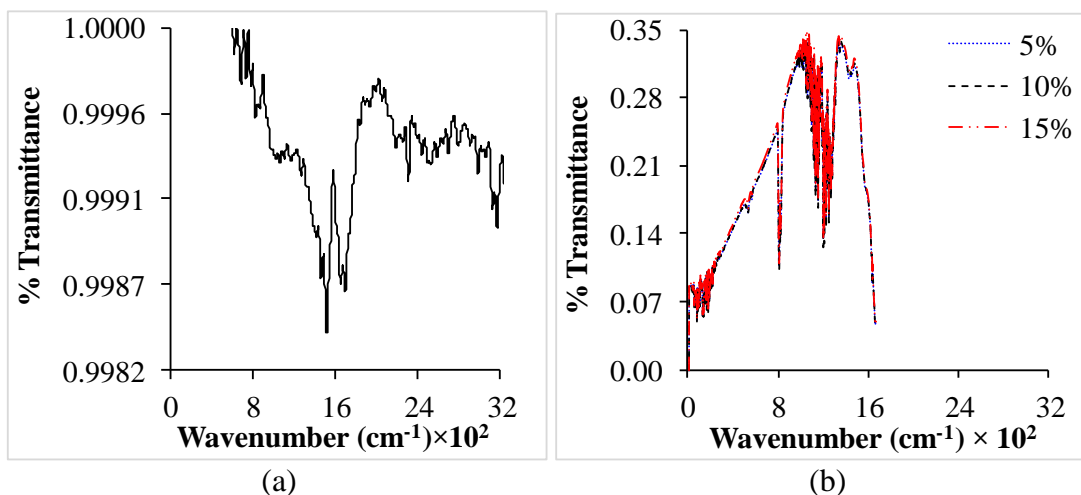


Figure 3.1 FTIR Spectra of (a) neat HDPE and (b) HDPE functionalized with 5, 10 and 15% DBM. Note that the y-scale is different in both figures.

Figure 3.2 presents freeze fractured micrographs of virgin and functionalized HDPE. High degree of surface roughness is observed in the fractured virgin specimen (Figure 3.2a) whereas a few large cracks are observed in the functionalized specimen surface (Figure 3.2b). Since total energy absorption in fracture depends on the area of the fracture surface, it is expected that the non functionalized and functionalized specimens would show different mechanical properties when the quantitative results are compared.

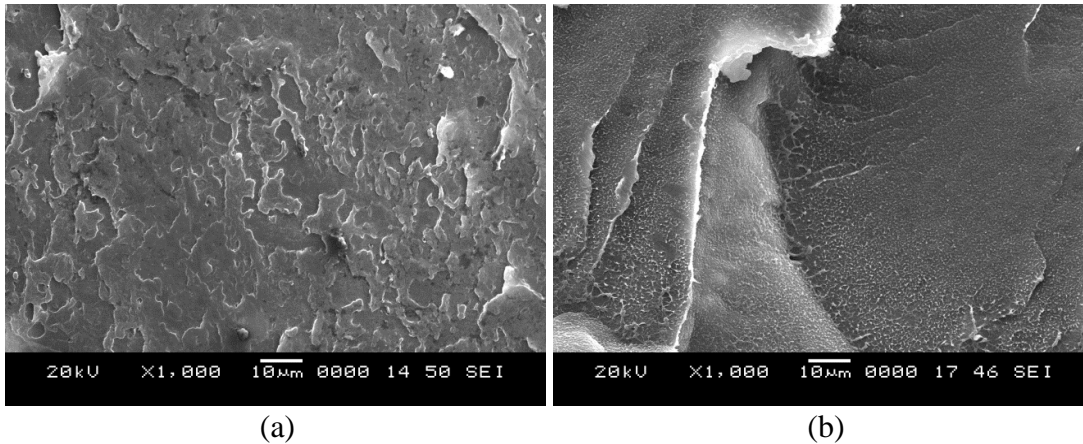


Figure 3.2 Freeze fractured micrographs of (a) non functionalized and (b) functionalized HDPE specimens at the same acquisition magnification.

FTIR results for untreated and silane treated cenospheres are presented in Figure 3.3. The spectrum confirms the presence of a silane surface layer and the -C-H- stretching of propyl group is observed at 2929 cm^{-1} .

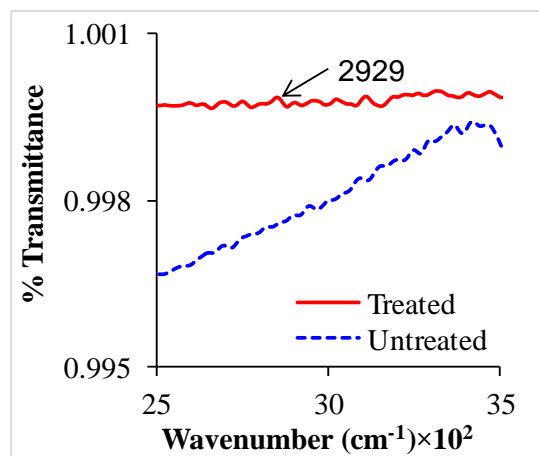


Figure 3.3 A section of the FTIR spectra of untreated and silane treated cenospheres.

Figure 3.4 shows the XRD diffraction results of constituents and representative syntactic foam composites. Untreated and treated fly ash cenospheres has a main peak at 2θ value of 26.6 and 26.04 and other numerous small peaks respectively as it consists of mainly metal oxides predominantly SiO_2 and $3\text{Al}_2\text{O}_3$. Virgin HDPE has two main peaks at 20.82 and 23.12 as it is semi-crystalline in nature. While functionalized HDPE shows two peaks at 20.6 and 22.92.

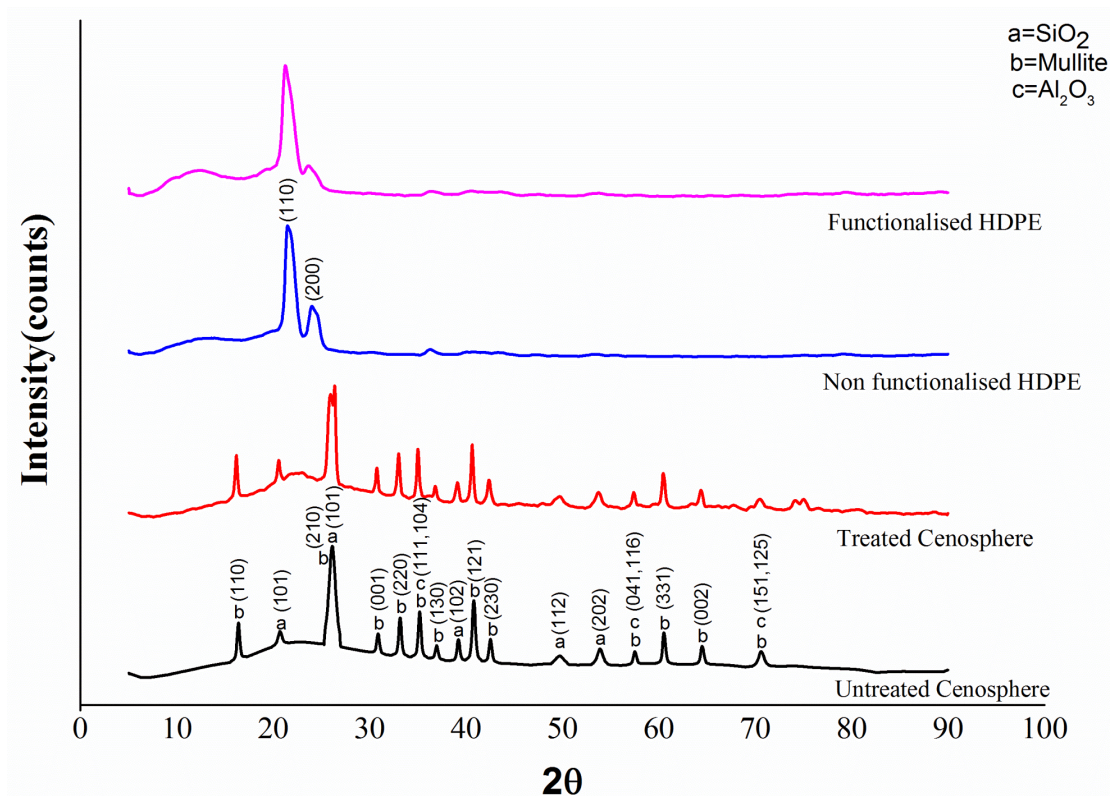


Figure 3.4 X-ray diffractogram of the constituents.

3.2 Particle size analysis

Micrographs of untreated and silane treated cenospheres are shown in Figure 3.5a and Figure 3.5b, respectively. Cenospheres contain surface defects as seen from these micrographs. The coating layer is not visibly identifiable in the micrographs due to its small thickness, despite the FTIR results providing evidence for its presence.

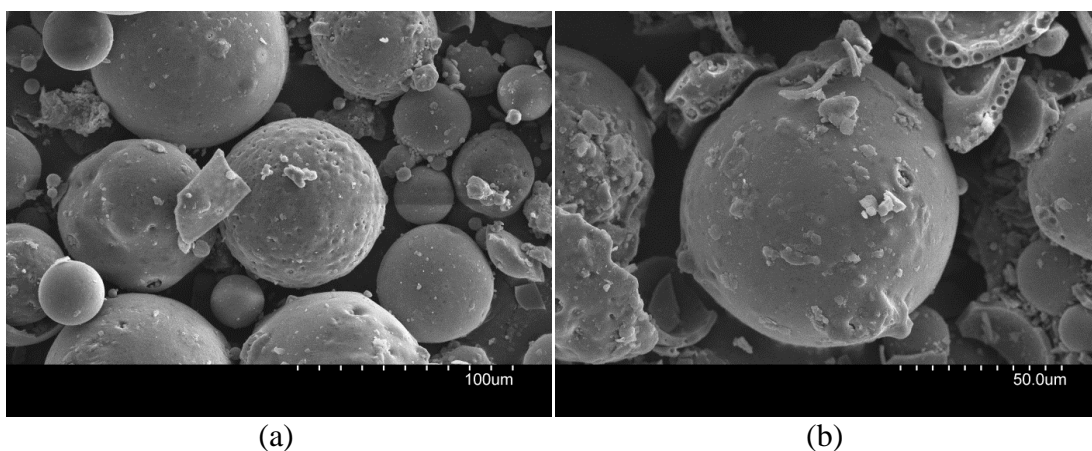


Figure 3.5 Micrographs of (a) untreated and (b) silane treated cenospheres.

Further observations are presented in Figure 3.6a and Figure 3.6b for broken untreated and silane treated cenospheres, respectively. It is observed in both figures that the wall thickness of cenospheres is irregular and there is significant amount of porosity in cenosphere walls.

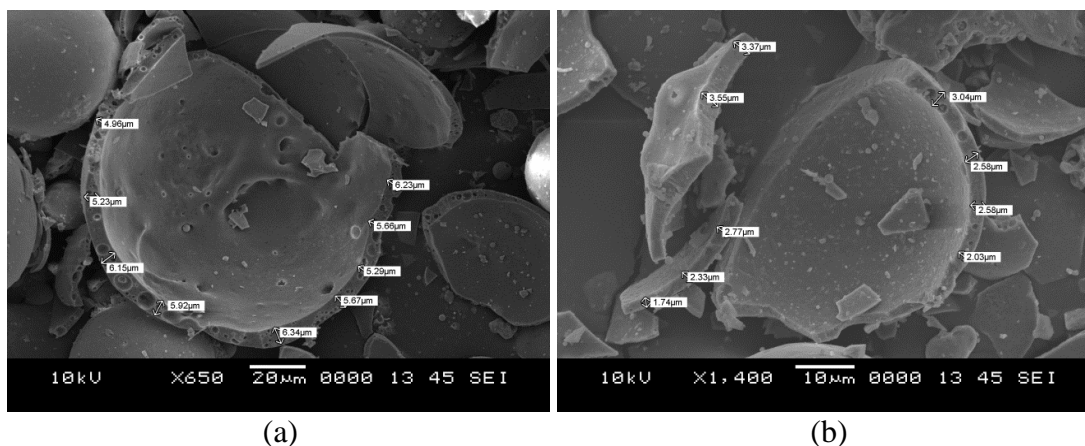


Figure 3.6 Micrographs of broken (a) untreated and (b) silane treated cenospheres. The wall thickness variations within one particle and porosity that exists in the walls of these cenospheres can be observed in these micrographs.

The porosity leads to lower strength of cenospheres than that expected from the fully dense walls of the same thickness. The results of particle size analysis for untreated and silane treated cenospheres are presented in Figure 3.7. It can be observed that the volume weighted mean particle size for untreated particles is 99.5 μm. The peak for the treated particles is broader and shows the average value of 110.2 μm. The X_{50} median particle sizes are 76.3 and 98.1 μm for the untreated and treated particles. The increase in the average diameter can be partly attributed to the silane coating.

It is also noted that, some of small size particles sink during the surface treatment due to their high density and are not recovered back contributing to the increased overall size of the coated particles. A shift in the initial part of the graph in Figure 3.7 provides evidence for this possibility. It can be observed in Figure 3.7 that the size distribution of untreated particles is very narrow and the upper range of particle size is about 170 μm. In comparison, the tail end of the curve for the treated particle extends considerably to a maximum size of about 475 μm.

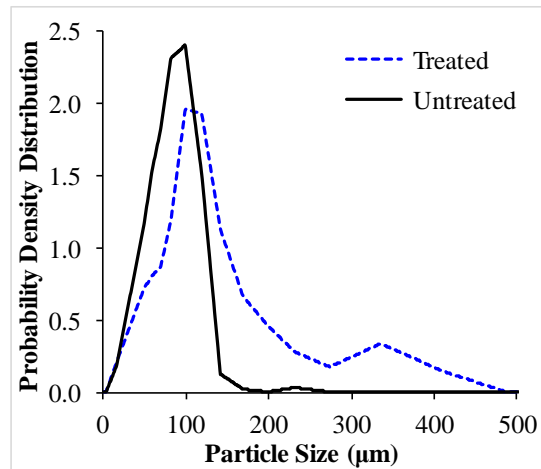


Figure 3.7 Particle size analysis of untreated and silane treated cenospheres.

The probability density distribution for the larger size particles is very low. This observation indicates the formation of a small amount of clusters as a result of silane treatment. It is expected that the shear forces applied during pre-mixing and injection molding will help in dispersing some of these clusters. Particle sphericity is observed to be in the range of 0.6-0.85 compared to 1 for perfectly spherical particles. Surface defects, observed in Figure 3.5, result in the variation in the measured particle sphericity.

3.3 PIM process optimization and specimen manufacturing

A pilot study is conducted for optimizing the parameters of PIM process. In this study temperatures of 160 and 180°C are used over a wide range of injection pressures (20-50 bars) for casting the tensile samples. Since no data is available for optimal parameters for developing cenosphere/HDPE syntactic foams using PIM technique, this parametric optimization is required for manufacturing high quality composites. Mechanical mixing route is adopted prior to loading the untreated constituents in the hopper of PIM. Composites with 30 and 60 wt.% cenospheres (labeled as H30-U-MM and H60-U-MM, respectively) are cast in this pilot study. The composites cast at different pressures are shown in Figure 3.8. Incomplete filling of mold cavity is obtained in Figure 3.8a for applied pressures of 20 and 25 bar for both 160 and 180°C temperatures. On the other hand, excessive material squeezing out of the mold is clearly seen in Figure 3.8b for pressures of 45 and 50 bar. Figure 3.8c shows that high quality specimens are cast at 30-40 bar pressures. High pressure can lead to greater

fraction of broken cenospheres, while higher temperature leads to lower viscosity of the resin resulting in runoff from the mold. Analysis of the density of fabricated specimens can help in measuring the fraction of broken cenospheres.

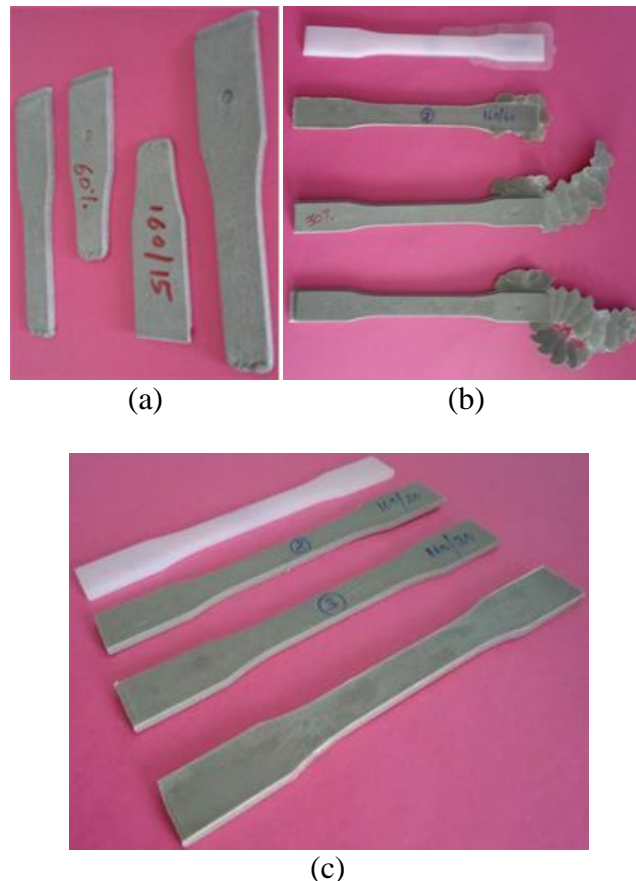


Figure 3.8 Syntactic foam samples molded at pressures (a) below 30 bar and (b) above 40 bar. (c) The specimens molded at 30, 35 and 40 bar pressures showed good quality. The figure includes a neat HDPE specimen with three H60-U-MM specimens molded at different pressures.

Density of matrix is measured to be $1.0563 \pm 0.0006 \text{ g/cm}^3$. The measured density values for H30-U-MM and H60-U-MM syntactic foams manufactured at different combinations of temperatures and pressures are presented in Table 3.1. It is observed in the table that syntactic foams fabricated at 160°C and 30 bar have the lowest densities for both compositions. Higher density values indicate fracture of cenospheres as the samples do not have any porosity in the matrix as observed in representative micrographs presented in Figure 3.9 Therefore, injection temperature

and pressure of 160°C and 30 bar, respectively, are selected for casting the syntactic foams in the present work.

Table 3.1 Density values of H30-U-MM and H60-U-MM cast in the pilot study for optimization of process parameters.

Syntactic foam type	Injection pressure (bar)	Density at 160°C (g/cm ³)	Density at 180°C (g/cm ³)
H30-U-MM	30	1.0122±0.0020	1.0261±0.0030
	35	1.0356±0.0021	1.0483±0.0035
	40	1.0461±0.0029	1.0551±0.0039
H60-U-MM	30	1.0219±0.0071	1.0774±0.0095
	35	1.0701±0.0092	1.1081±0.0140
	40	1.0802±0.0110	1.1271±0.0290

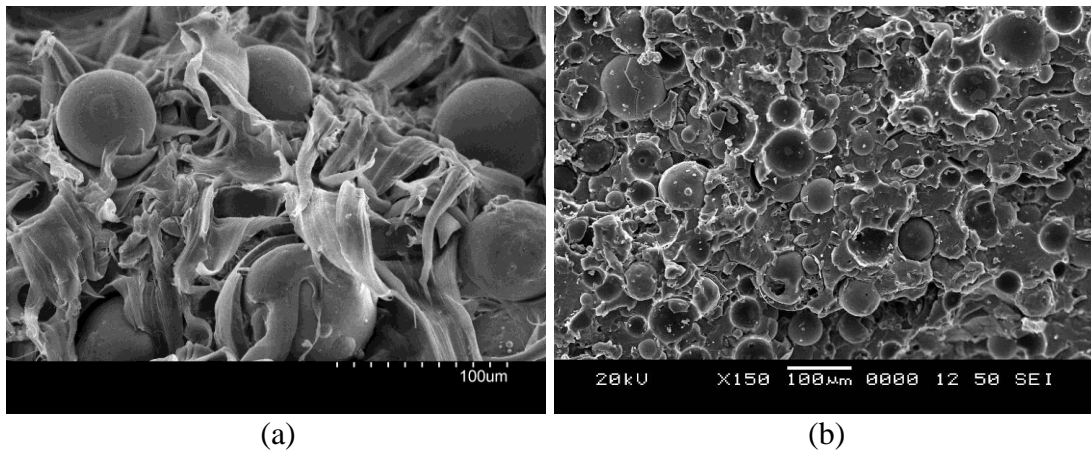
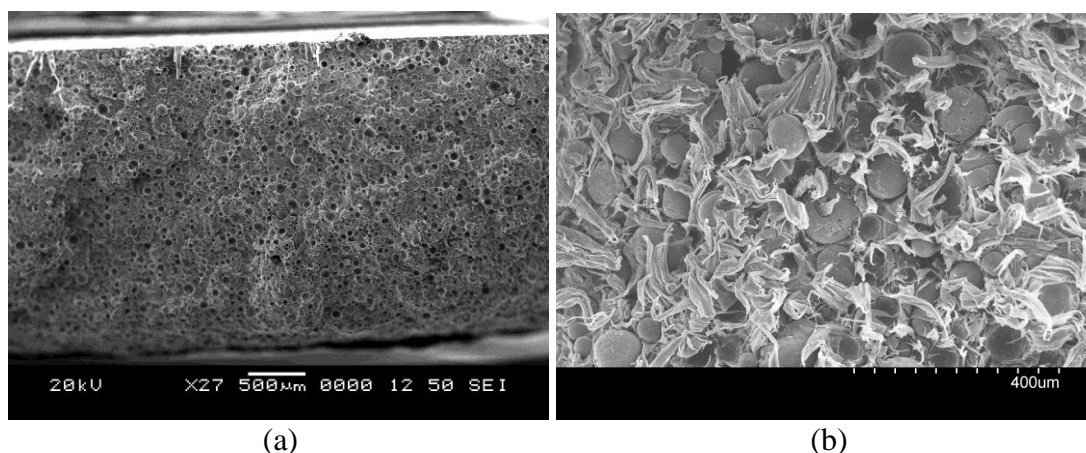


Figure 3.9 Micrographs of syntactic foam specimens containing (a) 30 (H30-U-MM) and (b) 60 wt.% (H60-U-MM) cenospheres manufactured at 160°C, 30 bar.

Obtaining uniform dispersion of cenospheres and minimizing their crushing in the matrix is a challenging task, especially when using pressurized techniques like PIM. Figure 3.10a presents a representative micrograph of syntactic foam containing untreated cenospheres and non functionalized HDPE. Uniform dispersion of hollow cenospheres in the matrix is observed in this micrograph demonstrating the feasibility of using PIM for developing syntactic foam composites. However, lack of interfacial bonding between cenospheres and HDPE is visible in Figure 3.10 b.

Improvement in the cenosphere-HDPE interfacial bonding is highly desired as the mechanical behavior strongly depends on the interfacial characteristics for effectively transferring load from the matrix to the particle. In order to promote strong interfacial

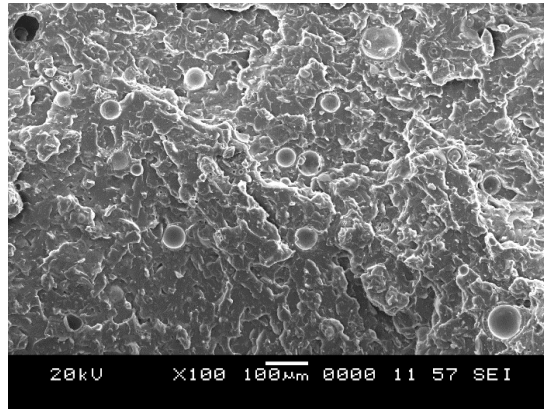
bonding, cenospheres are treated with silane and HDPE is functionalized with 10 vol.% DBM (Deepthi et al. 2014) as discussed earlier in section 2.2.



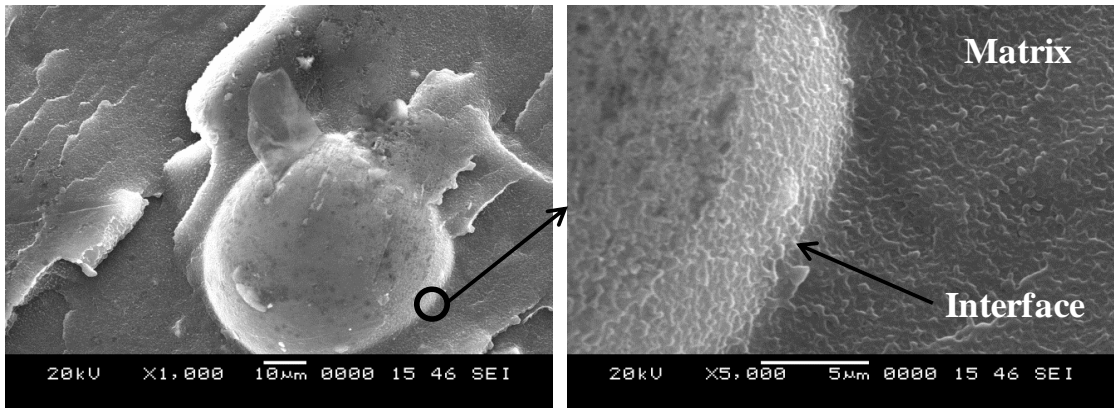
(a) (b)
Figure 3.10 Micrograph of freeze fractured HDPE matrix syntactic foams containing 60 wt.% cenospheres (H60-U-MM) showing (a) uniform dispersion of cenospheres, indicating feasibility of using PIM in developing syntactic foams and (b) lack of bonding between cenospheres and HDPE matrix.

Using the optimized processing parameters of PIM, syntactic foams with treated constituents are fabricated and representative microstructure is presented in Figure 3.11a. This figure shows that cenospheres are uniformly dispersed in functionalized HDPE resin and clusters of particles are not present. A higher magnification micrograph in Figure 3.11b shows that the bonding between silane treated cenospheres and the functionalized matrix is good, as evidenced by the presence of a continuous interface between them. No separation or discontinuity is observed at the particle-matrix interface. Strong interfacial bonding is desired in applications where these composites can be subjected to tensile or flexural loading to enable effective transfer of load between particle and matrix. The ester functionalized HDPE interacts with the amine group of silanized cenospheres, thereby, anchoring both HDPE and filler particles. Further, benefit in mechanical properties, if any, is based on cenospheres survival owing to PIM process.

Quantification of cenosphere survival is estimated by density test and is discussed in the next section.



(a)



(b)

(c)

Figure 3.11 (a) Freeze fractured micrographs of H2O-T-BM syntactic foam showing dispersion of cenospheres in HDPE resin and (b) the interface between functionalized HDPE matrix and silane treated cenospheres. (c) The region marked by a circle in (b) is shown at higher magnification, where continuity across the interface can be observed. These micrographs are taken prior to the test.

3.4 Density

Using the optimized parameters of 160°C temperature and 30 bar pressure, all the syntactic foam specimens are manufactured using mechanical and brabender mixing. The difference between experimental and theoretical (calculated using rule of mixtures) densities are presented for all syntactic foams in Table 3.2. Since no porosity is present in HDPE matrix (Figure 3.9 and Figure 3.11), the difference between theoretical and experimental density values is attributed to the cenosphere breakage during manufacturing and is estimated by,

$$V_{mp} = \frac{\rho_t - \rho_m}{\rho_t} \quad (3.1)$$

where, V_{mp} , ρ_t and ρ_m are cenosphere porosity, theoretical and measured densities of syntactic foams respectively. Negative porosity values indicate cenosphere breakage. During the syntactic foam synthesis using pressurized techniques like PIM, some cenospheres fracture. The matrix resin fills the cavity exposed due to cenosphere fracture, increasing the density of the syntactic foam. Some of the previous studies have shown measured density of syntactic foams to be higher than their theoretical densities despite the presence of matrix porosity, which leads to a conclusion that there is fracture of hollow particles in those foams during synthesis (Huang, J S and Gibson, L J 1991). In the present case, experimental density is higher than the theoretical density values, implying particle breakage.

Table 3.2 Theoretical and experimental density values of syntactic foams and cenosphere breakage during fabrication.

Syntactic foam type	Φ_f	Theoretical density (g/cm ³)	Experimental density (g/cm ³)	Cenosphere failure (wt. %)
H20-U-MM	0.229	0.9976	1.0159±0.0016	1.83
H40-U-MM	0.442	0.9430	1.0078±0.0036	6.87
H60-U-MM	0.664	0.8923	1.0219±0.0071	14.5
H20-T _M -MM	0.229	0.9976	1.0326±0.0316	3.51
H40-T _M -MM	0.442	0.9430	1.0293±0.0414	9.15
H60-T _M -MM	0.664	0.8923	1.0548±0.0527	18.21
H20-T-MM	0.229	0.9976	1.0830±0.0349	8.56
H40-T-MM	0.442	0.9430	1.1110±0.0455	17.82
H60-T-MM	0.664	0.8923	1.1140±0.0657	24.85
H20-T-BM	0.229	0.9976	1.0490±0.0394	5.15
H40-T-BM	0.442	0.9430	1.0710±0.0434	13.57
H60-T-BM	0.664	0.8923	1.0740±0.0537	20.36

* Φ_f = Cenospheres by volume %.

The particle fracture is low in composites containing 20 wt.% cenosphere. However, as the cenosphere content is increased in the syntactic foam, the proportion of cenosphere breakage also increases, likely because of particle to particle interaction. H60-T-MM syntactic foams showing the highest cenosphere breakage for both untreated and treated constituents, have 66.4 vol.% filler loading. In syntactic foams containing 60 wt.% cenospheres, 14-25 wt.% cenospheres are found to break due to the rigorous mixing procedure adopted. The results for both mechanical and Brabender mixing procedures are nearly the same. Higher particle breakage shows

that the selected method can be used for manufacturing syntactic foams having up to 40 wt.% cenospheres. Compatibilization of HDPE and cenospheres results in good interfacial bonding. During cenosphere/HDPE synthesis in PIM, owing to functionalized HDPE, matrix flow around the silane treated particles gets constrained and leads to higher shear forces during mixing in the screw zone (Figure 2.3b). Further, broken particle fragments have density (about 3.5 g/cm^3), which is 3.4 and 2.5 times higher than the density of cenospheres and HDPE matrix, respectively. Although fractured particles do not provide the reduction in density as planned, they still help in replacing more expensive HDPE resin and make the component cheaper. Observations on a freeze fractured surface in Figure 3.9b show a large number of intact particles in H60-U-MM syntactic foams manufactured at 160°C , 30 bar, apart from debris embedded in the HDPE matrix. The intact particles will be useful in density reduction as well as energy absorption under compression.

Higher quality specimens having lower fraction of particle breakage can be manufactured by other methods as has been demonstrated under laboratory conditions with greater control over environment. However, use of an industrial scale machine allows evaluating the actual material quality that can be delivered if a product is developed. The specimens containing 60 wt.% cenospheres will be evaluated to understand if broken particles provide any benefit in the material properties. Cenospheres contain defects in their walls. Such defects reduce the strength of cenospheres compared to the value estimated based on their true particle density and wall thickness. Previous studies on hollow SiC particles with porous walls have shown that such defects can drastically reduce the properties of the particles (Shunmugasamy et al. 2014).

3.5 Tensile behavior

3.5.1 Untreated constituents

A representative set of stress-strain graphs for HDPE and syntactic foams are presented in Figure 3.12. One of the major differences in the trend is that the HDPE specimens show failure strain over 120%, whereas the composite specimens fracture at 8-11% strain. The failure strain reduces with increasing cenosphere content. The

stress-strain graph for the neat resin shows a long perfectly plastic region that ranges from 40-120% strain.

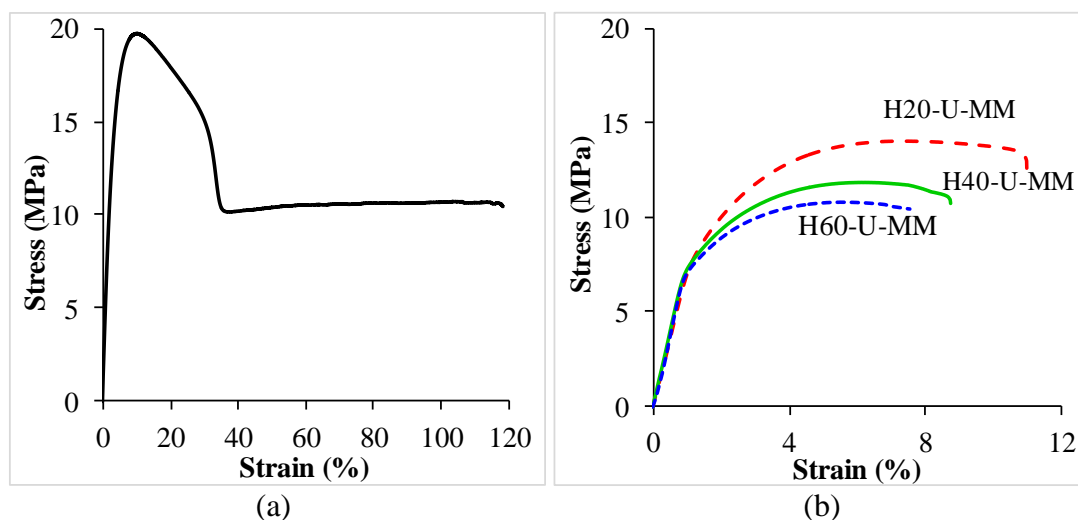
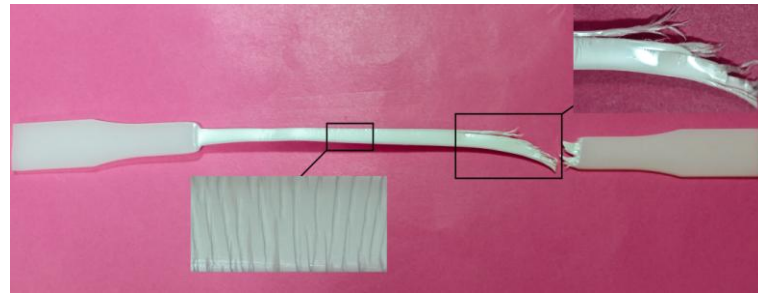


Figure 3.12 Tensile stress-strain curves for (a) neat HDPE and (b) syntactic foams having 20, 40 and 60% cenospheres by weight. Note x-scale is different in both the figures.

A representative fractured specimen of HDPE is shown in Figure 3.13a. The long necking region in the HDPE specimen corresponds to the large plastic deformation seen in the stress-strain graph. Inset in Figure 3.13a show the plastic deformation marks perpendicular to the direction of tensile loading throughout the specimen length. The final failure appears to be fibrous and has a broom-like fracture front. The inset of failure zone in Figure 3.13a shows such features clearly, where plastic deformation seems to draw the fibers leading to fracture.

The failure of syntactic foams appears to be relatively brittle with only a little plastic deformation. The failure surfaces presented in Figure 3.13b-e for syntactic foams do not show macroscopic deformation as is evident in neat HDPE specimens. Syntactic foams show relatively brittle fracture which can be attributed to stiff cenospheres present in ductile HDPE matrix. The measured tensile modulus, UTS, elongation at UTS, fracture strain and strength of HDPE and syntactic foams are listed in Table 3.3. The modulus of syntactic foams increases with cenosphere content.



(a)



(b)



(c)

(d)

(e)

Figure 3.13 A representative failed specimen of (a) HDPE and (b) syntactic foams. Fracture surface of (c) H20-U-MM (d) H40-U-MM and (e) H60-U-MM specimens. The fracture appears different from the fibrous fracture observed for the neat HDPE resin.

Table 3.3 Average modulus, strength, elongation and fracture behavior of HDPE and syntactic foams with untreated constituents.

Materials	Modulus (MPa)	UTS (MPa)	Elongation at UTS (%)	Fracture Strain (%)	Fracture strength (MPa)
H	529±19	19.9±0.26	10.21±0.13	120.85±6.86	19.9±0.19
H20-U-MM	574±25	14.1±0.10	7.40±0.16	10.38±0.44	12.95±0.38
H40-U-MM	723±27	12.1±0.44	6.40±0.34	9.42±0.72	11.18±0.33
H60-U-MM	661±65	11.0±0.55	5.60±0.41	7.76±0.37	10.30±0.55

It can also be noted from Table 3.3 that the UTS decreases with increasing cenosphere content. The matrix is the effective load bearing phase in particulate composites. Decrease in load bearing section of the composite because of lower matrix content at high cenosphere loading results in reduction in UTS.

The syntactic foam specimen's fracture at significantly lower strain compared to the neat HDPE specimens. The average fracture strain for H20-U-MM, H40-U-MM and H60-U-MM specimens is measured as 10.38, 9.42 and 7.76%, respectively. The lack of necking and large scale plastic deformation is apparent in the stress strain graphs of syntactic foams.

The fracture strength of syntactic foams is lower than that of the neat resin. Broken cenospheres owing to PIM process acts as stress concentrators, lowering fracture strength of SF's. The combination of ultimate tensile strength and fracture strength should be carefully analyzed.

In some applications where large scale plastic deformation after necking is not acceptable or desirable, the use of neat HDPE can be only up to about 10% strain, where the stress peak appears. This level of strain is comparable for HDPE and syntactic foams. It is also noted that syntactic foams fracture close to their UTS, whereas for neat resin the strength reduces significantly before becoming stable during the necking region.

The failure surface of HDPE resin is observed in Figure 3.14. Plastic deformation marks that are visible in Figure 3.13a, have deformation features that are smaller than 10 μm . The failure zone shows extensive fibrous failure. Some of these fibers are of submicron range diameter (Figure 3.14b). The failure surface of H40-U-MM is presented in Figure 3.15. Ductile fracture of the matrix is visible in this image in the form of wide deformation bands which formed due to plastic deformation of resin in the spaces between particles.

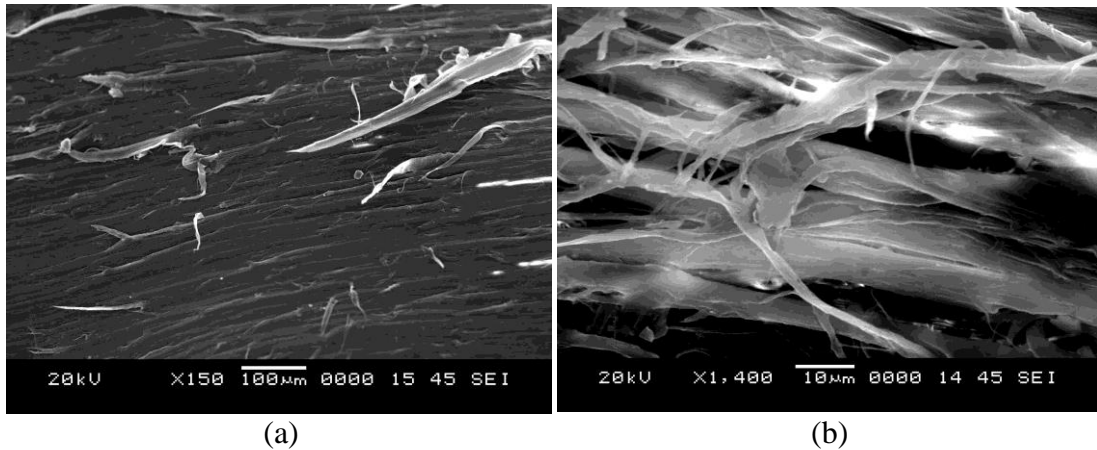


Figure 3.14 (a) Material flow lines with few separated fibers of HDPE before failure and (b) image close to the fracture zone showing formation of fibers that range from submicron to a few μm in diameter.

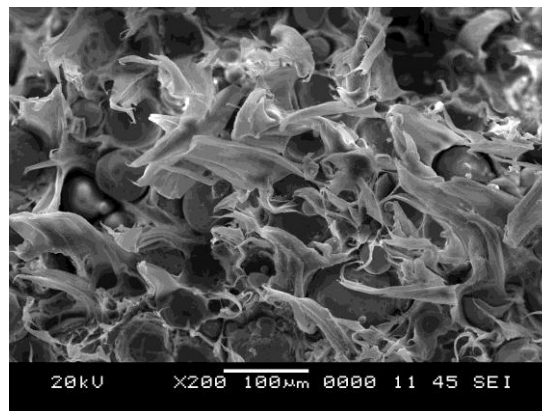


Figure 3.15 Failure surface of H40-U-MM showing HDPE matrix deformation.

A dimpled network with the debonded particles dispersed uniformly throughout the matrix is seen in all the fractured syntactic foam samples. Similar features are also observed in H60-U-MM (Figure 3.16a). The plastic deformation of HDPE resin results in formation of fibers that have submicron diameter range as observed in Figure 3.16b.

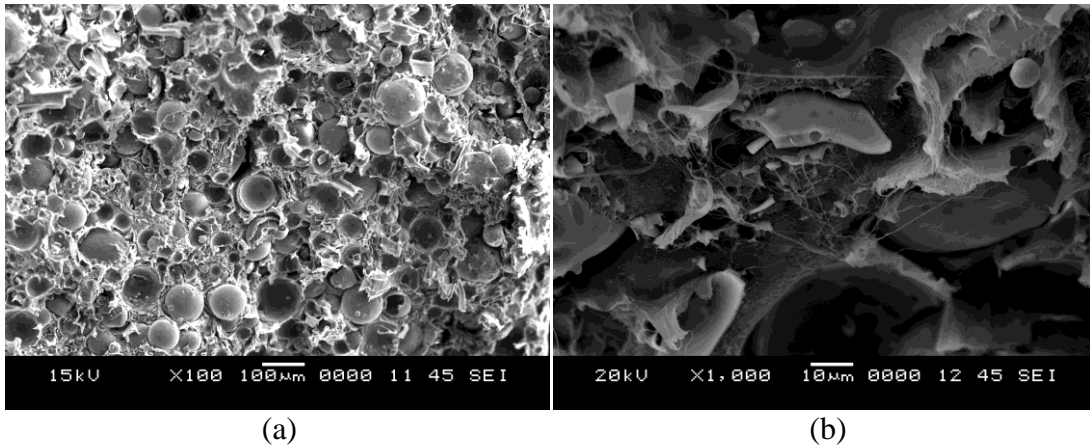


Figure 3.16 Fracture surface of H60-U-MM specimen showing (a) plastic deformation of matrix and several intact cenospheres that have not fractured and (b) the higher magnification shows local plastic deformation of HDPE resulting in sub-micron scale diameter fibers of HDPE.

Formation of such fine diameter fibers requires a significant amount of energy because of the creation of very high new surface area. However, comparing the HDPE failure in Figure 3.14 and syntactic foam failure surface in Figure 3.16, it is observed that the resin shows much more plastic deformation even at the microscopic level. Further observations on H60-U-MM foams in Figure 3.17a show debris of cenospheres on the fracture surface. Particle matrix interfacial bonding is poor in the present specimens as seen in Figure 3.17b.

Improvement in the interfacial bonding is expected to improve the load transfer from the matrix to the particle and improve the properties of syntactic foams. Previously, similar failure features are observed in tensile failure of epoxy matrix syntactic foams containing glass hollow particles (Gupta and Nagorny 2006). Use of silane coupling agents has been explored previously in cenosphere/HDPE syntactic foams processed by other methods (Deepthi et al. 2010).

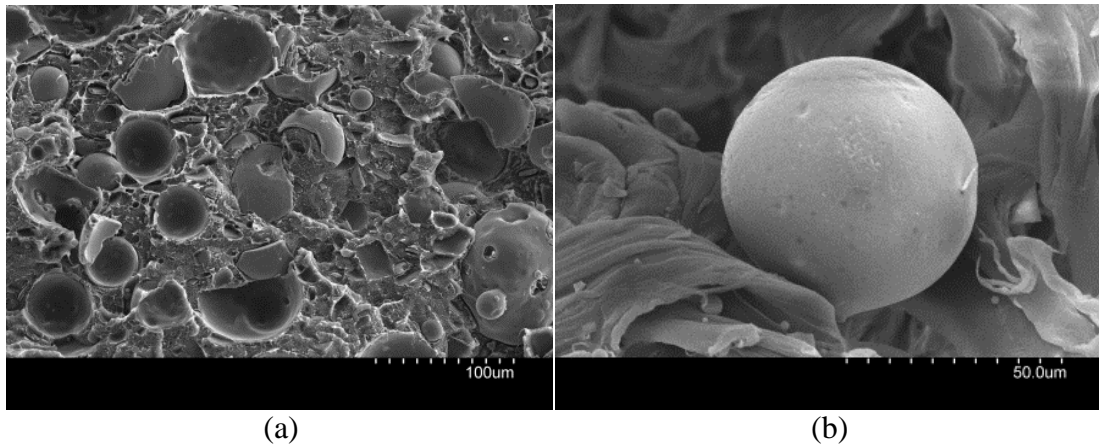


Figure 3.17 (a) Debris of cenospheres in a failed H60-U-MM specimen and (b) A cenosphere in a H60-U-MM syntactic foam specimen.

Table 3.4 presents specific properties of HDPE and syntactic foams, which are important in materials selection for weight sensitive applications. A decreasing trend is observed for specific strength with values within the range of 0.014-0.011 MPa/kg/m³ as the cenosphere content is increased. These values are lower than that for HDPE, which is 0.019 MPa/kg/m³. Compared to the E/ρ , E/ρ^2 and E/ρ^3 values of 0.501 (MPa/kg/m³), 0.474×10^{-3} (MPa/(kg/m³)²) and 0.449×10^{-6} (MPa/(kg/m³)³), respectively, all three parameters have higher values for syntactic foams. Higher values of E/ρ , E/ρ^2 and E/ρ^3 affirm that the use of syntactic foams can lead to weight savings in molded components. These three parameters appear to be the highest for H40-U-MM syntactic foams. Fracture of cenospheres in H60-U-MM syntactic foams increases their density and reduces the specific strength and modulus.

Table 3.4 Specific tensile properties of HDPE and syntactic foams.

Materials	Specific UTS (MPa/kg/m ³) $\times 10^{-3}$	E/ρ (MPa/kg/m ³)	E/ρ^2 (MPa/(kg/m ³) ²) $\times 10^{-3}$	E/ρ^3 (MPa/(kg/m ³) ³) $\times 10^{-6}$
H	18.84	0.501	0.474	0.449
H20-U-MM	13.88	0.565	0.556	0.547
H40-U-MM	12.01	0.717	0.712	0.706
H60-U-MM	10.76	0.647	0.633	0.619

3.5.1.1 Theoretical analysis for untreated constituents

A theoretical model developed for syntactic foams and extensively validated with epoxy/glass and vinyl ester/glass microballoon syntactic foams is applied to the

cenosphere/HDPE syntactic foams (Aureli et al. 2010). The model involves solving for the elastic properties of a composite containing an infinitely dilute dispersion of hollow particles and extending the results to high particle loadings using a differential scheme. The differential scheme, which contains a correction factor to account for the reduced volume available for hollow particles to occupy as the fraction of particles is increased, is given as,

$$\frac{dE}{E} = f_E(E_c, \nu_c, E_m, \nu_m, \eta) \frac{d\Phi_f}{1 - \Phi_f/\Phi_m} \quad (3.2)$$

where E_c and ν_c are the Young's modulus and Poisson's ratio of the ceramic particle wall, E_m and ν_m are the modulus and Poisson's ratio of the matrix material. In addition, Φ_f represents cenosphere volume fraction and Φ_m denotes the maximum packing factor of particles, taken to be 0.637, representing random packing factor of equal size spheres. The modulus of the matrix material is taken from the experimental data and the Poisson's ratio is assumed to be 0.425.

To determine the properties of the ceramic walls, the rule of mixtures approach (Matsunaga et al. 2002) is applied using the composition of the fly ash obtained for this study. The presence of minor constituents is ignored, and the modulus and Poisson's ratio of the ceramic are estimated to be 157 GPa and 0.19, respectively. The parameter η is the radius ratio of the hollow particles, defined as the ratio of the inner to outer radius. Assuming that the cenosphere wall is uniform and fully dense, the value of η can be determined by,

$$\eta = \sqrt[3]{1 - \frac{\rho_{TPD}}{\rho_c}} \quad (3.3)$$

where ρ_{TPD} is the true particle density and ρ_c is the density of the ceramic, also obtained by the rule of mixtures for cenosphere considering alumino-silicate composition. The properties of cenospheres are unknown in the present work as they

cannot be meaningfully measured through experiments due to defects in the cenosphere walls. Therefore, parametric studies are conducted using the theoretical model to get an insight into the properties of cenospheres.

In Figure 3.18a, the calculated wall material modulus is kept constant at 157 GPa and the radius ratio is varied to obtain an effective wall thickness for the cenospheres. Close agreement is seen for $\eta = 0.995$. Similarly, in Figure 3.18b the wall thickness obtained by density measurements is kept constant corresponding to estimated value of $\eta = 0.9$ and the ceramic modulus is varied, with good agreement seen when $E_c = 7.5$ GPa. These two pairs of effective properties are then used to calculate an effective modulus \bar{E} for the hollow particle using the method developed by Li G et al. (1999), which is given as,

$$\bar{E} = \frac{E_c(1-2\nu)(1-\eta^3)}{(1-2\nu) + \left(\frac{1+\nu}{2}\right)\eta^3} \quad (3.4)$$

For both pairs of properties obtained by fitting the theoretical model to the experimental data, the effective particle modulus is calculated to be 1.20 GPa using this method. A similar level of significant reduction in effective properties of hollow particles is observed previously for SiC particles having porous walls (Shunmugasamy et al. and Labella M et al. 2014). Selection of higher quality particles is possible with additional steps that involve pressurization of cenospheres to higher pressure and separating out the surviving particles. However, such additional processes add cost and are only justified if the end product can benefit from them.

The mathematical model considered perfect bonding between particle and matrix. Some reduction in predicted values is expected if no bonding is assumed. It is also known that change in wall thickness greatly influences the mechanical properties as previously reported (Gupta N and Nagorny 2006).

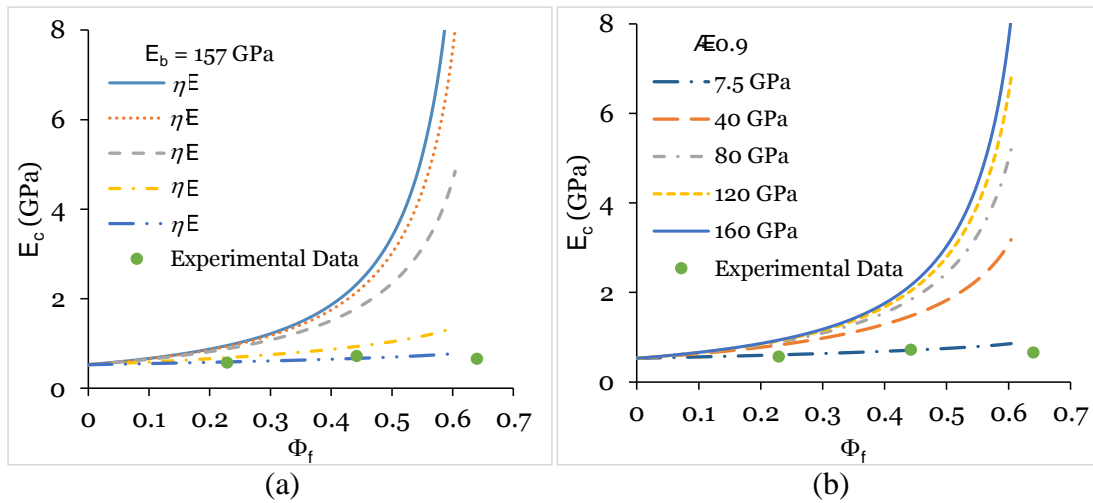


Figure 3.18 Results from Porfiri-Gupta model. In (a) the particle wall modulus obtained from the rule of mixtures method is kept constant and the radius ratio is varied. In (b) the radius ratio determined by density measurements is maintained constant and the ceramic modulus is varied.

3.5.2 Treated constituents

Virgin and functionalized HDPE resin

Figure 3.19 presents a representative set of stress-strain graphs for virgin and functionalized HDPE. Virgin HDPE exhibits failure strain of over 120% while the functionalized HDPE fails at 52% strain. With functionalization, failure strain reduces. The stress-strain graph for the virgin HDPE shows a long perfectly plastic region that ranges from 40-120% strain.

A representative fractured specimen of virgin HDPE is presented in Figure 3.13a and is discussed in earlier section. Long necking region, plastic deformation marks and broom like fracture front is seen in HDPE samples. The influence of functionalization on the failure pattern of HDPE specimens is in Figure 3.20, where the failure occurs at lower strain with only a little necking. In the virgin material, the polymer fibers act as separate entities (Figure 3.21a). These micro-fibers stretch before breaking into a broom like structure (Figure 3.13), leading to higher failure strain. Functionalization changes the failure features at the microstructure level (Figure 3.21b). It has been proposed that these changes following functionalization are likely related to the reduction in crystallinity due to the presence of the maleate groups and their interactions with one another (Wang Y et al. 1994).

The measured tensile modulus, ultimate tensile strength (UTS), elongation at UTS, and stress and strain at fracture of HDPE are listed in Table 3.5. The modulus, fracture strain, UTS and fracture strength are of 132, 133, 34 and 30% higher, respectively, for virgin HDPE compared to the functionalized polymer. However for functionalized HDPE the elongation at UTS is 349% higher than for the virgin material.

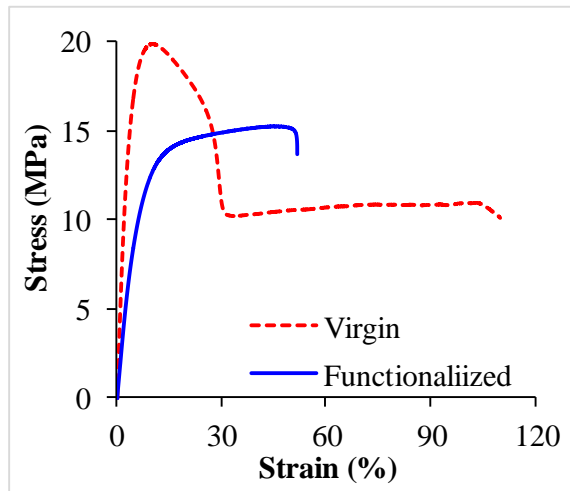


Figure 3.19 Comparison of representative stress-strain curves of virgin and functionalized HDPE.

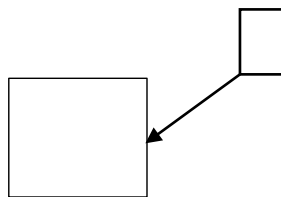
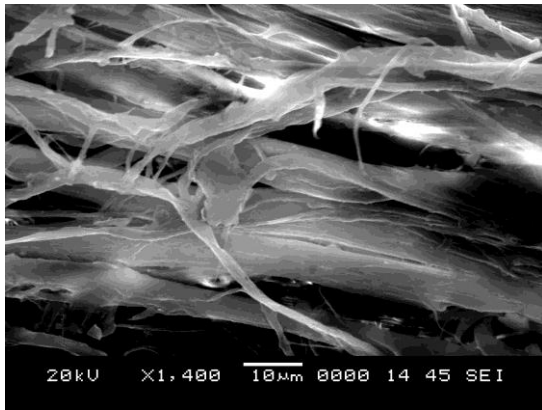


Figure 3.20 A representative failed specimen of functionalized HDPE.



(a)

(b)

Figure 3.21 Micrographs of representative tensile tested specimen of (a) virgin and (b) functionalized HDPE.

Table 3.5 Tensile properties of virgin and functionalized HDPE. The values are presented in average.

HDPE	Modulus (MPa)	Elongation at UTS (%)	Fracture strain (%)	UTS (MPa)	Fracture strength (MPa)
Virgin	529±19	10.21±0.13	120.85±6.86	19.9±0.26	19.9±0.19
Functionalized	228±9	45.83±1.12	51.91±2.21	14.9±0.19	15.3±0.24

Syntactic foams

Representative stress-strain curves of syntactic foams prepared by different blending routes are presented in Figure 3.22. Syntactic foams with treated constituents blended with both the mixing routes exhibit similar failure features as presented in Figure 3.13b-e. The characteristics of the stress-strain curves are similar for all syntactic foam types with distinct elastic and plastic regions.

Table 3.6 and Table 3.7 present the measured tensile properties of syntactic foams. The modulus of syntactic foams increases with cenosphere content except for H60-U-MM. This trend is very weak in the case of T_M-MM specimens (Figure 3.22b). The addition of stiffer filler particles that are strongly bonded to the matrix restricts the mobility of HDPE, increasing the modulus. Due to relatively lower filler content, H20 samples show the highest strain at UTS (Figure 3.22) and fracture strain among all syntactic foams and processing paths. Functionalization of the HDPE leads to a decrease in the modulus of the matrix, which is only partially compensated by the modulus gains resulting from improved interfacial bonding of the cenospheres.

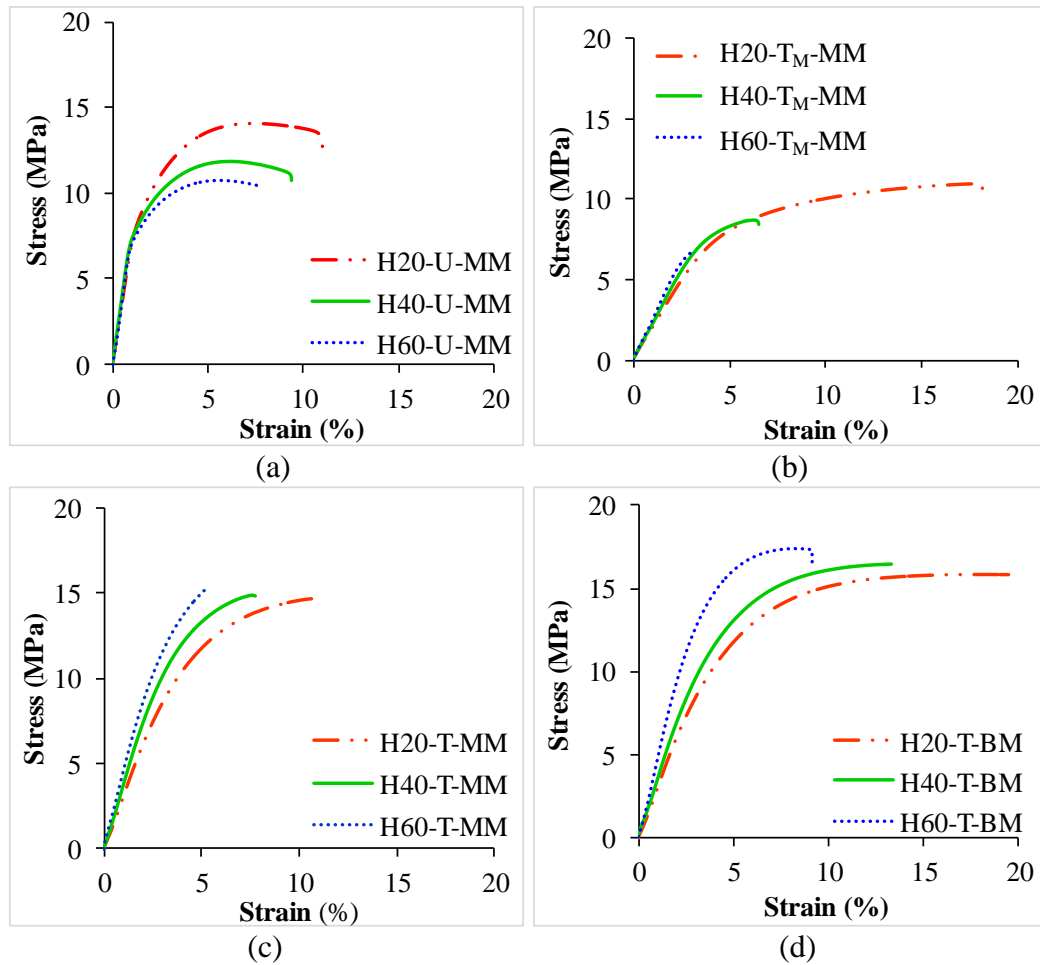


Figure 3.22 Stress-strain behavior of H20, H40 and H60 syntactic foams synthesized by (a) U-MM (b) T_M-MM (c) T-MM and (d) T-BM routes.

Table 3.6 Modulus, elongation at UTS and fracture strain of syntactic foams.

Syntactic foam type	Modulus (MPa)				Elongation at UTS (%)				Fracture strain (%)			
	U-MM	T _M -MM	T-MM	T-BM	U-MM	T _M -MM	T-MM	T-BM	U-MM	T _M -MM	T-MM	T-BM
H20	574 ±25	213 ±8	268 ±10	285 ±12	7.42 ±0.16	16.92 ±0.19	10.86 ±0.11	17.94 ±0.44	10.38 ±0.44	18.89 ±0.55	11.02 ±0.21	18.94 ±1.11
H40	723 ±33	226 ±11	351 ±14	327 ±11	6.37 ±0.34	6.25 ±0.22	7.61 ±0.28	12.82 ±0.69	9.42 ±0.72	7.09 ±0.35	7.97 ±0.33	13.29 ±0.89
H60	661 ±65	246 ±17	375 ±20	403 ±19	5.61 ±0.41	3.44 ±0.34	3.13 ±0.32	8.37 ±0.51	7.76 ±0.37	3.98 ±0.83	5.34 ±0.43	8.94 ±0.63

Table 3.7 UTS and fracture strength of syntactic foams.

Syntactic foam type	UTS (MPa)				Fracture strength (MPa)			
	U-MM	T _M -MM	T-MM	T-BM	U-MM	T _M -MM	T-MM	T-BM
H20	14.06 ±0.10	10.92 ±0.21	14.29 ±0.55	15.86 ±0.62	12.95 ±0.38	10.39 ±0.24	13.51 ±0.31	15.37 ±0.41
H40	12.07 ±0.44	8.92 ±0.39	14.81 ±0.67	16.53 ±0.51	11.18 ±0.33	8.39 ±0.31	14.21 ±0.56	16.39 ±0.71
H60	11.03 ±0.55	7.33 ±0.55	15.36 ±0.79	17.44 ±0.74	10.30 ±0.55	6.73 ±0.41	14.47 ±0.71	16.45 ±0.75

Among the treated composites, the greatest increase in modulus is observed for T-BM processing. Improved dispersion of cenospheres in HDPE and interfacial bonding due to reactive blending in brabender, results in such a trend. Elongation at UTS and fracture strain decreases with increase in filler content for all the blending routes. The presence of the stiff filler particles restricts the ability of the matrix to flow and form stable fibers as observed in the failure surfaces of virgin HDPE.

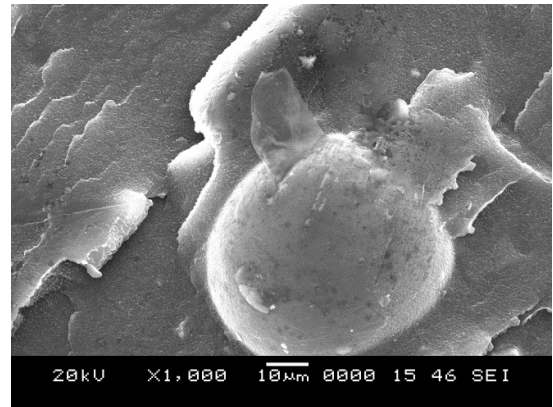
For the syntactic foams with treated constituents, elongation at UTS decreases in the range of 115-392% whereas this reduction for U-MM is merely 32% with respect to lowest filler content. The syntactic foams also fracture at significantly lower strain compared to the neat HDPE specimens. Fracture strain reduces by 34% in U-MM, while a decrease of 112-375% is seen with treated constituents with respect H20. The lack of necking and large scale plastic deformation is apparent in the stress-strain graphs for the syntactic foams.

It can be observed from Figure 3.22b-d and Table 3.7 that the strength of syntactic foams decreases for U-MM and T_M-MM and increases in case of T-MM and T-BM, with increasing cenosphere content.

Micrographs of representative H40 specimens acquired for all the blending routes are presented in Figure 3.23. Cenospheres-HDPE bonding is poor in U-MM as observed by Figure 3.23a. Further, though HDPE is functionalized, an absence of interfacial bonding in T_M-MM is observed due to untreated cenospheres in Figure 3.23b. Figure 3.23c shows linkages between cenospheres and HDPE resulting in improved interfacial strength in T-MM, which improves UTS and fracture strength in these syntactic foams compared to U-MM and T_M-MM specimens. Finally, reactive blending in T-BM forms a seamless interface between the filler and matrix as evident from Figure 3.23d, resulting in the highest ultimate strength levels.

(a)

(b)



(c)

(d)

Figure 3.23 Micrographs of H40 syntactic foams synthesized by (a) U-MM (b) T_M-MM (c) T-MM and (d) T-BM routes. All images are acquired at the same magnification.

It can also be noted in Table 3.7 that the UTS decreases with increasing cenosphere content for U-MM and T_M-MM, while a reverse trend is observed for T-MM and T-BM syntactic foams. Decrease in the load bearing section due to lower matrix content at higher filler loading results in a reduction of UTS in the specimens when the interfacial bonding is poor. Functionalization of HDPE promotes effective load transfer through the particle-matrix interface, which is evident from higher UTS and fracture strengths.

3.5.2.1 Theoretical analysis for treated constituents

In order to better understand the effects of the processing parameters on the properties of syntactic foams theoretical modeling approaches are applied to the experimental results. The existing models relate the elastic properties of syntactic foams to the elastic modulus of matrix, particle and the particle wall thickness (Bardella L et al.

2012, Bardella L and Genna F 2001, Porfiri M and Gupta N 2009). The particle wall thickness is modeled in the form of radius ratio ' η ' (Gupta N et al. 2004, Gupta N and Woldesenbet E 2004). The radius ratio of 1 corresponds to an air void while radius ratio of 0 corresponds to a solid particle. In tensile loading, the effect of these parameters on the ultimate strength is dominated by the effects of particle-matrix debonding in low stiffness polymer matrices. Therefore, the tensile strength of syntactic foams can often be modeled effectively using general solid particulate composite approaches with appropriate effective stiffness of particles, without considering the geometric effect of wall thickness or void. In this work, the tensile modulus is modeled using the Bardella-Genna model for syntactic foams (Bardella L and Genna F 2001) and the tensile strength is modeled using the Pukanszky model (Turcsanyi B et al. 1998). For both models, the volume fraction of hollow particles ' Φ ' in each syntactic foam is calculated from the nominal mass fraction and reduced according to the estimated particle breakage fraction obtained from density measurements of the fabricated specimens.

Tensile Modulus

The theoretical models for hollow particle composites, including the Bardella-Genna model used here, assume that there is perfect bonding between the particle and the matrix. As this may not be the case in the present work, an approach is taken where the model is used to obtain a least squares best fit estimate of the radius ratio parameter η in the model, while using the wall material modulus found according to the cenosphere composition. This effective value for η encapsulates information about the loss in reinforcing capability of cenospheres due to defects in the particle wall as well as due to the imperfect interfacial bonding. The rule of mixtures approach for determining the properties of the ceramic wall is described in a preceding section and yields the elastic modulus and Poisson's ratio to be 157.4 GPa and 0.185 respectively. Using these parameters, the measured modulus of the matrix and assuming the Poisson's ratio of HDPE to be 0.425, the model is fitted to the experimental data for each material type with the radius ratio as the free parameter. The full expression of this micromechanics-based model is lengthy and available in original article by Bardella L and Genna F (2001). The resulting model predictions are compared to the experimental data in Figure 3.24a. For U-MM, T_M-MM, T-MM,

and T-BM the effective radius ratios are found to be 0.9945, 0.9986, 0.9957 and 0.9956 respectively. These values are significantly higher than that obtained by density measurements and measurement in SEM images (Figure 3.8), which yield a radius ratio around 0.9. It indicates that for all the syntactic foams the stiffening efficiency of the particles is significantly lower than what is expected for particles of defect free walls having perfect bonding with the matrix. Testing in compression would likely yield a smaller effective radius ratio (greater stiffening effect) because the matrix is pushed into the interface reducing the importance of interfacial bonding. T-MM and T-BM have approximately the same effective cenosphere properties and T_M -MM shows the lowest effective properties (highest effective η). U-MM shows the lowest effective η of all the compositions because the higher matrix modulus leads to a lower particle wall to matrix modulus ratio, which the model compensates for by increasing the effective wall thickness.

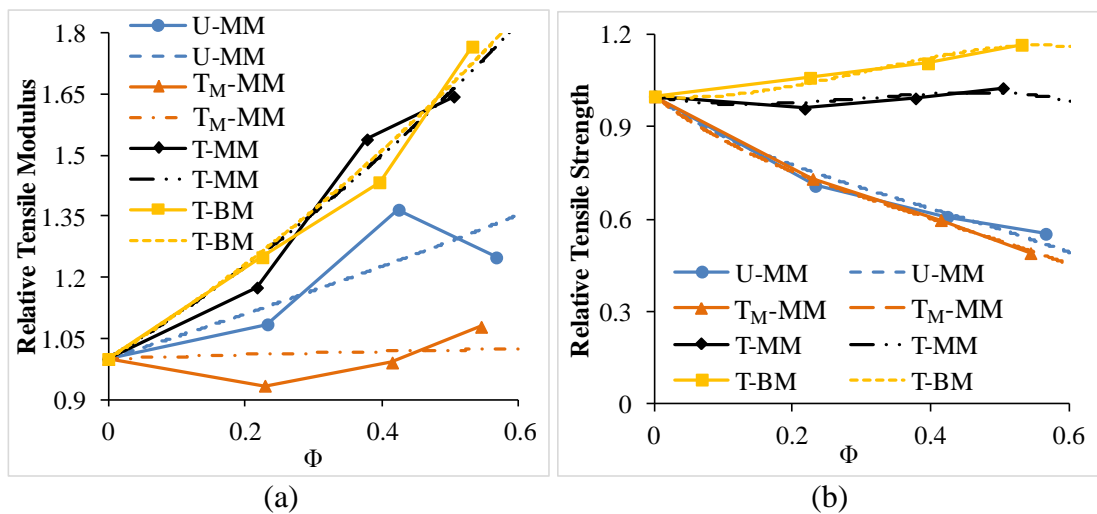


Figure 3.24 Least squares best fits of (a) Bardella-Genna model for modulus and (b) Pukánszky model for tensile strength represented with respect to the properties of neat resin. Solid lines with symbols represent experimental data and dashed lines are model fits. Note y-scale is different in both the figures.

Tensile Strength

The models for the tensile strength of particulate reinforced composites are strictly decreasing functions of filler volume fraction (Fu et al. 2008) as it is generally assumed that poor interfacial adhesion prevents load transfer from the matrix to the particle. For composites that do not necessarily follow this trend, the relationship

proposed by Turcsanyi B et al. (1998) and Pukanszky B (1990) can be applied. The expression is given by,

$$\sigma_c = \frac{1 - \Phi}{1 + 2.5\Phi} \sigma_m \exp(B\Phi) \quad (3.5)$$

where σ_c is the strength of the composite, σ_m is the strength of the matrix and the parameter B is related to the interfacial strength. There is no reinforcing effect when $B = 0$, while the strength of the composite increases with increasing filler content for $B > 3$. For U-MM and T_M-MM the value of B is approximately 1.81, while for the two types of syntactic foams with strong interfacial bonding, T-MM and T-BM, the value of B is found to be approximately 3.17. These results show that syntactic foams with untreated particles have poor interfacial bonding and the strength decreases with particle content as seen in Figure 3.24b. Treatment of the particles has a significant impact on the interfacial bonding, causing the strength to increase with particle content (Figure 3.24b).

3.6 Flexural behavior

Virgin and functionalized HDPE resin

A representative stress-strain curve obtained from the flexural testing for non functionalized and functionalized HDPE resin is presented in Figure 3.25. The HDPE resin shows a non-linear behavior in this graph for both the samples. Specimens did not fail even after 10% strain, therefore the test is stopped and the results are plotted upto 5% strain. There is no visible sign of fracture during testing. Stress magnitude of 23.25 and 10.84 MPa is noted at 5% strain for non functionalized and functionalized HDPE sample. Higher load bearing capability (114%) of non functionalized HDPE as compared to its counterpart might be due to absence of tiny islands (Figure 3.26a) as seen in Figure 3.26b for functionalized HDPE. Such tiny features in functionalized resin results in stress concentration leading to lowering the performance. It would be worth to investigate if cenospheres can minimize stress concentration effect due to reactive blending in syntactic foams.

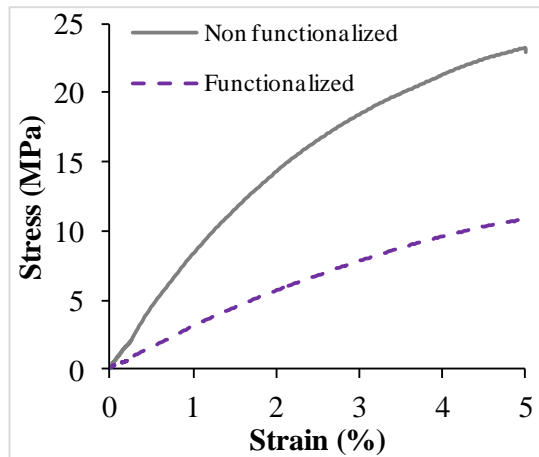


Figure 3.25 Stress-strain behavior of non functionalized and functionalized neat HDPE.

(a) (b)
Figure 3.26 Freeze fractured SEM images of (a) non functionalized and (b) functionalized HDPE samples after the test, acquired at same magnification. Tiny islands are observed for functionalized HDPE.

Syntactic foams

The stress-strain behaviors of syntactic foam specimens prepared by different blending routes are presented in Figure 3.27a-d. The trend of the stress-strain curves is similar for all composite types except for U-MM showing distinctly initial linear response followed by non-linear behavior. Load bearing capability decreases with increase in filler content as seen Figure 3.27a. Poor interfacial bonding between the constituents in U-MM (Figure 3.17b) results in such a behavior. For treated configurations of syntactic foams, only a small initial portion is linear elastic, while the most part of these curves is non-linear elastic and plastic (Figure 3.27b-d).

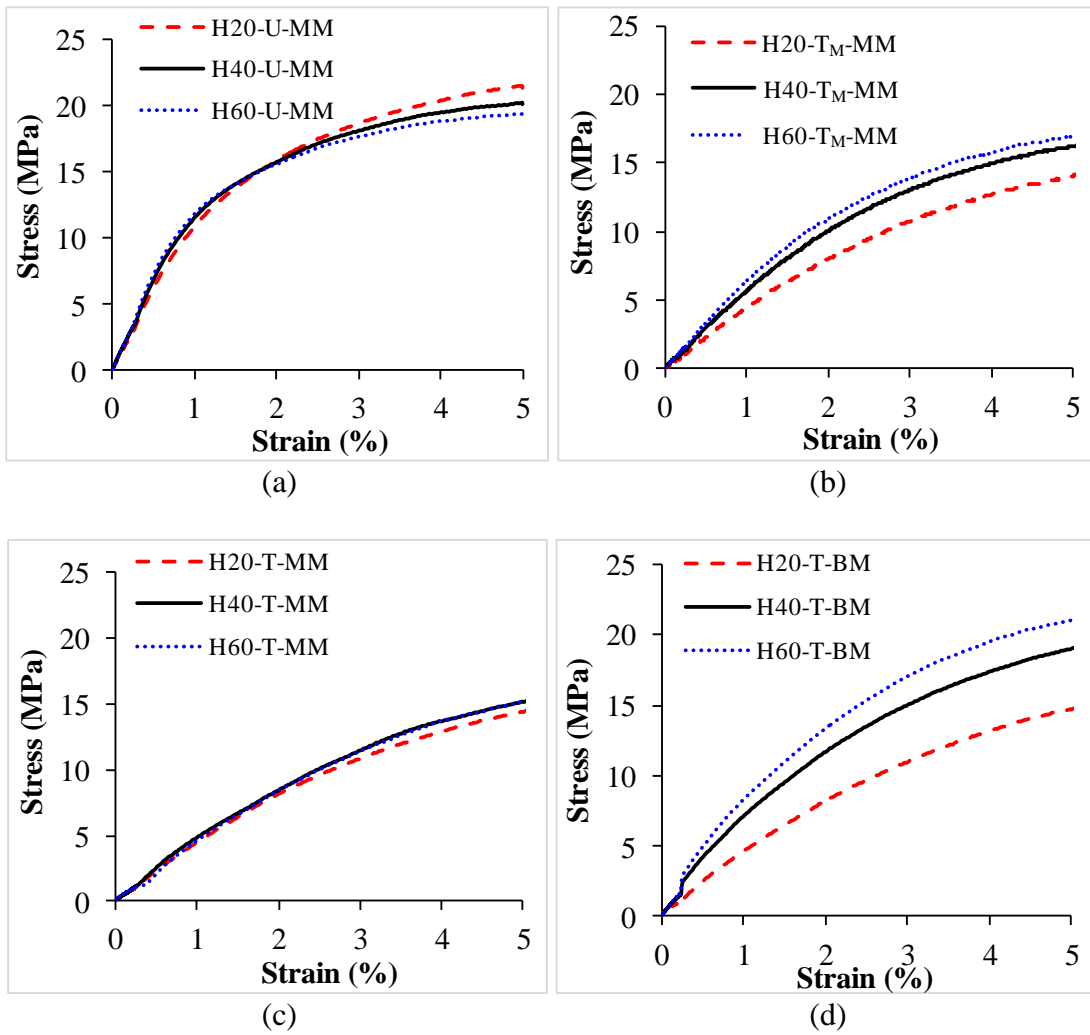


Figure 3.27 Stress-strain behavior of H20, H40 and H60 prepared by (a) U-MM (b) T_M -MM (c) T-MM and (d) T-BM routes.

It can be observed from Figure 3.27b-d that the strength of syntactic foam increases with the cenosphere content. This trend is very weak in the case of T-MM specimens (Figure 3.27c). This combination of materials and processing method resulted in the lowest survival rate of cenospheres as seen from Table 3.2. Figure 3.28 presents a comparison of stress-strain graphs with respect to different blending methods. Syntactic foams processed by brabender mixing show the highest level of strength in treated constituents regime, especially when the particle content is high. Untreated constituents (U-MM) presented better performance as compared to treated counterparts owing to higher particle survival rate (Table 3.2).

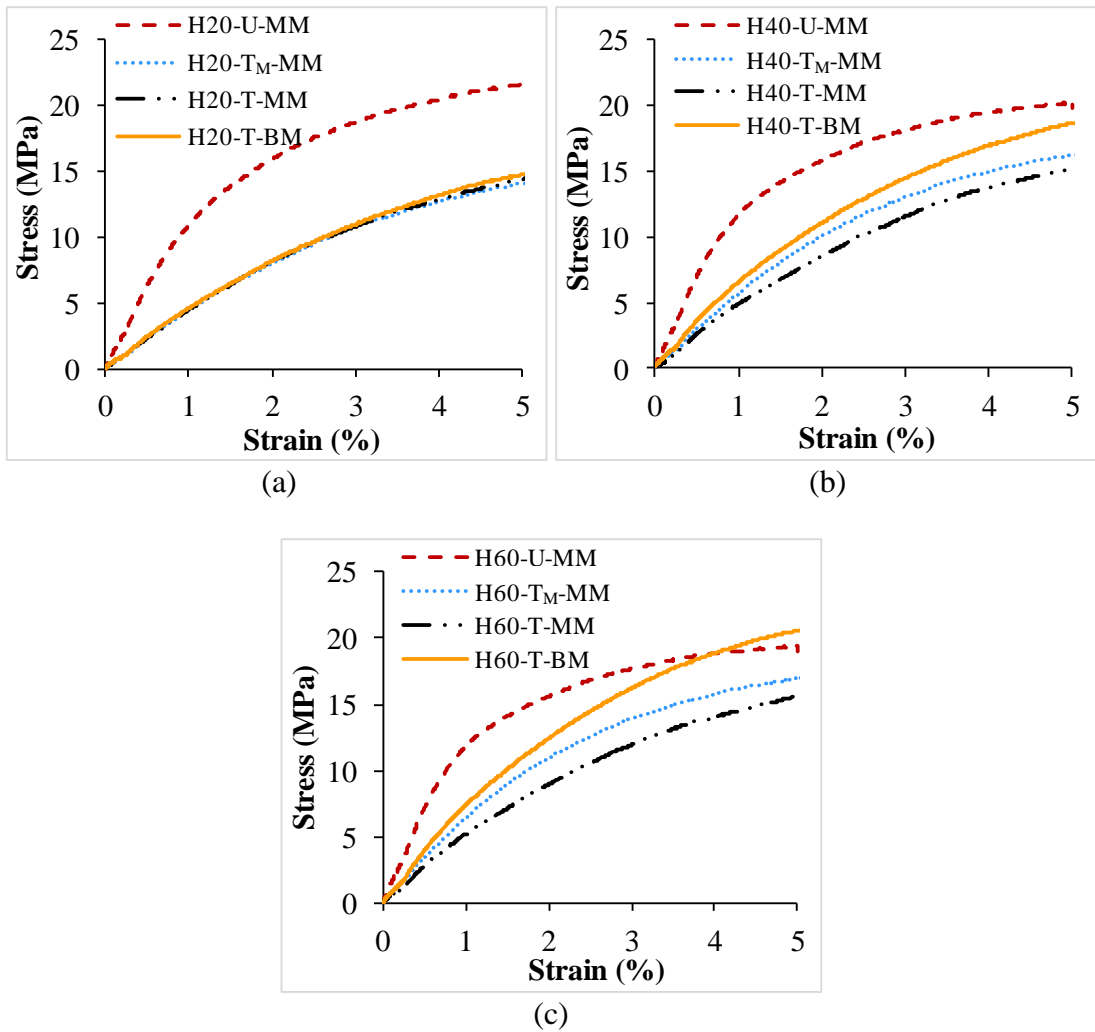


Figure 3.28 Comparison of stress-strain response for (a) H20 (b) H40 and (c) H60 syntactic foams as a function of blending methodology.

These results show the effectiveness of injection molding in dispersing cenospheres in the resin. Improved dispersion results in enhancing the mechanical properties of syntactic foams. Table 3.2 shows that the cenosphere fracture is lower in U-MM compared to other routes with treated constituents. Reduced particle breakage is also likely to contribute to increased strength. Flexural modulus and strength values for all syntactic foams and neat HDPE are presented in Table 3.8 and Figure 3.29. The modulus is found to increase with cenosphere content. Higher stiffness of cenosphere material compared to the HDPE resin helps in obtaining improvement in the stiffness of syntactic foams as the cenosphere content is increased. Highest modulus is observed in U-MM for all the variations of filler content compared to treated constituents.

Table 3.8 Flexural modulus and strength of materials.

Material	Modulus (MPa)				Strength (MPa)			
	U-MM	T _M -MM	T-MM	T-BM	U-MM	T _M -MM	T-MM	T-BM
H	713.8 ±1.2	204.67 ±5.2	-----	204.67 ±5.2	22.60 ±0.03	12.37 ±0.05	-----	12.37 ±0.05
H20	1108.14 ±10.8	407.85 ±19.8	341 ±9.5	365.94 ±12	21.13 ±0.59	16.21 ±1	15.73 ±0.04	15.83 ±0.79
H40	1192.5 ±20.1	514.75 ±12.4	382.11 ±12.5	534.23 ±15.2	19.54 ±0.42	17.6 ±0.54	15.98 ±0.08	18.98 ±0.73
H60	1253.68 ±35.2	677.29 ±28.4	417.11 ±14.8	659.44 ±16.8	19.17 ±0.21	17.79 ±0.92	16.81 ±0.13	21.07 ±0.53

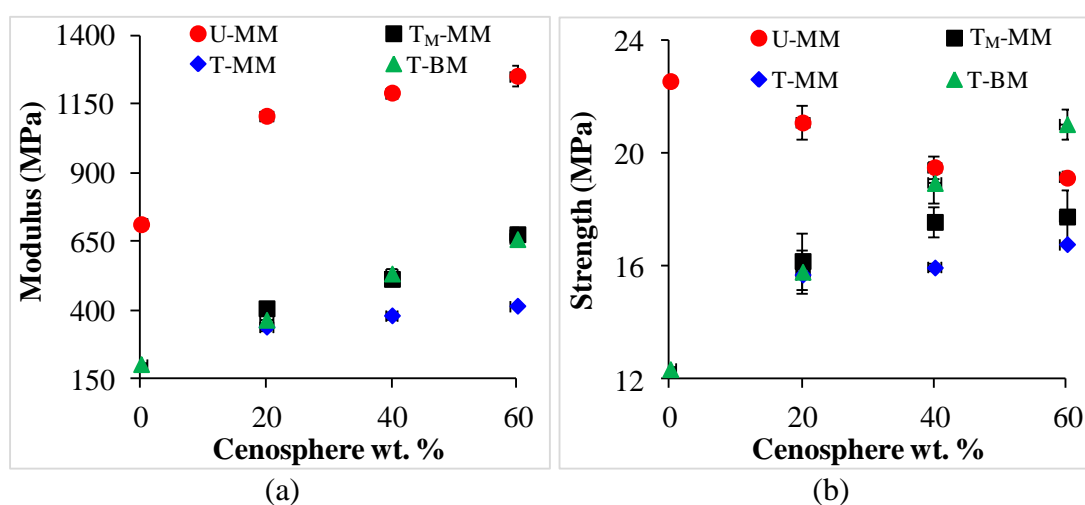


Figure 3.29 (a) Flexural modulus and (b) flexural strength of syntactic foams at different cenosphere contents.

Compared to the modulus of functionalized HDPE (T_M-MM) 204.7 MPa, the H60-T_M-MM, H60-T-MM and H60-T-BM syntactic foams had 231, 104 and 222% higher modulus. The flexural strengths for syntactic foams are presented in Figure 3.29b. The flexural strength is also found to increase with cenosphere content. All syntactic foams have higher strength than that of the HDPE resin. Compared to the strength of functionalized HDPE (12.4 MPa), the H60-T_M-MM, H60-T-MM and H60-T-BM syntactic foams had 44, 36 and 70% higher strength. Untreated constituents provide the highest benefit in flexural modulus. Rise in modulus is in the range of 201-249% for U-MM compared to all the treated configurations. For strength, untreated constituents have outperformed the treated ones except at H60.

3.6.1.1 Theoretical Analysis for flexural behavior

The bending behavior of the syntactic foams is analyzed using two theoretical models namely, Porfiri-Gupta and Bardella-Genna model. Porfiri-Gupta model has been

validated for epoxy and vinyl ester matrix syntactic foams containing engineered glass hollow particles (Porfiri, M and Gupta N. 2009, Gupta N et al. 2010, Aureli M et al. 2010). Further, Bardella-Genna model (Bardella L and Genna F 2001, Bardella L et al. 2012) considers a representative volume element and uses a homogenization scheme to estimate the bulk and shear moduli of the composite. The bulk modulus of the composite is given as,

$$K = K_m \frac{\delta(1 + \Phi\gamma) + \kappa(1 - \Phi)\gamma}{\delta(1 - \Phi) + \kappa(\gamma + \Phi)} \quad (3.6)$$

where

$$\gamma = \frac{4G_m}{3K_m}, \delta = \frac{4G_c}{3K_m}(1 - \eta^3), \kappa = \frac{4G_c}{3K_c} + \eta^3 \quad (3.7)$$

The G and K terms represent the shear and bulk moduli of the materials, which are derived from the elastic modulus and Poisson's ratio for each material (Bardella L and Genna F 2001, Bardella L et al. 2012). These two elastic constants then allows for the determination of the elastic modulus of syntactic foams by,

$$E = \frac{9KG}{3K + G} \quad (3.8)$$

The modulus of the matrix is taken from the experimental data, Poisson's ratio is taken as 0.425 which leads to estimates for the modulus and Poisson's ratio of 157 GPa and 0.19, respectively (Section 3.5.1.1). Radius ratio is determined to be 0.903 for the cenospheres as discussed in Section 3.5.1.1, yields similar results to the particle wall thickness measurements shown in Figure 3.6, giving an average radius ratio of 0.897. The predictions of the two models are compared to the experimental data in Figure 3.30. The volume fractions of cenospheres are reduced by the calculated fraction of broken particles. The two models are in close agreement for a dilute dispersion of particles, or up to 20 vol.%, but diverge at higher particle loadings due to increased particle to particle interactions and lower matrix content

except for composites with untreated constituents. At higher volume fractions the Porfiri-Gupta model shows closer agreement with U-MM, while the Bardella-Genna model shows closer agreement with the experimental data for T_M-MM and T-BM syntactic foams. The Bardella-Genna model can be used for identifying the parameters such as cenosphere volume fraction and true particle density that are expected to provide syntactic foams of desired properties. It is noted that the experimental values of modulus are lower than the predictions for 40 and 60 wt.% particles for treated constituents. This kind of trend is likely due to the presence of broken particles as stress concentration sites due to thin walls of cenospheres.

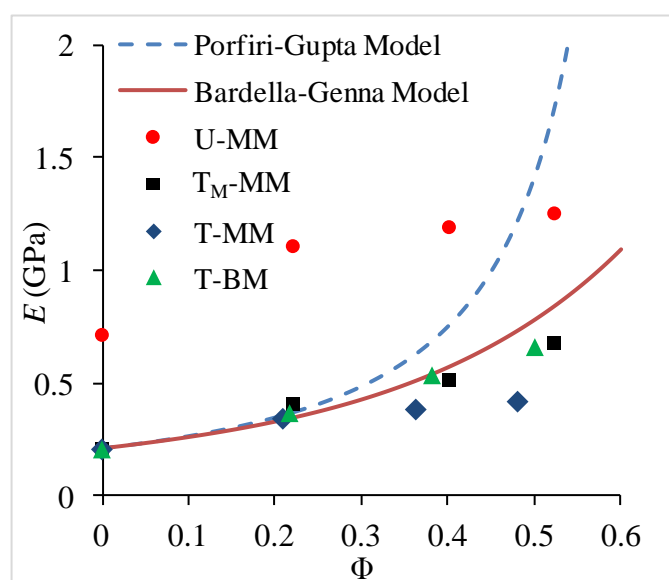


Figure 3.30 Comparison of model predictions with experimental data on modulus of syntactic foams.

*Syntactic foams prepared by injection molding technique registered higher tensile modulus and better flexural performance for U-MM route. While improvement in the interfacial bonding has improved the properties of syntactic foams in particular tensile strength, the decision to use these treatment methods must weigh the property benefits against increased processing time, costs and the environmental impacts in the context of the proposed application of syntactic foams. Thereby, **hereafter syntactic foams prepared through U-MM route are investigated.***

3.7 Quasi-static and high strain rate compression

3.7.1 Quasi-static

The quasi-static compressive stress-strain plots for the HDPE resin and syntactic foams at different strain rates are presented in Figure 3.31.

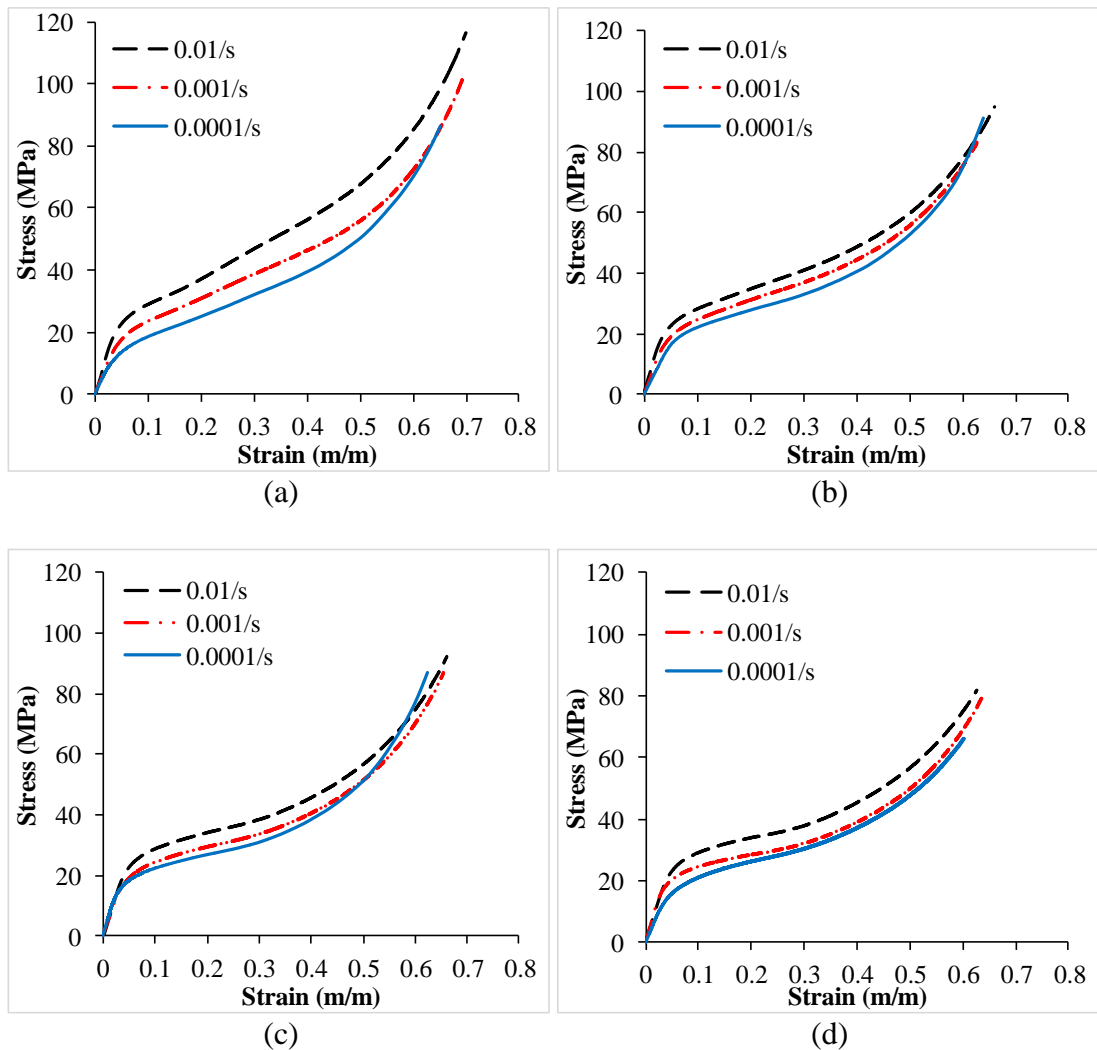


Figure 3.31 Comparison of stress-strain curves at different quasi-static compressive strain rates for (a) H (b) H20 (c) H40 and (d) H60.

The stress-strain behavior of HDPE syntactic foams is different from that observed for epoxy and vinyl ester matrix syntactic foams. Since epoxy and vinyl ester resins are brittle, a significant drop in stress is observed at the end of the initial linear elastic region followed by a stress plateau (Gupta N et al. 2010, Wouterson E M et al. 2005, Zhang L et al. 2014). The drop of stress is due to successive failure of brittle particles

in the matrix because of stress concentration in the localized region around broken particles (Kim J I et al. 2000). Such effects are mitigated in significantly more compliant HDPE resin above its glass transition temperature (T_g) at room temperature. Figure 3.31 also indicates that the strength and modulus of HDPE and syntactic foams increase with strain rate. As shown in Figure 3.32, the representative curve can be divided into three regions: (I) the initial elastic region with constant slope, (II) a post yield plastic deformation region with smaller slope and (III) plastic deformation region with higher and increasing slope that appears after densification. There is no clearly distinguishable stress plateau region that is a characteristic of foams and porous materials; instead, the thermoplastic syntactic foams continue to harden at all strains.

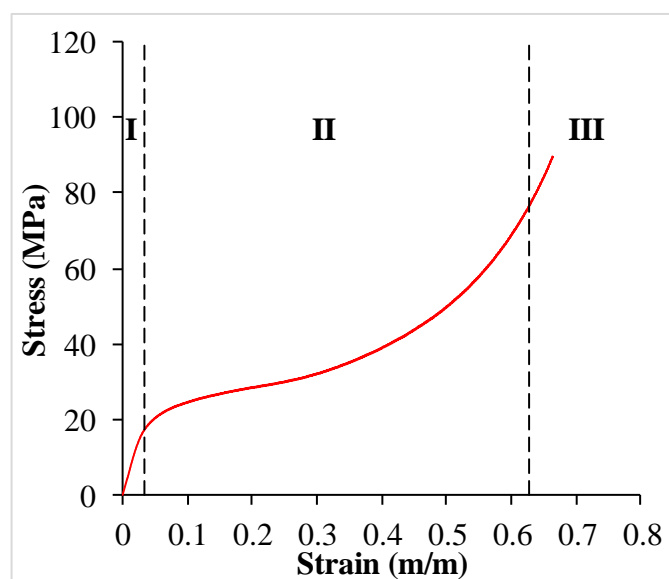


Figure 3.32 A representative compressive stress-strain curve at 10^{-3} strain rate for H60 syntactic foam showing three regions of different deformation behaviors (I: elastic deformation, II: post yield plastic deformation, III: plastic deformation beyond densification).

The measured mechanical properties of syntactic foams are presented in Table 3.9. Although some of the values have overlapping standard deviations, the average elastic modulus and compressive yield strength are observed to increase with strain rate for syntactic foams. H60 shows the highest yield strength for all compressive strain rates among all syntactic foams.

Table 3.9 Mechanical properties of HDPE and its composites under varying low strain rate compression conditions.

Material	Strain rate (s ⁻¹)	Elastic Modulus (MPa)	Yield strength (MPa)	Yield strain (%)	Energy absorption to 50% strain (MJ/m ³)	Densification stress (MPa)	Densification strain (%)
H	10 ⁻⁴	406 ± 56	10 ± 1.0	2.8 ± 0.1	16 ± 1.1	-	-
	10 ⁻³	454 ± 46	14 ± 1.4	3.1 ± 0.5	17 ± 0.7	-	-
	10 ⁻²	572 ± 23	17 ± 0.5	3.2 ± 0.2	21 ± 0.2	-	-
H20	10 ⁻⁴	358 ± 16	14 ± 2.3	4.3 ± 0.8	15 ± 0.5	70 ± 2.1	58 ± 1.8
	10 ⁻³	460 ± 17	15 ± 0.9	3.4 ± 0.1	17 ± 0.4	81 ± 0.7	62 ± 0.5
	10 ⁻²	532 ± 58	17 ± 0.7	3.5 ± 0.4	18 ± 0.6	100 ± 7.5	66 ± 2.6
H40	10 ⁻⁴	471 ± 28	14 ± 0.8	3.8 ± 0.8	15 ± 0.6	67 ± 2.7	56 ± 2.1
	10 ⁻³	472 ± 17	15 ± 0.7	3.4 ± 0.1	16 ± 0.2	77 ± 1.3	63 ± 0.5
	10 ⁻²	545 ± 14	19 ± 0.4	3.7 ± 0.1	18 ± 0.2	88 ± 2.2	65 ± 0.6
H60	10 ⁻⁴	451 ± 36	14 ± 0.5	3.2 ± 0.1	17 ± 2.5	66 ± 4.2	49 ± 6.2
	10 ⁻³	519 ± 45	16 ± 2.4	3.3 ± 0.6	16 ± 0.2	77 ± 7.1	63 ± 1.0
	10 ⁻²	546 ± 25	20 ± 0.5	4.0 ± 0.3	18 ± 0.3	83 ± 2.9	63 ± 3.1

Compared to yield strength of neat resin, the yield strengths at 10⁻², 10⁻³ and 10⁻⁴ s⁻¹ strain rates for H20, H40 and H60 are -0.3, 9.8, 14.2; 7.2, 9.3, 17.1 and 40.8, 37.9, and 31.1% respectively higher. The slope and y-intercept for linear trends of yield strength with respect to strain rates are presented in Table 3.10.

Table 3.10 Slope and y-intercept values of yield strength (MPa) trend lines with respect to varying low strain rates for the different composites.

Material type	Slope (MPa-s)	y-intercept (MPa)
H	574	12
H20	273	14
H40	459	14
H60	534	14

Specific compressive yield strengths (ratio of yield strength and experimentally measured density) of the materials are depicted by Figure 3.33 for various material compositions. Some of the syntactic foams are found to have higher performance than the neat resin. These compositions are useful in reducing the use of thermoplastic resin in relevant applications. It is also anticipated that further optimization of the process may result in reduction in crushed particles during syntactic foam fabrication,

which will provide syntactic foams with lower densities and improve the weight saving benefits.

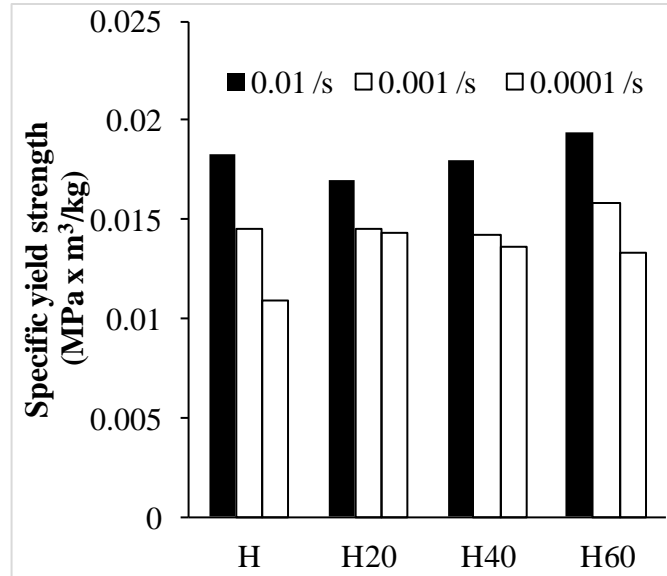


Figure 3.33 Yield strength of HDPE and its syntactic foams normalized by their density at different compressive strain rates.

A method devised by Smith et al. (2012) is used to determine the densification point. $E_{t,0.01}(\varepsilon)$ is assumed to be the tangent modulus at strain ε of the material determined by performing a linear regression on the stress-strain curve over the range $(\varepsilon - 0.01, \varepsilon + 0.01)$ and $E_{t,0.01}(\varepsilon_y)$ to be the tangent modulus at the yield strain. The densification strain is then defined as the minimum strain for which the tangent modulus becomes greater than the value of tangent modulus at the yield point and is given by,

$$\varepsilon_d = \min(\varepsilon : E_{t,0.05}(\varepsilon) > E_{t,0.05}(\varepsilon_y)) \quad (3.9)$$

The densification stresses and strains obtained by this method are presented in Table 3.9. The corresponding densification stresses are also reported. The densification strain increases as strain rate is increased from 10^{-4} to 10^{-2} s^{-1} for all syntactic foams. SEM images of the compressed samples are presented in Figure 3.34.

It can be observed from Figure 3.34 that some cenospheres are intact in all syntactic foams even after densification strain is reached. The thicker walled cenospheres having high strength are likely to survive the compression process. Extensive deformation of the matrix and debris from fractured cenospheres are visible in all these figures. Although the compressive strain rate is changed by two orders of magnitude, the difference is not high enough to provide any change in the failure mode of syntactic foams as seen from these figures. These features will be useful in studying the HSR failure features.

3.7.2 High strain rate compression

A representative set of strain histories obtained from the incident and transmitted bars during SHPB testing is shown in Figure 3.35a for a randomly selected HDPE specimen to illustrate general trends. Eqs. (2.3) - (2.5) assume that the specimen is under dynamic stress equilibrium and is experiencing a constant strain rate during the deformation (Dass Goel M et al. 2013). The radial inertia and dispersion effects are neglected in calculations. The strain rate reported is the average of nearly constant strain rate region in the strain rate-strain curve shown in Figure 3.35b.

The HSR stress-strain relationships at selected strain rates for HDPE and syntactic foams are presented in Figure 3.36. The slope of curve in the plastic region decreases as the cenosphere content is increased. This trend is attributed to the higher strain rate sensitivity of HDPE compared to the particle material. The strain rate cannot be directly controlled during the SHPB setup and is recovered from the test results thereby the graphs for various syntactic foam compositions are not compared at the exact same strain rates. Yield strength values are compared in Figure 3.37 for different strain rates. It is observed in this figure that yield strength increases with strain rate for H20 and H40. The results for H60 show that the yield strength saturates at higher strain rates.

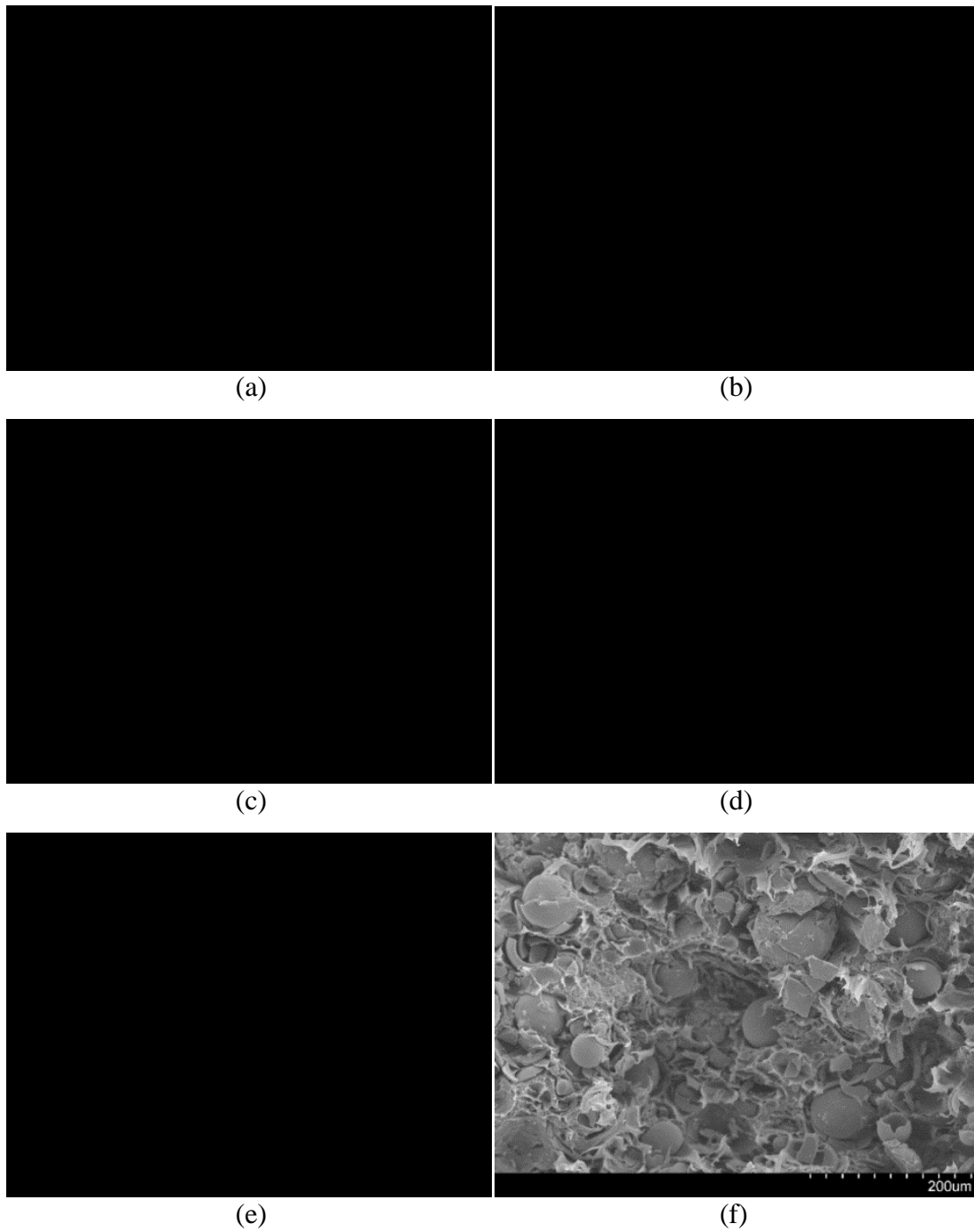


Figure 3.34 SEM image of compressed (a) H20 specimen at $0.01s^{-1}$ (b) H20 specimen at $0.001s^{-1}$ (c) H40 compressed at $0.01s^{-1}$ (d) H40 specimen at $0.001s^{-1}$ (e) H60 specimen at $0.01s^{-1}$ and (f) H60 specimen at $0.001s^{-1}$. Intact cenospheres are found in the material even after densification strain is reached. No significant change in the failure mode is observed in the material even after two orders of magnitude change in strain rate.

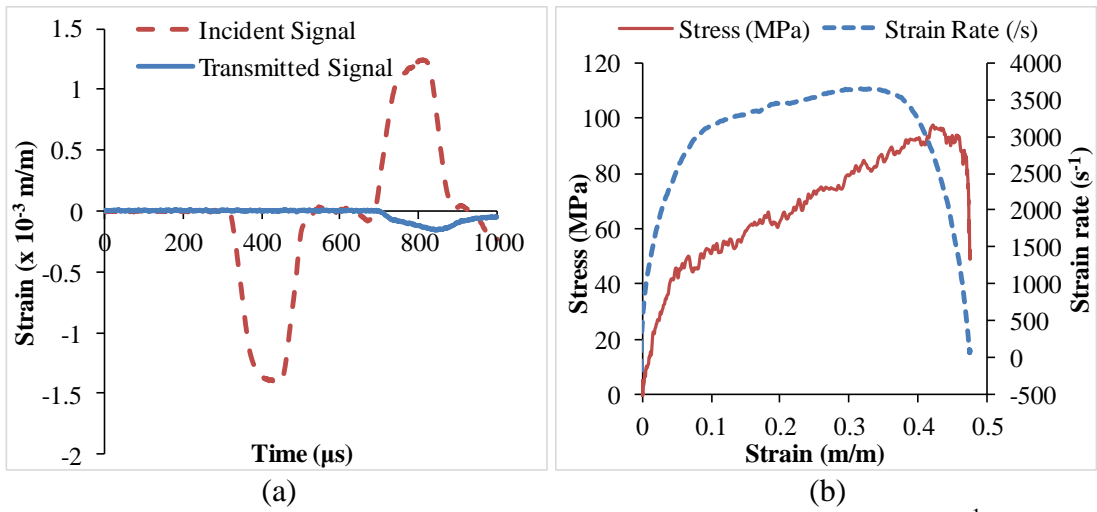


Figure 3.35 A representative set of strain signals for HDPE tested at 3430 s^{-1} showing (a) incident and transmitted signals and (b) stress and strain rate with respect to strain.

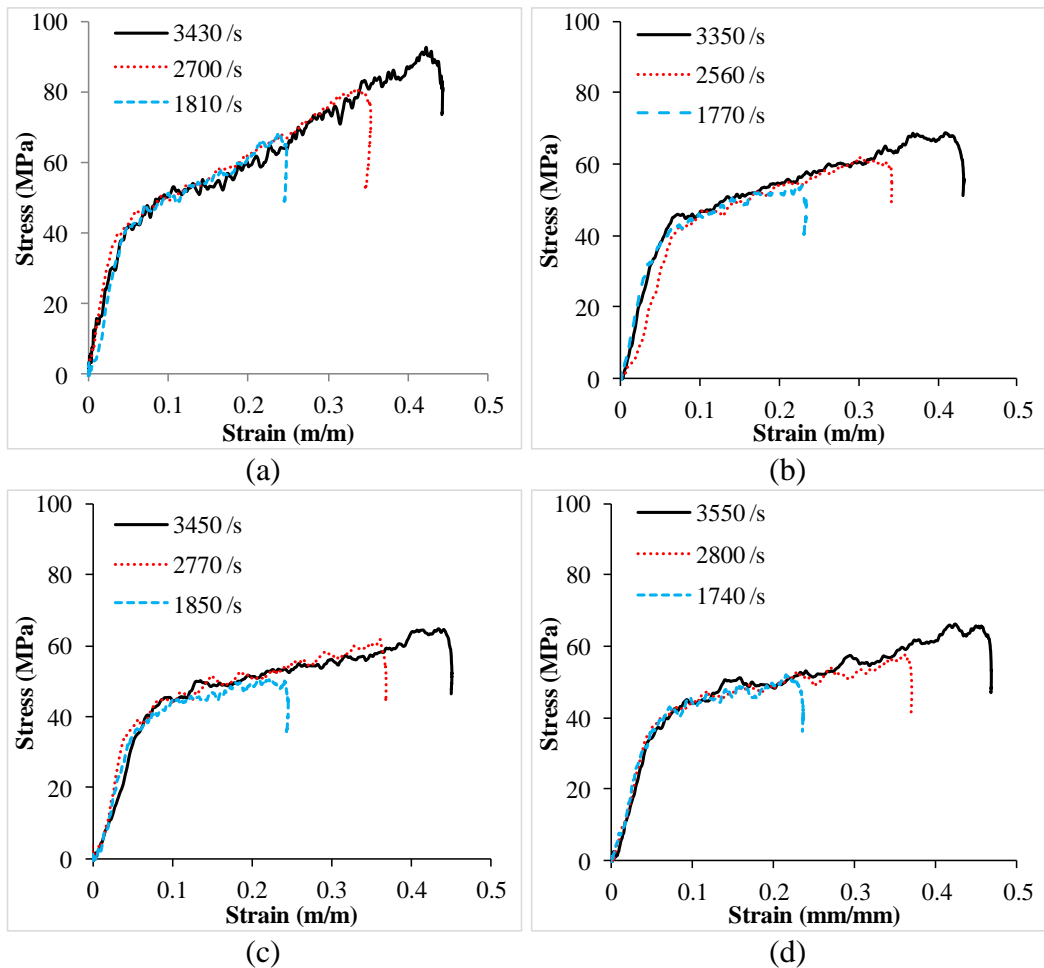


Figure 3.36 Compressive stress-strain curves at three different high strain rates for (a) HDPE (b) H20 (c) H40 and (d) H60. The strain rates are recovered from the test results so they are not exactly the same for all materials.

Figure 3.37 shows that the yield strength values are higher than those obtained under quasi-static compression. For example, yield stress for H20 syntactic foam at 3350 s^{-1} strain rate is 2.73, 3.20 and 3.23 times higher than those at 10^{-2} , 10^{-3} and 10^{-4} s^{-1} strain rates, respectively. For H40 and H60 also, the yield strength increases at high strain rates. The factor of increase is found to be between 1.91 and 2.54. These results shows strong strain rate sensitivity in the compressive yield strength for HDPE matrix syntactic foams.

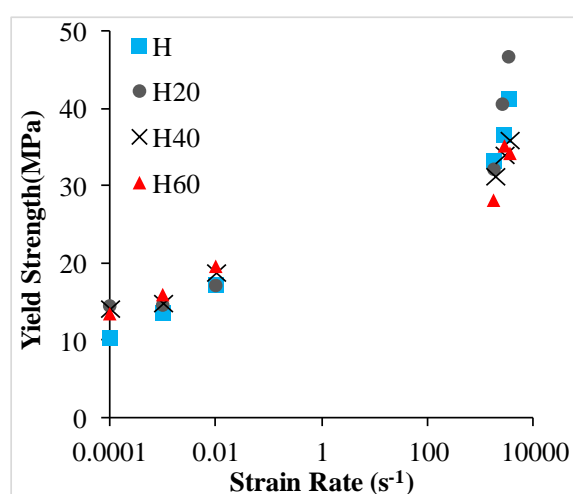


Figure 3.37 Yield strength of HDPE and its syntactic foams at low and high strain rates.

Figure 3.38 presents SEM images of syntactic foam specimens compressed at strain rates around 1800 s^{-1} . Since the maximum strain that the SHPB test could provide at this strain rate is around 0.25, several surviving cenospheres are observed from these micrographs as densification is not completed at this strain.

It should be noted that the end of the stress-strain curve in Figure 3.36 does not necessarily represent specimen failure. SHPB is a wave propagation technique with finite width of the strain pulse that is used to compress the specimen. If the specimen does not fail, the end of the test means that, the strain pulse reflected back in the incident bar and the specimen loading is terminated.

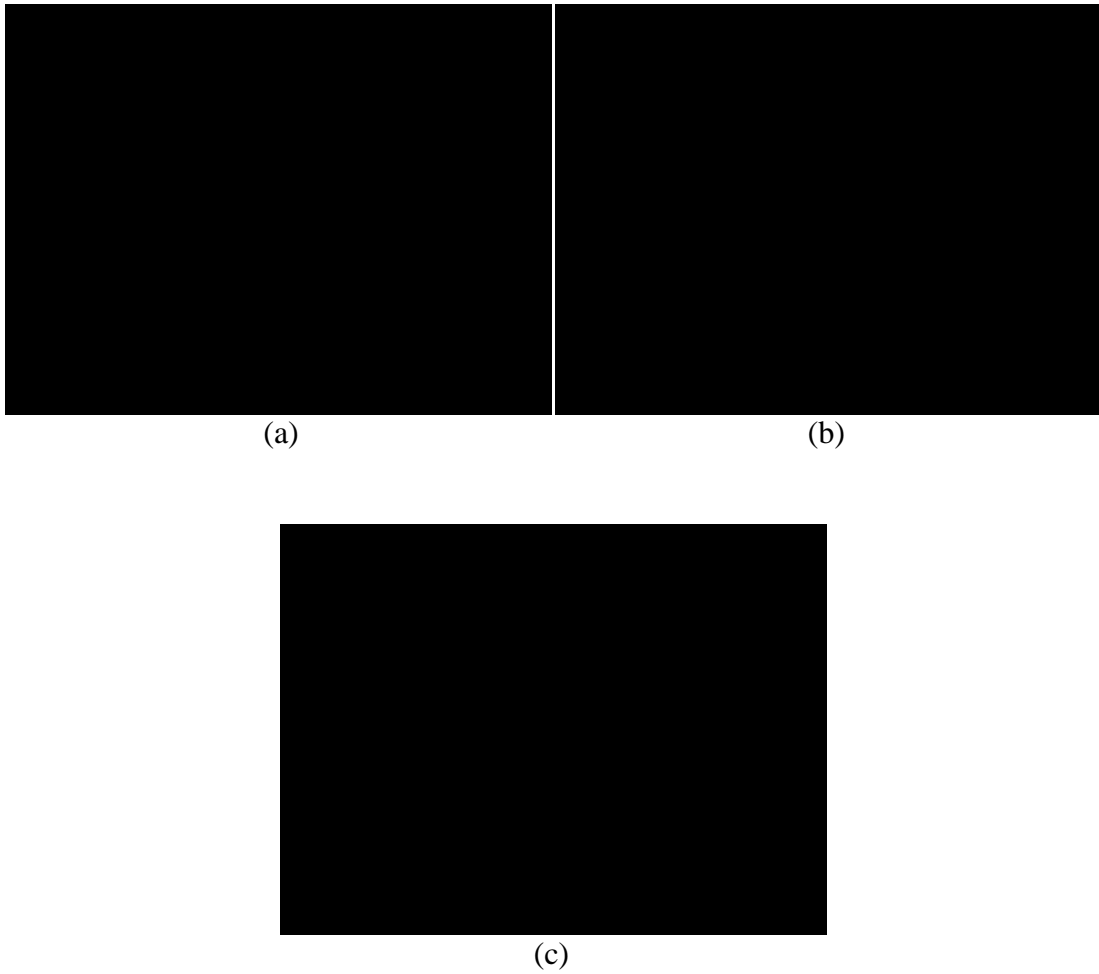


Figure 3.38 SEM images of (a) H20 specimen compressed at 1770 s^{-1} (b) H40 specimen compressed at 1850 s^{-1} and (c) H60 specimen compressed at 1740 s^{-1} .

Increase in the specimen temperature may be a concern during rapid compression at high strain rates. Due to the short time scale during high speed compression, the heat generated in the specimen may not be dissipated. Since T_g of HDPE is below the testing temperature, changes in temperature during the test may cause significant impact on the measured properties. The temperature of the specimens is calculated as a function of strain, assuming that κ is the fraction of the work that goes in heating of the specimen.

$$\kappa \Delta W \approx \Delta Q \quad (3.10)$$

$$\kappa \int_0^{\varepsilon} \sigma d\varepsilon = \rho C_v \Delta T \quad (3.11)$$

$$\Delta T = \frac{\kappa}{\rho C_v} \int_0^{\varepsilon} \sigma d\varepsilon \quad (3.12)$$

where ΔW is the work done, ΔQ is the heat generated, σ is the true stress, ε is the true strain, ρ is the material density, C_v is the specific heat capacity at constant volume (plastic flow is essentially isochoric) and ΔT is the rise in temperature, $\kappa = 1$ assuming all the work is used to heat the sample without any heat loss (Kapoor, R and Nemat-Nasser, S. 1998), which will provide the upper bound in temperature rise.

For HDPE compressed at 25°C under 3430, 2700 and 1810 s⁻¹ strain rates, the calculated temperature rise is 16.1, 9.6 and 5.2°C respectively. A functional relation between Young's modulus and temperature is not available for HDPE. However, viscoelastic properties of HDPE are documented by Sewda, K and Maiti, S. N. (2013) and Kim et al. (2000) with respect to temperature. These studies provide a relationship between temperature and the storage and loss moduli of HDPE resin. The storage and loss moduli of HDPE at 20°C are 1299 MPa and 75 MPa, respectively (Sewda, K and Maiti, S. N. 2013) but the storage modulus reduces to 996 MPa and loss modulus increases to 107 MPa at 41.1°C as listed in Table 3.11. These results show that increase in temperature may have an effect in the measured high strain rate properties.

Table 3.11 Storage modulus and loss modulus values of HDPE at different temperatures.

Temperature (°C)	Storage Modulus (MPa)	Loss Modulus (MPa)
25	1299	75
30.2	1207	88
34.6	1124	97
41.1	996	107

3.8 Dynamic Mechanical Analysis

3.8.1 Temperature sweep

Results of the temperature sweep for storage modulus E' , loss modulus E'' and $\tan \delta$ are shown in Figure 3.39. As the glass transition temperature of the HDPE matrix is approximately -110°C (Khanna, Y. P et al. 1985), the experiments in the present work are conducted entirely in the rubbery region and the variation of the dynamic

properties with temperature does not show step changes or peaks which indicate phase transitions. In Figure 3.39a it is observed that at all temperatures the syntactic foams have higher storage modulus than the virgin HDPE resin. Storage modulus increases with increasing hollow particle content, though the difference between H40 and H60 is slight. From Table 3.12 it can be observed that the standard deviations of these compositions overlap at the three selected reference temperatures. The significantly higher fraction of broken particles may be responsible for the lack of increased stiffening effect at higher particle loading. However, the use of high weight fraction of particles is still highly beneficial from the standpoint of reducing consumption of HDPE. It is also observed that the syntactic foams are all able to withstand approximately 5°C higher temperature before the storage modulus drops below the 20 MPa threshold.

Loss modulus results are presented in Figure 3.39b and at selected temperatures in Table 3.13. As with storage modulus, the loss modulus is higher at all temperatures for syntactic foams and increases with increasing hollow particle content. The difference between H40 and H60 are within the standard deviations. The peak in loss modulus at around 50°C corresponds to the α -relaxation in HDPE (Khanna, Y. P et al. 1985). The peak appears to occur at higher temperatures with increasing particle loading, which may indicate an increase in the crystallinity of the specimens due to the presence of the hollow particles.

Tan δ results are presented in Figure 3.39c and at selected temperatures in Table 3.14. This property, also known as the damping parameter, loss factor or loss tangent, is the ratio of the loss and storage moduli and represents the relative magnitudes of the elastic and viscous behavior of the material. While all of the syntactic foams have lower damping parameter than the virgin HDPE at all temperatures, the damping parameter is less sensitive to the hollow particle content than the storage and loss moduli.

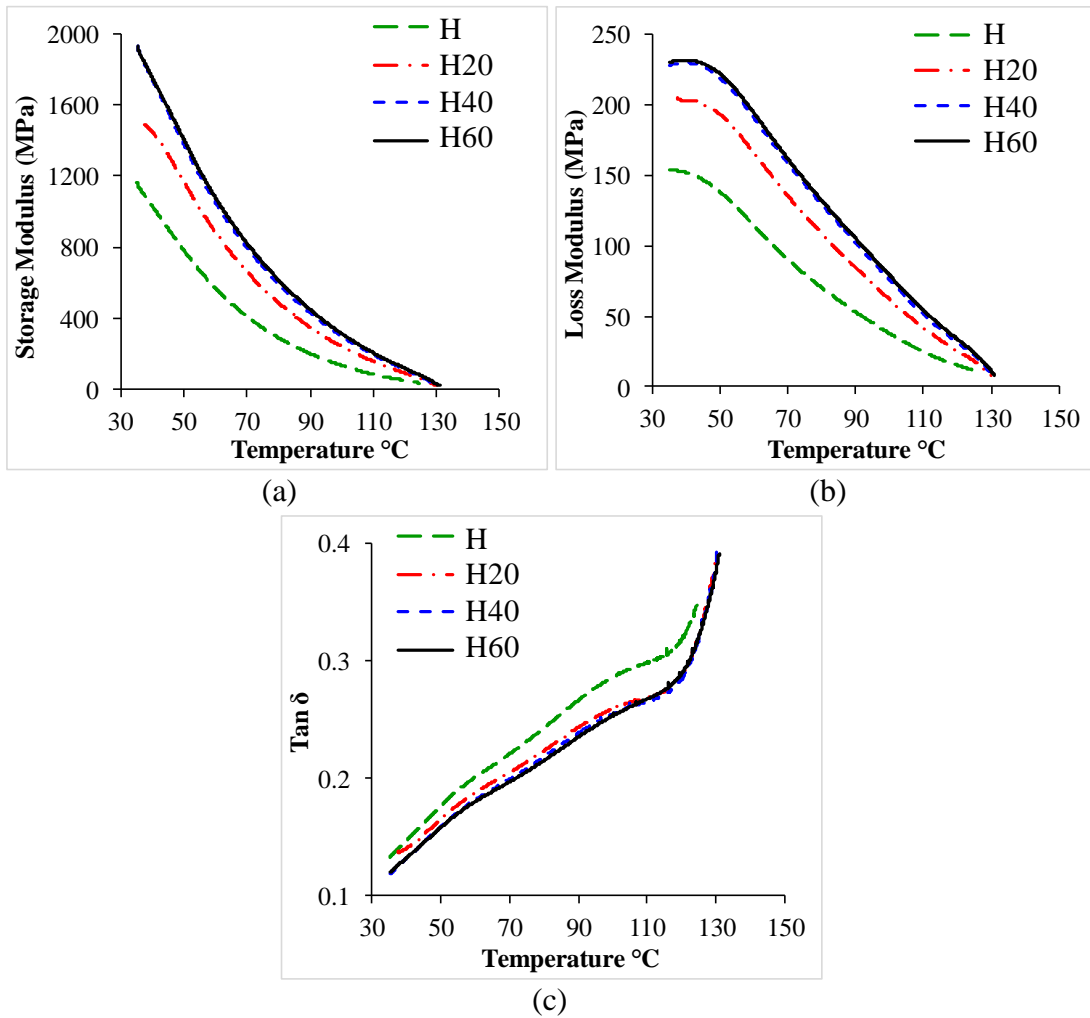


Figure 3.39 (a) Storage modulus (b) loss modulus and (c) $\tan \delta$ results from DMA temperature sweep at 1 Hz.

Table 3.12 Comparison of storage modulus at three representative temperatures.

Syntactic foam type	E' at 50 °C (MPa)	E' at 80 °C (MPa)	E' at 120 °C (MPa)
H	786.23±4.8	292.59±3.7	48.57±1.3
H20	1169.93±0.8	485.84±2.3	88.92±0.73
H40	1375.55±21.9	590.11±9.6	109.06±1.9
H60	1374.11±26.7	593.98±17.5	109.61±6.1

Table 3.13 Comparison of loss modulus at three representative temperatures.

Syntactic foam type	E'' at 50 °C (MPa)	E'' at 80 °C (MPa)	E'' at 120 °C (MPa)
H	139.03±0.9	70.63±0.7	15.29±0.2
H20	193.81±0.9	108.87±0.6	25.09±0.3
H40	217.35±1.9	129.07±1.7	30.86±0.7
H60	216.78±5.2	129.92±1.8	31.71±1.7

Table 3.14 Comparison of damping parameter at three representative temperatures.

Syntactic foam type	$\tan \delta$ at 50 °C ($\times 10^{-2}$)	$\tan \delta$ at 80 °C ($\times 10^{-2}$)	$\tan \delta$ at 120 °C ($\times 10^{-2}$)
H	17.68±0.006	24.1±0.005	31.5±0.001
H20	16.6±0.002	22.4±0.001	28.2±0.002
H40	15.8±0.001	21.9±0.001	28.3±0.004
H60	15.8±0.004	21.9±0.003	28.9±0.003

3.8.2 Time-temperature superposition

In the second phase of DMA measurements, isothermal frequency sweeps are conducted at a selection of temperatures. According to the time-temperature superposition principle, the effects of changing temperature and varying frequency are interchangeable. This allows for the extension of data, collected over a limited frequency domain to be expanded by many orders of magnitude, by applying a shift factor to data collected over a range of temperatures (Ferry, J. D 1961). These shift factors are determined from the experimental data by shifting the curves obtained at different temperatures along the frequency axis to obtain a single smooth master curve. The shift factors for most polymers have been found to obey the Williams-Landel-Ferry (WLF) equation (Williams, M. L et al. 1955) and is given by,

$$\log a_T = \frac{-c_1(T - T_0)}{c_2 + T - T_0} \quad (3.13)$$

where a_T is the frequency shift factor, c_1 and c_2 are the WLF coefficients, T is the temperature each data set is acquired at and T_0 is the reference temperature. Once the shift factors for a given material are determined, the corresponding WLF coefficients are independent of the choice of reference temperature.

A representative set of DMA curves obtained by varying frequency at various temperature steps for H60 is shown in Figure 3.40. These curves are shifted to produce a master curve for the material based on a chosen reference temperature. The master curves for storage modulus of all of the compositions at three arbitrarily selected reference temperatures are presented in Figure 3.41. The curves are shown in the frequency range 10^{-2} - 10^6 Hz, which is the range encountered in most applications. The total frequency range covered depends on the selection of reference temperature.

At all of the reference temperatures, the sensitivity of the storage modulus to weight fraction of hollow particles increases with increasing frequency.

The WLF constants corresponding to the shift factors used in generating the master curves are presented in Figure 3.42. The constants are approximately a linearly increasing function of cenosphere weight fraction. The shift factors for the cenosphere syntactic foams are of the same magnitude as those calculated for vinyl ester/hollow glass microsphere syntactic foams (Shunmugasamy, V. C et al. 2013) and shift factors for the virgin HDPE are similar to those reported in the literature (Goldman, A. Y and Grinman 1974). However, direct comparison of the shift factors for virgin HDPE is difficult because they are affected by the degree of crystallinity.

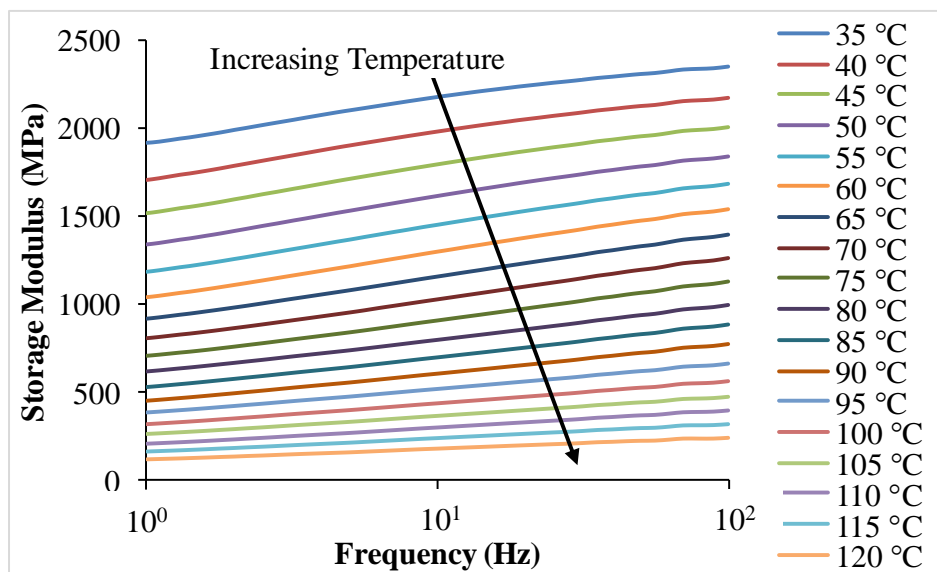


Figure 3.40 Representative data set from combined temperature-frequency sweep on a specimen of H60.

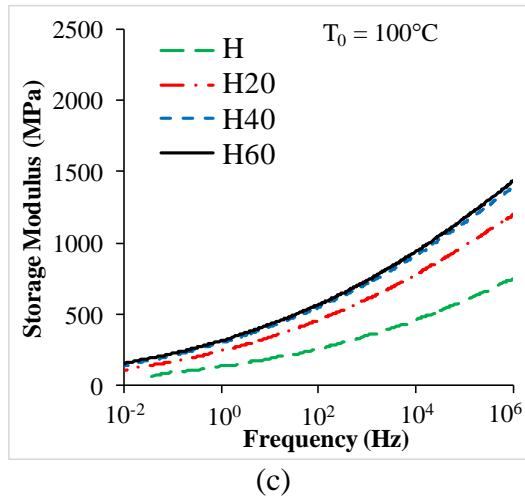
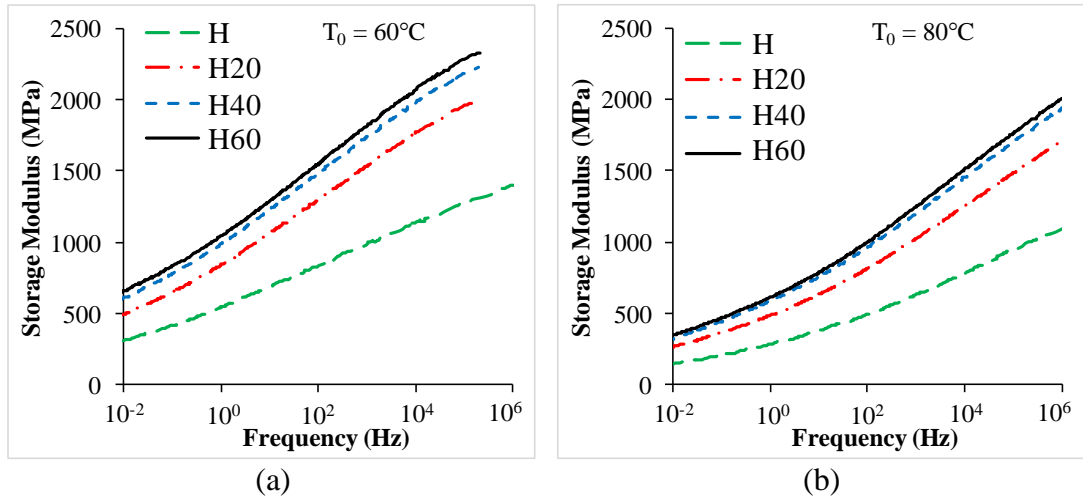


Figure 3.41 Time-temperature superposition results from DMA frequency sweep calculated for reference temperatures of (a) 60° (b) 80° and (c) 100°C .

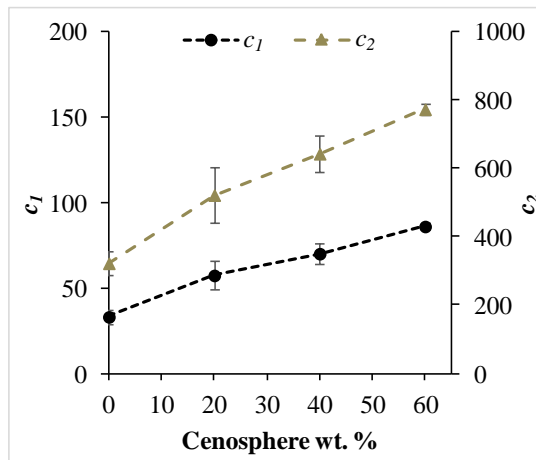


Figure 3.42 Williams-Landel-Ferry constants for syntactic foams.

Mechanical property characterization of cenosphere/HDPE syntactic foam composites as dealt in the present work, gives a valuable insight for a materials designer to select most appropriate configuration. As seen from the preceding discussions, H40-U-MM is the most favorable choice for casting industrial scale components using PIM.

As a deliverable/tangible outcome of this work, several industrial scale components are casted using optimized parameters of PIM and are presented in the section to follow.

4 CASTING OF PROTOTYPE COMPONENTS

HDPE is widely used in manufacturing consumer products. Many of the existing components can be identified where cenosphere filled HDPE syntactic foams can be beneficial either to provide lightweight or to reduce HDPE consumption to make the part cheaper and more eco-friendly. Reduction in failure strain may be a limitation for some applications. In addition, concerns such as mismatch in coefficient of thermal expansion of particle and matrix leading to interfacial separation or material failure can be important considerations. Therefore, the potential applications of such new materials should be carefully selected. Several existing HDPE components are identified and the process parameters optimized in the present work are used to cast these parts in syntactic foams using PIM process. A snapshot of the cast parts is presented in Figure 4.1 and close-up images of few components are shown in Figure 4.2

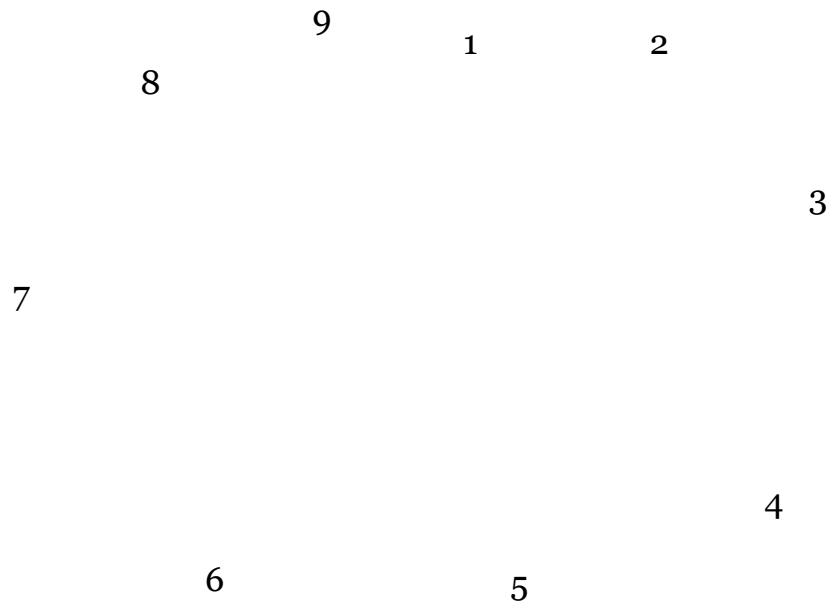


Figure 4.1 Eco-friendly components cast using injection molding technique 1. Bearing cover 2. Automobile component used in liquefied petroleum gas cylinder for gas mixtures 3. Gear 4. Electrical junction box 5. Water filter cap 6. End cap for closure 7. Square base attachment for pipes 8. Jerry can cap and 9. Bottle cap. Several original components made of pure HDPE are also displayed in the center.

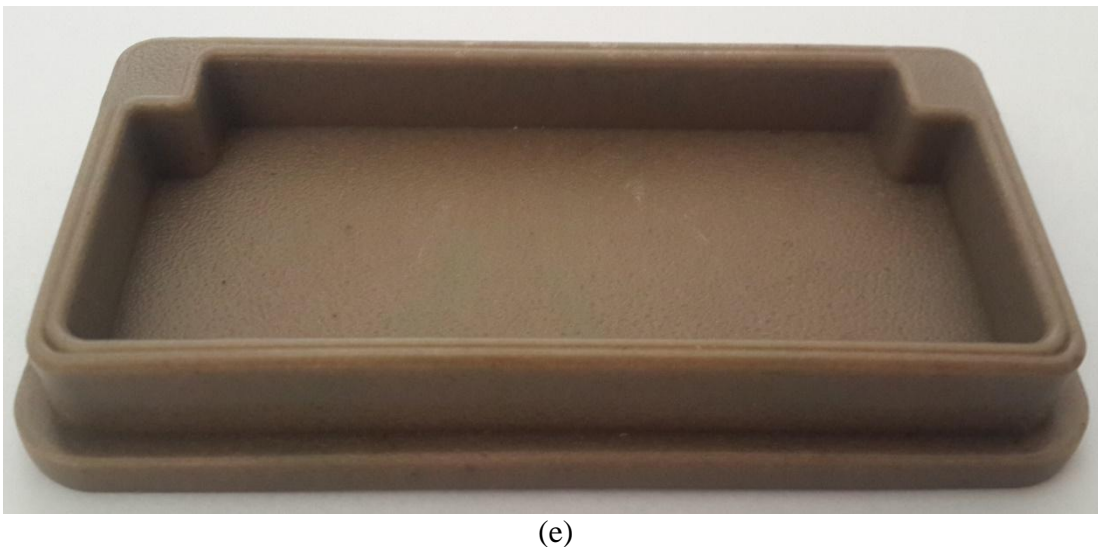
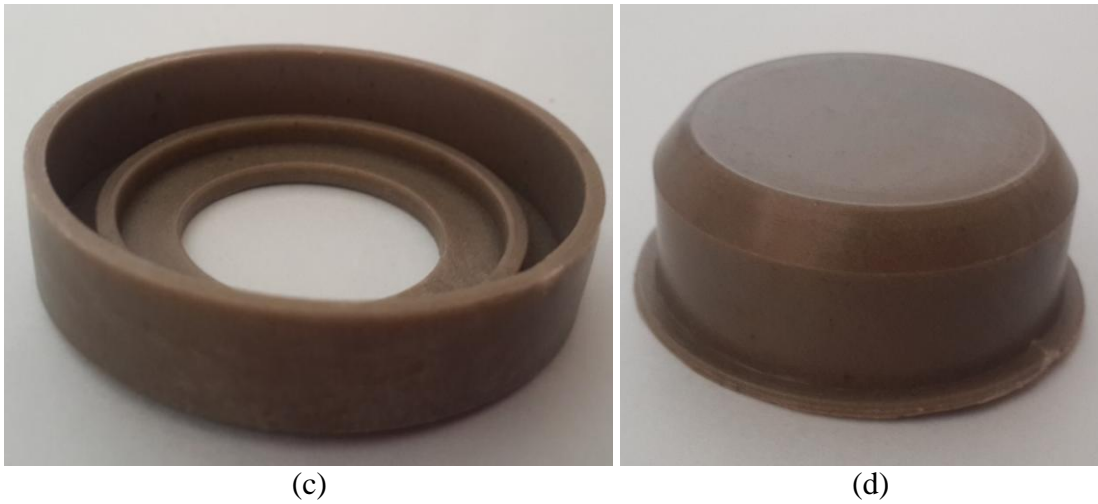
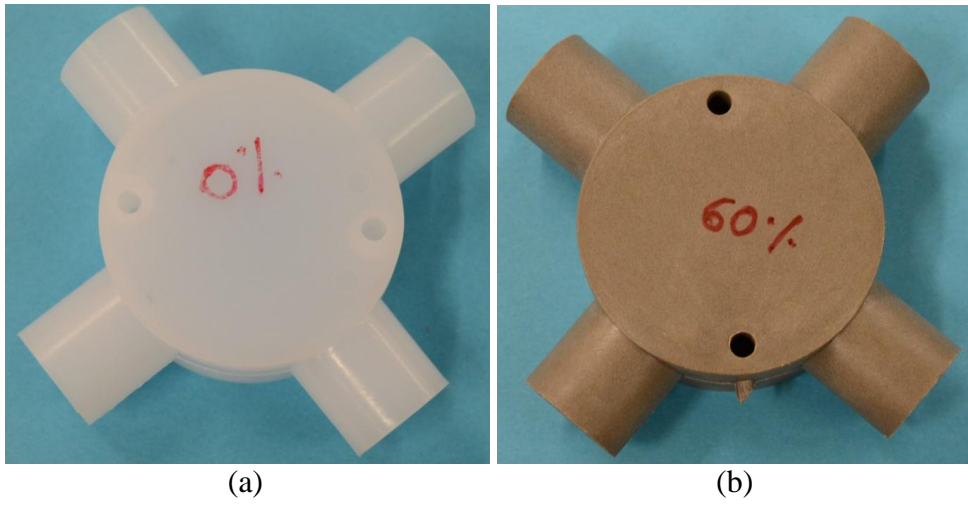


Figure 4.2 Prototype components cast in the study: (a) an example of an electrical junction box cast of pure HDPE (b) the electrical junction box cast on the same machine with syntactic foam. Other syntactic foam prototypes: (c) a part bearing cover (d) a bottle cap and (e) bottom cap of a chair leg.

Table 4.1 provides details on each of these components and the impact of using syntactic foams for their manufacture.

Table 4.1 Details of cast syntactic foam components.

No.	Component Name	Wt. of HDPE component (g)	Wt. of Composite Component (g)	Wt. saving (%)	Features	Component functionality	*Annual total HDPE Saving
01	Bearing cover	11.3	10.7	5	Stepped thin section	Compliant for being press fit, sealing, wear resistance	
02	Automobile component used in liquefied petroleum gas driven cars	16.8	15.9	5.5	Thin slender section, localized steps, Multiple features in different planes	Sustain compressive forces, chemically inert, dimensionally stable, low coefficient of thermal expansion, fire retardant	
03	Gear for small motors	33.5	31.9	4.9	Thick section, sharp edges,	Torsional strength, high stiffness, wear resistance, vibration damping, dimensional stability at elevated temperature	
04	Electrical connector	25.95	24.6	5.3	Thin section, thread pockets	Fire retardant, compliant, long term durability	5%, 2.9 Million tons
05	Water filter cap	13.4	12.7	5.2	Thin section, screw threads	Close dimensional tolerances, sealing	
06	End cap for closure	28.5	27.1	5	Thick section	Dimensional stability, compressive and torsional strength	
07	Square base attachment for pipes	10.7	10.2	5.3	Thin section, multiple features in different planes	Dimensional stability, compressive strength, provide good damping	
08	Jerry can cap	28.7	27.3	5.1	Thick section, threads	Compressive strength, wear resistance, chemical resistance	
09	Oil container packing cap	5.6	5.3	5	Thin section with step	Compressive strength, chemical resistance, fire retardant	

*Report on Global HDPE demand to grow 4.2% annually through 2022, March 9, 2015 by Canadian plastics, Toronto, Canada. <http://www.canplastics.com/materials/global-hdpe-demand-to-grow-4-2-annually-through-2022-report/1003434693>

The parts are cast with an aim of reducing the weight of the component by 5%. From Figure 4.1 it is very clear that, complex shaped, thin sectioned, intricate parts can be manufactured in large volume leading to lower costs. Further, the product is more eco-friendly due to use of fly ash. It is also noted that apart from mixing cenospheres

in the initial feed and adjusting molding pressure and temperature, the overall machine settings and parameters have been maintained constant so that the industrial adaptation of lighter components can be easily adopted. Based on the estimate of using HDPE in the selected 9 components, cenosphere usage can save around 2.9 million tons of HDPE globally per year.

Conclusive remarks of this study are presented hereafter.

CONCLUSIONS

A comprehensive study is conducted to optimize the processing parameters for the PIM to enable casting of cenosphere/HDPE components. Use of cenospheres can make products lighter and reduce consumption of HDPE. In addition, fly ash is an industrial waste and use of cenospheres in consumer products can reduce the burden on landfills addressing the environmental concern of fly ash disposal. An industrial scale PIM machine is used to develop the cenosphere/HDPE syntactic foam specimens, which are characterized for mechanical properties. Optimized processing parameters for PIM process are used based on the pilot study. Syntactic foams with 20, 40 and 60 wt.% of cenospheres in HDPE matrix are fabricated. The effect of surface treatment and blending method on the tensile and flexural behavior of cenosphere/HDPE syntactic foams produced by an industrial scale injection molding technique are investigated first.

Theoretical models are used to estimate the properties of cenospheres by conducting parametric studies and the effectiveness of cenospheres in reinforcing HDPE matrix is evaluated. Based on these results, cenosphere/HDPE samples prepared using untreated constituents by mechanical mixing route are investigated for compressive and dynamic characterizations. Compressive properties at quasi-static and high strain rate are dealt with next. Temperature rise during HSR compression is calculated using an analytical expression. Finally, effect of temperature in the range 35-130°C on the dynamic mechanical properties of cenosphere/HDPE syntactic foams has been studied. The results are expended to cover over eight magnitudes of frequency by using the time-temperature superposition principle for measurements taken in the frequency range 1-100 Hz.

The main conclusions can be summarized as:

PIM process

- The most favorable processing parameters for manufacturing syntactic foam with the selected cenospheres and HDPE grade are 160°C temperature and 30 bars pressure.

Density

- Measured density of syntactic foams is higher than their theoretical values suggesting failure of some cenospheres during fabrication. H20 and H40 syntactic foams have lower density than the neat HDPE.
- The breakage of cenospheres increases with their weight fraction due to increased particle to particle interaction during mixing in the present industrial scale manufacturing method.
- It is desired to reduce the particle breakage in higher loading compositions. However, syntactic foams containing up to 40 wt.% particles can be fabricated with these processes with good quality.

Tensile behavior

- Syntactic foam samples fracture at significantly lower strain compared to the neat HDPE specimens but the fracture strength of syntactic foams is significantly higher than that of the neat resin. The modulus of syntactic foams increases with cenosphere content.
- It is also noted that the syntactic foams fracture close to their ultimate strength, whereas for neat resin the strength reduces significantly after reaching a peak and the fracture strength is less than 20% compared to the peak strength.
- Microscopic observations reveal poor interfacial bonding between as-received cenospheres and HDPE. The surface treatment of cenospheres and functionalization of HDPE promote interfacial bonding.
- Strength increases with cenosphere content in treated configuration and decreases otherwise.
- The modulus and strength are found to be the highest for H40-U-MM (723 MPa) and H60-T-BM (17.44 MPa) specimens. These values are 37 and 17% higher than those for their respective matrices.
- While surface treatment yields benefits in the reinforcing capabilities of cenospheres, the use of untreated constituents (U-MM) may still be beneficial where modulus is important criteria, rather than the strength.
- From environmental perspective untreated constituents are the better proposition.

Flexural behavior

- Flexural modulus and strength are found to increase with cenosphere content for syntactic foams manufactured by all methods.
- Syntactic foams processed through mechanical mixing resulted in the highest flexural modulus of 1253.68 MPa in comparison to 713.8 MPa of virgin HDPE. Highest strength is observed in case of Brabender mixing (21.07 MPa) as against 12.37 MPa of functionalized HDPE. Modulus and strength values are 76 and 70% higher than the corresponding values for the HDPE resin.
- Two theoretical models are used for prediction of flexural modulus of the syntactic foams. Bardella-Genna model predictions are close to the experimental results. This model can be used for designing syntactic foam microstructures with desired properties.

Quasi-static compression and High strain rate testing

- Several compositions of syntactic foams have higher yield strength than the matrix material. Syntactic foam compositions can also be identified to have higher specific yield strength than the neat matrix material. This observation points to possibilities of weight saving by using syntactic foams.
- The yield strengths under HSR are found to be greater than those under quasi-static or low strain compression, with higher strain rate sensitivity as the percentage of cenospheres is increased.
- Modulus of elasticity for HDPE and syntactic foams increases with strain rates in the quasi-static strain rate regime.
- In the present investigation, it is apparent that the 60 wt.% of cenospheres is too high to have high quality syntactic foams because of cenosphere fracture due to particle to particle interaction during mixing.

Dynamic Mechanical Analysis

- Storage and loss modulus increase with increasing weight fraction of cenospheres, but with little difference between 40 and 60 wt.%, at all temperatures. The sensitivity of storage modulus to weight fraction of cenospheres increases with increasing frequency.

- Storage and loss modulus decrease with increasing temperature in the range of 35-130°C, while $\tan \delta$ increases. The WLF constants are a linearly increasing function of cenosphere weight fraction.

Present work successfully demonstrated feasibility of industrial scale PIM for developing thermoplastic syntactic foam composites. Components are eco-friendly, lightweight and more importantly saves approximately 5% of plastic (2.9 million tons annually at global scale). Further, usage of fly ash cenospheres reduces landfill burden and environmental linked issues. Complex shaped, intricate parts of cenosphere/HDPE syntactic foams can be manufactured in large volume leading to lower costs by using injection molding technique. As far as the guidelines for PIM industries are concerned, H40-U-MM would be the best choice based on the work presented here.

The experimental results presented as part of this work can be used by industry professionals for development of syntactic foams for specific applications. Theoretical models can help researchers and industry professionals in predicting the properties of various compositions of syntactic foams and reduce experimentation. The data can be used in design and evaluation of consumer products for manufacture with this lower cost lightweight material. Optimization data on industrial scale machine for syntactic foam manufacture can help other industries to adopt similar practices.

SCOPE OF FUTURE WORK

Present work demonstrates feasibility of industrial scale PIM in developing thermoplastic syntactic foams. Though, the approach is successful, hollow cenospheres are observed to break in such pressurized techniques. Filler breakage needs to be addressed and minimized further, by adopting CFD simulations to get the optimized temperature profile with shearing forces creeping in due to screw rotation across heating zones. Further, theoretical models adopted for comparing the experimental data lacks in considering the interaction between the hollow particles and HDPE matrix.

REFERENCES

- Agarwal, B. D. and Broutman, L. J. (1980). "Analysis and performance of fiber composites." *Journal of polymer science: Polymer Letters Edition*, 18(10), 689-690.
- Alkan, C., Arslan, M. Cici, M. Kaya, M. and Aksoy, M. (1995). "A study on the production of a new material from fly ash and polyethylene." *Resources, Conservation and Recycling*, 13(3-4), 147-154.
- Arza Seidel (2012). "Fillers." *Encyclopedia of Polymer Science and Technology*, 4th edition. John Wiley & Sons, New York.
- Arzamasov B. (1989). *Materials Science*, Mir publishers, Moscow.
- ASTM C618-15, *Standard Specification for Coal Fly Ash and Raw or Calcined Natural Pozzolan for Use in Concrete*, ASTM International, PA, USA.
- ASTM D3878-07, *Standard Terminology for Composite Materials*, ASTM International, PA, USA.
- ASTM D638-10, *Standard Test Method for Tensile Properties of Plastics*, ASTM International, PA, USA.
- ASTM D790-10, *Standard Test Methods for Flexural Properties of Unreinforced and Reinforced Plastics and Electrical Insulating Materials*, ASTM International, PA, USA.
- ASTM D792-13, *Standard Test Methods for Density and Specific Gravity (Relative Density) of Plastics by Displacement*, ASTM International, PA, USA.
- Atikler, U., Basalp, D. and Tihminlioglu, F. (2006). "Mechanical and morphological properties of recycled HDPE, filled with calcium carbonate and fly ash." *Journal of Applied Polymer Science*, 102(5), 4460-4467.
- Aureli, M., Porfiri, M. and Gupta, N. (2010). "Effect of polydispersivity and porosity on the elastic properties of hollow particle filled composites." *Mechanics of Materials*, 42(7), 726-739.
- Bachmatiuk, A., Bornert, F. Schaffel, F. Zaka, M. Martynkova, G. S. Placha, D. Schonfelder, R. Costa, P. M. F. J. Ioannides, N. Warner, J. H. Klingeler, R. Buchner, B. and Rummeli, M. H. (2010). "The formation of stacked-cup carbon nanotubes

using chemical vapor deposition from ethanol over silica.” *Journal of Carbon*, 48(11), 3175-3181.

Bajaj, P., Jha, N. K. and Ananda, K. R. (1992). “Effect of coupling agents on the mechanical properties of mica/epoxy and glass fiber/mica/epoxy composites.” *Journal of Applied Polymer Science*, 44(11), 1921-1930.

Bardella, L. and Genna, F. (2001). “On the elastic behavior of syntactic foams.” *International Journal of Solids and Structures*, 38(40-41), 7235-7260.

Bardella, L., Sfreddo, A. Ventura, C. Porfiri, M. and Gupta, N. (2012). “A critical evaluation of micromechanical models for syntactic foams.” *Mechanics of Materials*, 50, 53-69.

Benckechou, B., Coni, M. Howarth, H. V. C. and White, R. G. (1998). “Some aspects of vibration damping improvement in composite materials.” *Composites Part B*, 29(6), 809-817.

Bunn, P. and Mottram, J. T. (1993). “Manufacture and compression properties of syntactic foams.” *Composites*, 24(7), 565-571.

Burgiel, J., Butcher, W. Halpern, R. Oliver, D. Tangora, P. Tangora, R. W and Kirk D. R. (1994). *Cost evaluation of automated and manual post consumer plastic bottle sorting systems*. EPA report EPA/600/R-94/165, 1-10.

Chawla, K. K. (2001). *Composite materials*. Springer, New York.

Das, A. and Satapathy, B. K. (2011). “Structural, thermal, mechanical and dynamic mechanical properties of cenosphere filled polypropylene composites.” *Materials & Design*, 32(3), 1477-1484.

Dass Goel, M., Matsagar, V. A. Gupta, A. K. and Marburg, S. (2013). “Strain rate sensitivity of closed cell aluminium fly ash foam.” *Transactions of Nonferrous Metals*, 23(4), 1080-1089.

Deepthi, M. V., Sailaja, R. R. N. Sampathkumaran, P. Seetharamu, S. and Vynatheya, S. (2014). “High density polyethylene and silane treated silicon nitride nanocomposites using high-density polyethylene functionalized with maleate ester: Mechanical, tribological and thermal properties.” *Materials & Design*, 56, 685-695.

- Deepthi, M. V., Sharma, M. Sailaja, R. R. N. Anantha, P. Sampathkumaran, P. and Seetharamu, S. (2010). "Mechanical and thermal characteristics of high density polyethylene–fly ash Cenospheres composites." *Materials & Design*, 31(4), 2051-2060.
- Demjen, Z. and Pukanszky, B. (2004). "Effect of surface coverage of silane treated CaCO₃ on the tensile properties of polypropylene composites." *Polymer Composites*, 18(6), 741-747.
- Dimchev, M., Ryan Caeti and Gupta, N. (2010). "Effect of carbon nanofibers on tensile and compressive characteristics of hollow particle filled composites." *Materials and Design* 31(3), 1332-1337.
- Divya., V. C. Ameen Khan, M. Nageshwar Rao, B. and Sailaja, R. R. N. (2015). "High density polyethylene/cenosphere composites reinforced with multi-walled carbon nanotubes: Mechanical, thermal and fire retardancy studies." *Materials and Design*, 65, 377-386.
- Esha Shah and Rajaram (1997). "Plastic Recycling in Bangalore-India." *Urban Waste Expertise Programme (UWEP)*, CS-plast India, 8-10.
- Farinha J. P. S., Winnik, M. A. and Hahn K. G. (2000). "Characterization of oil droplets under a polymer film by laser scanning confocal fluorescence microscopy." *Langmuir*, 16(7), 3391-3340.
- Ferreira J. A. M., Capela, C. and Costa J. D. (2010). "A study of mechanical behaviour on fibre reinforced hallow microballoon hybrid." *Composites: Part A*, 41(3), 345-352.
- Ferrigno, T. H. (1978). "Handbook of fillers and reinforcements for plastics." *H. S. Katz and J.V. Milewski eds*, Van Nostrand Reinhold, New York, 66-71.
- Ferry, J. D. (1961). *Viscoelastic Properties of Polymers*, John Wiley & Sons, New York.
- Fu, S. Y., Feng, X. Q. Lauke, B. and Mai, Y. W. (2008). "Effects of particle size, particle/matrix interface adhesion and particle loading on mechanical properties of particulate-polymer composites." *Composites Part B: Engineering*, 39(6), 933-961.

Goldman, A. Y. and Grinman, A. M. (1974). "Variant of time-Temperature superposition for partially crystalline polymers (high-density polyethylene)." *Polymer Mechanics*, 10(2), 224-230.

Guhanathan, S., Devi, M. S. and Murugesan, V. (2001). "Effect of coupling agents on the mechanical properties of fly ash/polyester particulate composites." *Journal of Applied Polymer Science*, 82(7), 1755-1760.

Gupta, N. (2002). "Effect of Wall Thickness of Cenospheres on the Compressive Properties of Syntactic Foams." *ME Graduate Student Conference*, Louisiana State University, New York.

Gupta, N. (2007). "A Functionally Graded Syntactic Foam Material for High Energy Absorption under Compression." *Materials Letters*, 61(4-5), 979-982.

Gupta, N. and Nagorny, R. (2006). "Tensile properties of glass microballoon-epoxy resin syntactic foams." *Journal of Applied Polymer Science*, 102(2), 1254-1261.

Gupta, N. and Woldesenbet, E. (2004). "Microballoon Wall Thickness Effects on Properties of Syntactic Foams." *Journal of Cellular Plastics*, 40(6), 461-480.

Gupta, N., Pinisetty, D. and Shunmugasamy, V. C. (2013). *Reinforced Polymer Matrix Syntactic Foams: Effect of Nano and Micro-Scale Reinforcement*, Springer New York.

Gupta, N., Woldesenbet, E. and Mensah, P. (2004). "Compression properties of syntactic foams: effect of cenosphere radius ratio and specimen aspect ratio." *Composites Part A: Applied Science and Manufacturing*, 35(1), 103-111.

Gupta, N., Gupta, S. K. and Benjamin, J. M. (2008). "Analysis of a functionally graded particulate composite under flexural loading conditions." *Materials Science and Engineering A*, 485(1-2), 439-447.

Gupta, N., Karthikeyan, C. S. Sankaran, S. and Kishore (1999). "Correlation of Processing Methodology to the Physical and Mechanical Properties of Syntactic Foams With and Without Fibers." *Materials Characterization*, 43(4), 271-277.

- Gupta, N., Maharsia, R. and Jerro, H. D. (2005). "Enhancement of energy absorption characteristics of hollow glass particle filled composites by rubber addition." *Materials Science and Engineering A*, 395(1-2), 233-240.
- Gupta, N., Zeltmann, S. Shunmugasamy, V. and Pinisetty, D. (2013). "Applications of Polymer Matrix Syntactic Foams." *The Journal of The Minerals, Metals & Materials Society*, 66(2), 245-240.
- Gupta, N., Ye, R. and Porfiri, M. (2010). "Comparison of tensile and compressive characteristics of vinyl ester/glass microballoon syntactic foams." *Composites Part B: Engineering*, 41(3), 236-245.
- Harris, B. (1999). *Engineering composite materials*, IOM communications, The university press, Cambridge.
- Hu, G. and Yu, D. (2011). "Tensile, thermal and dynamic mechanical properties of hollow polymer particle-filled epoxy syntactic foam." *Materials Science and Engineering: A*, 528(15), 5177-5183.
- Huang, J. S. and Gibson, L. J. (1991). "Fracture toughness of brittle foams." *Acta Metallurgica et Materialia*, 39(7), 1627-1636.
- Hull, D. and Clyne, T. W. (1996). *An introduction to composite materials*, Cambridge University press, Cambridge.
- Jena, H., Pandit, M. K. and Pradhan, A. K. (2013). "Effect of cenosphere on mechanical properties of bamboo-epoxy composites." *Journal of Reinforced Plastics and Composites*, 32(11), 794-801.
- John, B., Nair, C. P. R. and Ninan, K. N. (2010). "Effect of nanoclay on the mechanical, dynamic mechanical and thermal properties of cyanate ester syntactic foams." *Materials Science and Engineering: A*, 527(21-22), 5435-5443.
- Kapoor, R. and Nemat Nasser, S. (1998). "Determination of temperature rise during high strain rate deformation." *Mechanics of Materials*, 27(1), 1-12.
- Khanna, Y. P., Turi, E. A. Taylor, T. J. Vickroy, V. V. and Abbott, R. F. (1985). "Dynamic mechanical relaxations in polyethylene." *Macromolecules*, 18(6), 1302-1309.

Kim, J. I., Ryu, S. H. and Chang, Y. W. (2000). "Mechanical and dynamic mechanical properties of waste rubber powder/HDPE composite." *Journal of Applied Polymer Science*, 77(12), 2595-2602.

Kishore., Shankar, R. and Sankaran, S. (2005). "Short-Beam Three-Point Bend Tests in Syntactic Foams Part II: Effect of Microballoons Content on Shear Strength." *Journal of Applied Polymer Science*, 98(2), 680-686.

Kruger, R. A. (1997). "Fly ash beneficiation in South Africa: creating new opportunities in the market-place." *Fuel*, 76(8), 777-779.

KSSPMA, (Karnataka Small Scale Plastic Manufacturers Association). (1992). *A Guide to Plastics*. Bangalore.

Kulkarni, M. B. and Mahanwar, P. A. (2014). "Studies on the effect of maleic anhydride-grafted polypropylene with different MFI on mechanical, thermal and morphological properties of fly ash-filled PP composites." *Journal of Thermoplastic Composite Materials*, 27(12), 1679-1700.

Kulkarni, S. M. and Kishore (2002). "Effect of contact at the interface on the compressive properties of fly ash-epoxy composites." *Journal of Adhesion*, 78(2), 155-166.

Labella, M., Zeltmann, S. Shunmugasamy, V. C. Gupta, N. and Rohatgi, P. K. (2014). "Mechanical and thermal properties of fly ash/vinyl ester syntactic foams." *Fuel*, 121, 240-249.

Li, G., Zhao, Y. and Pang, S. S. (1999). "Analytical modeling of particle size and cluster effects on particulate-filled composite." *Materials Science and Engineering A*, 271(1-2), 43-52.

Maharsia, R., Gupta, N. and Jerro, H. D. (2006). "Investigation of flexural strength properties of rubber and nanoclay reinforced hybrid syntactic foams." *Materials Science and Engineering A*, 417(1-2), 249-258.

Manas chanda. and Salil Roy (2006). *Plastics Technology Handbook*, CRC press, New York, 2-6.

- Manz, O. E. (1999). "Coal fly ash: a retrospective and future look." *Fuel*, 78(2), 133-136.
- Mathew, G., Huh, M. Y. Rhee, J. M. Lee, M. H. and Nah, C. (2004). "Improvement of properties of silica filled styrene – butadiene rubber composites through plasma surface modification of silica." *Polymers for Advanced Technologies*, 15(7), 400-408.
- Matsunaga, T., Kim, J. K. Hardcastle, S. and Rohatgi, P. K. (2002). "Crystallinity and selected properties of fly ash particles." *Materials Science and Engineering: A*, 325(1-2), 333-343.
- Mohapatra, R. and Rajagopala Rao. (2001). "Some aspects of characterisation, utilisation and environmental effects of fly ash." *Journal of Chemical Technology and Biotechnology*, 76(1), 9-26.
- Nabil A. N., Alkadasi, D. G. Hundiwale and Kapadi, U. R. (2004). "Effect of Coupling Agent on the Mechanical Properties of Fly Ash-Filled Polybutadiene Rubber." *Journal of Applied Polymer Science*, 91(2), 1322-1328.
- Nanavaty, K. (1997). "Recycling of Plastics: Indian Experience." *3rd International Plastics Exhibition and Conference on Environment/Recycling of Plastics*, New Delhi.
- Navin Chanda, Prabhat Sharma and Fahim, M. (2010). "Correlation of mechanical and tribological properties of organosilane modified cenosphere filled high density polyethylene." *Materials Science and Engineering A*, 527, 5873-5878.
- Pedlow, J. W. (1978). *Cenospheres, in Coal ash utilization Fly ash, Bottom ash and Slag*, S. Torrey, eds., Noyes, New Jersey, 353-362.
- Phueakbuakao, N., Prissanaroon-Ouajai, W. and Kreua-Ongarjnkool, N. (2008). "Effect of coupling agents on mechanical properties and morphology of CaCO₃ filled recycled HDPE." *Journal of Metals, Minerals & Materials Society*, 18(2), 131-135.
- Porfiri, M. and Gupta, N. (2009). "Effect of volume fraction and wall thickness on the elastic properties of hollow particle filled composites." *Composites Part B: Engineering*, 40(2), 166-173.

Poveda, R. L., Achar, S. and Gupta, N. (2014). "Viscoelastic properties of carbon nanofiber reinforced multiscale syntactic foam." *Composites Part B: Engineering*, 58, 208-216.

Poveda, R. L., Dorogokupets, G. and Gupta, N. (2013). "Carbon nanofiber reinforced syntactic foams: Degradation mechanism for long term moisture exposure and residual compressive properties." *Polymer Degradation and Stability*, 98(10), 2041-2053.

Pukanszky, B. (1990). "Influence of interface interaction on the ultimate tensile properties of polymer composites." *Composites*, 21(3), 255-262.

Ramakrishna, H. V., Padma Priya, S. and Rai, S. K. (2006). "Utilization of Granite powder as Filler in Epoxy Phenol Cashew Nut Shell Liquid-Toughened Epoxy Resin for Impact and Compression Strength." *Journal of Reinforced Plastics and Composites*, 25(3), 227-234.

Ranney, M. W., Berger, S. E. and Marsden, J. G. (1974). *Interfaces in Polymer Matrix Composites*, Academic press, New York.

Reinhart Theodore, J. (1998). "Overview of composite materials." *Handbook of Composites*. Edited by S.T. Peters. Published by Chapman & Hall, London.

Rigoberto Burguen., Mario, J. and Geeta Mehta. (2004). "Load bearing natural fiber composite cellular beams and panels." *Composites: Part A*, 35(6), 645-656.

Rizzi, E., Papa, E. and Corigliano, A. (2000). "Mechanical behavior of syntactic foam: experiments and Modeling." *International Journal of Solids and Structures*, 37(40), 5773-5794.

Sailaja, R. R. N. (2006). "Mechanical and thermal properties of bleached kraft pulp-LDPE composites: Effect of epoxy functionalized compatibilizer." *Composites Science and Technology*, 66(13), 2039-2048.

Sailaja, R. R. N. and Deepthi, M. V. (2010). "Mechanical and thermal properties of compatibilized composites of polyethylene and esterified lignin." *Materials & Design*, 31(9), 4369-4379.

- Sailaja, R. R. N. and Seetharamu, S. (2008). "Itaconic acid-grafted-LDPE as compatibilizer for LDPE-plasticized Tapioca starch blends." *Reactive and Functional Polymers*, 68(4), 831-841.
- Sankaran, S., Sekhar, K. R. Raju, G. and Kumar, M. N. J. (2006). "Characterization of epoxy syntactic foams by dynamic mechanical analysis." *Journal of Materials Science*, 41(13), 4041-4046.
- Scheetz, B. E. and Earle, R. (1998). "Utilization of fly ash." *Current Opinion in Solid State and Material Science*, 3(5), 510-520.
- Scott, G. (2000). "Green polymers." *Polymer Degradation Stability*, 68(1), 1-7.
- Seena Joseph., Bambola, V. A. Sherhtukade, V. V. and Mahanwar, P. A. (2010). "Effect of Flyash Content, Particle Size of Flyash, and Type of Silane Coupling Agents on the Properties of Recycled Poly(ethylene terephthalate)/Flyash Composites." *Journal of Applied Polymer Science*, 119(1), 201-208.
- Sewda, K. and Maiti, S. N. (2013). "Dynamic mechanical properties of high density polyethylene and teak wood flour composites." *Polymer Bulletin*, 70(10), 2657-2674.
- Shaikh, A. A. and Channiwala, S. A. (2006). "Experimental and Analytical Investigation of Jute Polyester Composite for Long Continuous Fiber Reinforcement." *Journal of Reinforced Plastics and Composites*, 25(8), 863-873.
- Shekhar, B. (2012). "Roadmap to 13 Million Tons." *Plastindia in-house journal*, 37, 6-11.
- Shim, J. and Mohr, D. (2009). "Using split Hopkinson pressure bars to perform large strain compression tests on polyurea at low, intermediate and high strain rates." *International Journal of Impact Engineering*, 36(9), 1116-1127.
- Shunmugasamy, V. C., Gupta, N. Nguyen, N. Q. and Coelho, P. G. (2010). "Strain rate dependence of damage evolution in syntactic foams." *Materials Science and Engineering A*, 527(23), 6166-6177.
- Shunmugasamy, V. C., Pinisetty, D. and Gupta, N. (2013). "Viscoelastic properties of hollow glass particle filled vinyl ester matrix syntactic foams: effect of temperature and loading frequency." *Journal of Materials Science*, 48(4), 1685-1701.

Shunmugasamy, V. C., Zeltmann, S. E. Gupta, N. and Strbik, O. M. (2014). "Compressive Characterization of Single Porous SiC Hollow Particles." *The Journal of The Minerals, Metals & Materials Society*, 66(6), 892-897.

Singh, A. K. and Siddhartha (2015). "Leverage of cenosphere filler size on mechanical and dry sliding wear peculiarity of polyester composites." *Journal of Composite Materials*, 49(22), 2789-2802.

Smith, B. H., Hajjar, J, F. Schafer, B. W. and Arwade, S. A. (2012). "Characterization of Steel Foams for Structural Components." *Metals*, 2(4), 399-410.

Srinivasan, N. K. and Ramakrishnan, S. S. (1983). *The science of engineering materials*, Oxford & IBH publishing, New Delhi.

Srivastva, V. K. and Shembekar, P. S. (1990). "Tensile and fracture properties of epoxy resin filled with fly ash particles." *Journal of Material science*, 25(8), 3513-3516.

Thakur, S. and Chauhan, S. (2014). "Effect of micron and submicron size cenosphere particulate on mechanical and tribological characteristics of vinylester composites." *Proceedings of the Institution of Mechanical Engineers, Part J: Journals of Engineering Tribology*, 228(4), 415-423.

Thongsang, S. and Sombatsompap, N. (2006). "Effect of NaOH and Si69 treatments on the properties of fly ash/natural rubber composites." *Polymer Composites*, 27(1), 30-40.

Turcsanyi, B., Pukanszky, B. and Tudos, F. (1998). "Composition dependence of tensile yield stress in filled polymers." *Journal of Materials Science Letters*, 7(2), 160-162.

Wang, Y., Ji, D., Yang, C., Zhang, H., Qin, C. and Huang, B. (1994). "Structure and properties of maleated high-density polyethylene." *Journal of Applied Polymer Science*, 52(10), 1411-1417.

Williams, M. L., Landel, R. F. and Ferry, J. D. (1955). "The Temperature Dependence of Relaxation Mechanisms in Amorphous Polymers and Other Glass-forming Liquids." *Journal of the American Chemical Society*, 77(14), 3701-3707.

Wouterson, E. M., Boey, F. Y. C. Hu, X. and Wong, S. C. (2005). "Specific properties and fracture toughness of syntactic foam: Effect of foam microstructures." *Composites Science and Technology*, 65(11-12), 1840-1850.

Yu, M., Zhu, P. and Ma, Y. (2012). "Experimental study and numerical prediction of tensile strength properties and failure modes of hollow spheres filled syntactic foams." *Computational Materials Science*, 63, 232-243.

Zhang, L., Roy, S. Chen, Y. Chua, E. K. See, K. Y. Hu, X. and Liu, M. (2014). "Mussel-inspired polydopamine coated hollow carbon microspheres, a novel versatile filler for fabrication of high performance syntactic foams." *ACS Applied Materials and Interfaces*, 6(21), 18644-52.

LIST OF PUBLICATIONS

INTERNATIONAL JOURNALS

1. Bharath Kumar, B. R., Doddamani, M. Zeltmann, S. E. Gupta, N. Ramesh, M. R. and Ramakrishna, S (2016). “Processing of cenosphere/HDPE syntactic foams using an industrial scale polymer injection molding machine.” *Materials & Design*, 92, 414-423. (**Elsevier, 3.501**)
2. Bharath Kumar, B. R., Doddamani, M. Zeltmann, S. E. Gupta, N. Uzma, Gurupadu, S. and Sailaja, R. R. N (2016). “Effect of surface treatment and blending method on flexural properties of injection molded cenosphere/HDPE syntactic foams.” *Journal of Materials Science*, 51(8), 3793–3805. (**Springer, 2.371**)
3. Bharath Kumar, B. R., Doddamani, M. Zeltmann, S. E. Gupta, N. and Ramakrishna, S (2016). “Data characterizing tensile behavior of cenosphere/HDPE syntactic foam.” *Data in Brief*, 6, 933-941. (**Elsevier**)
4. Bharath Kumar, B. R., Singh, A. K. Doddamani, M. Luong, D. and Gupta, N. (2016). “Quasi-static and high strain rates compressive response of injection molded cenosphere/HDPE syntactic foam.” *JOM*, DOI: 10.1007/s11837-016-1912-3, 01-11. (**Springer, 1.757**)
5. Bharath Kumar, B. R., Zeltmann, S. E. Doddamani, M. Gupta, N. Uzma, Gurupadu, S. and Sailaja, R. R. N (2016). “Effect of cenosphere surface treatment and blending method on the tensile properties of thermoplastic matrix syntactic foams.” *Journal of Applied Polymer Science*, 133(35), 10.1002/app.43881. (**Wiley, 1.768**)
6. Zeltmann, S. E., Bharath Kumar, B. R. Doddamani, M. Gupta, N. (2016). “Prediction of strain rate sensitivity of high density polyethylene using integral transform of dynamic mechanical analysis data.” *Polymer*, 101, 1-6. (**Elsevier, 3.586**)

INTERNATIONAL CONFERENCES

1. Zeltmann S. E., Gupta, N., Bharath Kumar, B. R. and Doddamani, M. (2016). “Dynamic mechanical analysis of HDPE-cenosphere syntactic foams.” *American Society for Composites, 31st Technical Conference and ASTM Committee D30 Meeting*, September 19-22, Williamsburg Virginia, USA, Paper No. 1814.
2. Bharath Kumar, B. R., Singh, A. K. Doddamani, M. Luong, D. and Gupta, N (2016). “Compressive behavior of cenosphere/HDPE syntactic foams under different strain rates.” *American Society for Composites, 31st Technical Conference and ASTM Committee D30 Meeting*, September 19-22, Williamsburg, Virginia, USA, Paper No. 1905.
3. Bharath Kumar, B. R., Doddamani, Gupta, N. Sailaja, R. R. N (2015). “Flexural behaviour of cenosphere/HDPE syntactic foam composite.” *Proceedings of the 17th ISME Conference*, October 3-4, IIT Delhi, New Delhi, Paper ID – ISME-M-032, 2015.
4. Rakesh Dhaka., Bharath Kumar, B. R. Doddamani, M (2015). “Free vibration response of HDPE syntactic foam composite.” *Proceedings of the 17th ISME Conference*, October 3-4, IIT Delhi, New Delhi, Paper ID-ISME-D-027.
5. Bharath Kumar, B. R., Doddamani, M. Gupta, N (2015). “Tensile properties of cenosphere/HDPE syntactic foams manufactured using an industrial scale injection molding technique.” *American Society for Composites-30th Technical Conference*, September 28-30, Kellogg Centre, Michigan State University, East Lansing, Michigan, USA, Paper ID-1498.
6. Bharath Kumar, B. R. and Doddamani, M (2015). “Mechanical Behavior of HDPE Syntactic Foam Composite.” *4th International Engineering Symposium - IES 2015* March 4-6, Kumamoto University, Japan.
7. Bharath Kumar, B. R., Doddamani, M. Zeltmann, S. E. Gupta, N. Ramesh, M. R. and Ramakrishna, S (2014). “Processing and tensile characteristics of cenosphere/hdpe syntactic foams.” *1st International conference in Sports science and Technology-Advanced Materials for Sports Technology*, 11-12 December, Singapore.

BIO-DATA

1. **Name** : Bharath Kumar B. R.
2. **Father's Name** : Rangaswamy B. S.
3. **Date of Birth** : 3rd September 1987
4. **Nationality** : Indian
5. **Marital Status** : Single
6. **Address** : Department of Mechanical Engineering
National Institute of Technology Karnataka
Surathkal, PO Srinivasnagar 575 025
Karnataka, India.
7. **Mobile Number** : +91 96113 45720
8. **E-mail id.** : *bharathrangaswamy@gmail.com*
9. **Educational Qualification** :

Qualification	University/Board	Year of Passing
Ph.D. (Mechanical Engineering)	National Institute of Technology Karnataka	Pursuing
M.Tech. (Mechanical Engineering)	Visvesvaraya Technological University, Belgaum	2012
B.E. (Mechanical Engineering)	Visvesvaraya Technological University, Belgaum	2010
